ONTOGENY AND FUNCTION OF REGULATORY T CELLS DURING ESTABLISHED INFLAMMATION AND AT INTESTINAL MUCOSA

by

Zhongmin Wang

A Dissertation

Presented to the Faculty of the Louis V. Gerstner, Jr.

Graduate School of Biomedical Sciences,

Memorial Sloan-Kettering Cancer Center

in Partial Fulfillment of the Requirements for the Degree of

Doctor of Philosophy

New York, NY

September 2022

Alexander Y. Rudensky, Ph.D.
Dissertation Mentor

Date

Copyright by Zhongmin Wang 2022

DEDICATION

I would like to dedicate this dissertation to my grandparents, Li Fang-Lan, Sun Mei-Ran, Wang Mao-Li, and Wang Qing-Chun, for their unwavering love.

ABSTRACT

Regulatory T (Treg) cells, characterized by the lineage-defining transcription factor *Foxp3*, are specialized $CD4^+$ T cells with immunosuppressive function. Treg cell deficiency causes lethal autoimmune inflammation in mice and humans. Although an indispensable role for Treg cells in preventing the onset of fatal autoimmunity has been clearly demonstrated, whether Treg cells can effectively function under conditions of established systemic inflammation or reverse severe autoimmunity remains unclear. To address this question, we created a reversible *Foxp3* null allele ($Foxp3^{LSL}$) whose expression is by default prevented by a transcriptional termination cassette but can be rescued by tamoxifen-activatable cre recombinase. This allowed for acute and specific activation of *Foxp3* expression *in vivo* in the Treg cell lineage-committed "Treg wannabe cells", which were originally devoid of suppressive properties. Restoration of *Foxp3* expression in these mice when the disease was pronounced completely reversed tissue pathologies and dysfunction, and resolved the lethal autoimmune inflammation. The rescued Treg cells were more suppressive, elaborated higher levels of effector molecules, and participated in tissue repair. Surprisingly, Treg cells generated as a cohort in response to a single dose of tamoxifen treatment persisted stably without exhibiting signs of exhaustion and provided long-term protection against relapse of autoimmunity. Therefore, Treg cells are highly functional in a severely inflammatory environment and are capable of reversing, in addition to preventing, complex autoimmune inflammation, which paves the way for developing Treg cell-based therapies for autoimmune diseases.

In addition to autoimmunity, Treg cells are also involved in restraining pathogenic immune responses against innocuous foreign antigens, including allergens, dietary components, and commensal microbes. Treg cells specific for self and foreign antigens are thought to be generated from distinct precursor cells in separate anatomic locations: thymocytes develop into thymic Treg (tTreg) cells in response to self antigens, while environmental antigens of barrier site origin stimulate naïve conventional T cells to differentiate into peripheral Treg (pTreg) cells. Due to a lack of tools that allow for specific identification and manipulation of these cell populations, whether tTreg and pTreg cells represent separate lineages with unique function and properties remains elusive. Therefore, we sought to selectively ablate pTreg cells through deletion of *Foxp3* enhancers responsive to pTreg cell-inducing signals in a temporally controlled manner. By knocking out *Foxp3*-CNS0 immediately before weaning in *Foxp3*-CNS1 deficient mice, the resulting conventional T cells had severely diminished response to IL-2, TGF-β, or retinoic acid signaling in *in vitro* induction assays and failed to express *Foxp3.* pTreg cell-deficient mice spontaneously developed mucosal inflammation in the large intestine at 3-4 months featuring mastocytosis, expansion of T helper 2 cells, and heightened production of type 2 cytokines. Furthermore, germinal center B cells in the gut-associated lymphoid tissues of pTreg cell-deficient mice preferentially switched to the type 2 immunoglobulin IgG1, and serum IgE titer in these mice was also elevated. In conclusion, intestine-related pTreg cells restrain exuberant type 2 immunity and safeguard the health of the gastrointestinal mucosa, dysregulation of which might underlie food allergy.

BIOGRAPHICAL SKETCH

Zhongmin Wang (also spelt professionally as Zhong-Min Wang, pronounced *Jone Meen Wahng,* Chinese: 王鐘民), was born to mother Donghui Wang and father Kewei Wang in July 1994 in Dalian, Liaoning Province, P.R. China. He attended Dalian No. 24 High School before receiving his high school diploma in 2012. He then attended The University of Hong Kong (HKU) and majored in Biochemistry. During his tenure at HKU, Zhongmin conducted research in the laboratory of Prof. Dong-Yan Jin to develop novel therapeutics for nasopharyngeal carcinoma caused by Epstein-Barr virus infection, served as Student Representative on the BSc in Biochemistry Curriculum Committee and as Student Peer Advisor, and spent 8 months of his junior year in 2015 as an exchange student at University of California, Berkeley. In 2016, he graduated from HKU and was awarded a Bachelor of Science degree with First Class Honors. He thereafter moved to New York to begin his doctoral study at Louis V. Gerstner Jr. Graduate School of Biomedical Sciences, Memorial Sloan-Kettering Cancer Center, where he served on the Student Council as Curriculum Advisor.

ACKNOWLEDGMENTS

I would like to thank my colleagues who provided tremendous help with and contribution to my research. The following people contributed to the research described in Chapter One: Wei Hu, Yongqiang Feng, Michail Schizas, Beatrice E. Hoyos, Joris van der Veeken, Jacob G. Verter, and Regina Bou-Puerto. Wei Hu was in particular instrumental to this project, who generously shared with me her insight and technical expertise without reserve. Through working alongside Wei, I have been greatly influenced by her ingenuity, meticulousness, scientific acumen, integrity, technical competence, and work ethics as I was being trained to become a scientist. The following people contributed to research described in Chapter Two: Stanislav Dikiy, Wei Hu, Regina Bou-Puerto, Beatrice E. Hoyos, Emma Andretta, and Alejandra Mendoza. Doing the large experiments in this chapter would not have been possible without the profuse help that they offered. In addition, I would like to thank all past and current members of the Rudensky Lab from 2017 onward for scientific discussions.

I would like to thank my thesis committee members, Drs. Jayanta Chaudhuri, Danwei Huangfu, Steven Josefowicz, and Christina Leslie for bringing their expertise to discussion of my research and providing me with insightful guidance. I would also like to thank Dr. Thomas Norman for helping me devise a mathematical model for enhancer synergy, and Dr. Eric G. Pamer for being my rotation and first year mentor.

I would like to thank my parents for their steadfast support for me to pursue my aspirations throughout my doctoral studies and beyond, and for taking tremendous interests in my research.

I would like to thank GSKGS leadership, Deans Michael Overholtzer, Kenneth Marians, Linda Burnley, and Tomas Magaldi, as well as David McDonagh and Maria Torres for their dedication to the education and wellbeing of GSK students. I would also like to thank my friends both within and outside the GSK community for taking the ride of graduate school with me and providing moral support.

I would like to thank the Geoffrey Beene Graduate Student Fellowship, the Bruce Charles Forbes Pre-doctoral Fellowship, and the GSKGS Chairman's Award for recognizing my research and providing me with financial support.

Last but not the least, I would like to thank my mentor, Dr. Sasha Rudensky, for the invaluable guidance and stringent training I have been receiving, and for his dedication to and support for my success and wellbeing during and after my graduate studies. I have also learned greatly from the talented group that Sasha has built, in particular Drs. Stanislav Dikiy, Wei Hu, Clarissa Campbell, Alejandra Mendoza, Ariella Glasner, and Joris van der Veeken, and Miss Regina Bou-Puerto and Deeksha Deep for their altruism and kindness that helped me through periods of difficulties. What I have gained from the Rudensky lab was not only professional training, but also camaraderie that will last for a lifetime.

TABLE OF CONTENTS

LIST OF FIGURES

LIST OF ABBREVIATIONS

4-OHT: 4-hydroxytamoxifen

APC: Antigen presenting cell

BM: Bone marrow

CD4SP: CD4 single-positive thymocyte

CNS: Conserved non-coding sequence

cTEC: Cortical thymic epithelial cell

DC: Dendritic cell

DKO: Double knockout

DP: Double-positive thymocyte

DT: Diphtheria toxin

DTR: Diphtheria toxin receptor

GF: Germ-free

GFP: Green fluorescent protein

H3K4me1: Histone H3 lysine 4 monomethylation

IFN: Interferon

IL: Interleukin

ILC: Innate lymphoid cells

isoalloLCA: isoallolithocholic acid

isoDCA: 3β-hydroxydeoxycholic acid

iTreg: Induced regulatory T (cell)

KO: Knockout

LILP: Large intestine lamina propria

MHC: Major histocompatibility complex

MLN: Mesenteric lymph node

mTEC: Medullary thymic epithelial cell

nTconv: Naïve conventional T (cell)

nTreg: Natural regulatory T (cell)

OVA: (Chicken egg) Ovalbumin

P: Postnatal day

pLN: Peripheral lymph nodes

PP: Peyer's patch

pTreg: Peripheral regulatory T (cell)

RA: Retinoic acid

scRNA-seq: Single cell RNA sequencing

SPF: Specific pathogen free

Tconv: Conventional T (cell)

TCR: T cell receptor

Treg: Regulatory T (cell)

tTreg: Thymic regulatory T (cell)

WT: Wild-type

CHAPTER ONE:

Introduction

The emergence of the adaptive immune system allows vertebrates to amplify the innate immune response, mobilize dedicated effector modules tailored for different types of pathogens, and form immunological memory. T and B lymphocytes utilize germline-encoded receptors generated via VDJ recombination to recognize virtually any antigen with high specificity. Due to its stochastic nature, however, the very mechanism that confers vertebrate unlimited pathogen recognition capacity can also give rise to lymphocytes that respond to and attack self, commensal microorganisms, and innocuous dietary and environmental antigens. If left unchecked, these cells would cause debilitating and even lethal autoimmune, inflammatory, or allergic disorders. Therefore, dedicated mechanisms have evolved to ensure that tolerance can be developed for self antigens and induced for harmless foreign substances.

For T cells, such mechanisms include both central and peripheral tolerance. Central tolerance happens in the thymus where signaling through T cell receptors (TCRs) triggers apoptosis of autoreactive thymocytes, thus preventing them from maturation and emigration to the periphery (1). Even when central tolerance fails to eliminate autoreactive T cells, those that evade negative selection will not become activated upon encountering antigen presenting cells (APCs) that present the cognate self antigens on their major histocompatibility complexes (MHCs), because T cell activation requires a second signal, or co-stimulation, by CD28 ligation. Ligands of CD28, namely CD80 and CD86, are only upregulated in APCs upon pattern recognition receptor signaling, so that autoreactive T cells that signal

only through their TCR in the absence of pathogen- or danger-associated molecular patterns will instead become anergic or hyporesponsive (2).

In addition to the aforementioned cell-intrinsic tolerogenic programs, another mechanism of peripheral tolerance has been postulated which involves a specialized T cell population that suppresses conventional T (Tconv) cell activation *in trans*. The first evidence in support of the presence of such inhibitory cells came from neonatal thymectomy experiments performed in mice. Surgical removal of thymus on postnatal day (P) 3 causes systemic autoimmune inflammation that can be prevented with adoptive transfer of splenocytes from adult euthymic mice (3-5). This indicates cells that are capable of inhibiting the activation of other immune cells, in particular T cells generated within the first 2 days of life develop after P3 in the thymus. These cells, named regulatory T (Treg) cells, were first identified as a population of $CD4^+$ T cells that constitutively express CD25, the high affinity subunit of the interleukin (IL) -2 receptor complex (6). The suppressive function of euthymic mice splenocytes is highly enriched in these cells, as transfer of $CD4^+CD25^+$ cells but not $CD4^+CD25^-$ cells subdues autoimmune inflammation in P3 thymectomized mice as well as in mouse models of various autoimmune diseases (7, 8). However, the utility of CD25 as a marker for Treg cells is limited because it is also upregulated in Tconv cells upon activation, thus rendering the differentiation of Treg cells and activated Tconv cells difficult under settings of active inflammation.

Foxp3 is the lineage-defining transcription factor of Treg cells

Our understanding of Treg cell biology was largely facilitated by the identification and study of murine spontaneous loss-of-function *scurfy* mutation in the *Foxp3* gene and human IPEX (Immune dysregulation, polyendocrinopathy, enteropathy, X-linked) patients (9-12). Mice and human carrying inactivating mutations in *Foxp3* develop rampant, early-onset and lethal systemic inflammation featuring lympho- and myelo-proliferation, splenomegaly, lymphadenopathy, exudative dermatitis, polyneuropathy, hepatitis, endocrinopathy (insulitis, thyroiditis, adrenal dysfunction), enteropathy (autoimmune gastritis, inflammatory bowel disease), hyper-IgE syndrome, autoimmune hematopoietic disorders (hemolytic anemia, autoimmune thrombocytopenia), and pulmonary and nephrotic pathologies (13). Of note, only mutant hemizygous males but not heterozygous females are affected, because the latter harbor T cells that express either the mutant or the wild-type (WT) *Foxp3* gene due to random X inactivation (14). The WT *Foxp3*-expressing cells are sufficient for keeping autoreactive T cells in check, hence preventing fatal autoimmunity.

Based on these findings, three labs examined Foxp3 expression in mouse T cell populations. Foxp3 is stably expressed at high levels in $CD4^+CD25^+$ T cells but is undetected in $CD4^+CD25^-$ naïve T cells or effector T cells (15-17). *Foxp3* knockout (KO) mice developed lethal multi-organ inflammation similar to those carrying spontaneous *Foxp3* mutations, with severely diminished $CD25^+$ CD4 single-positive thymocyte (CD4SP) populations (16, 17). Importantly, in healthy mixed bone marrow chimeras using congenically marked *Foxp3*-sufficient and -deficient bone marrow as donors and mice lacking T cells as recipients, only

Foxp3^{WT} bone marrow is able to give rise to CD4$^+$CD25$^+$ T cells in the periphery (17). This indicates that the CD4$^+$CD25$^+$ T cells in the secondary lymphoid organs of *Foxp3*^{KO} mice after disease onset are activated Tconv cells rather than Treg cells. Transfer of WT but not *Foxp3*^{KO} bone marrow into *Foxp3*^{KO} recipients cures systemic inflammation, whereas transfer of *Foxp3*^{KO} bone marrow into *Foxp3*^{WT} T cell-deficient recipients causes fatal autoimmunity (17). Therefore, expression of Foxp3 in the hematopoietic compartment instead of cortical or medullary thymic epithelial cells (cTECs or mTECs, respectively) is required for the generation of Treg cells, in agreement with its expression pattern (18).

Generation of the *Foxp3*^{GFP} reporter allele which consists of an N-terminal fusion of green fluorescent protein (GFP) to Foxp3 enabled further examination of Foxp3 expression among CD4$^+$ T cells (19). The majority of Foxp3$^+$ cells in the secondary lymphoid organs express CD25, while a small population of Foxp3$^+$CD25$^-$ cells are present. Albeit at a lower frequency, CD25$^-$ Foxp3$^+$ cells isolated from *Foxp3*^{GFP} mice are capable of suppressing APC-induced proliferation of Tconv cells *in vitro* as well as lethal T cell activation *in vivo* upon co-transfer into T cell-deficient mice similar to their CD25$^+$ counterparts, whereas Foxp3$^-$ cells cannot suppress regardless of CD25 expression (19). Ectopic expression of Foxp3 in Tconv cells confers upregulation of Treg cell markers and suppressive function, while ablation of Foxp3 in differentiated Treg cells either through knockdown or by use of tamoxifen-activatable cre in combination of a loxP-flanked *Foxp3* allele (*Foxp3*^{fl}) causes them to lose suppressive function and adopt pro-inflammatory properties, including upregulation of interferon (IFN) γ, IL-4, IL-17, and IL-2 (20,

21). Taken together, Foxp3 is necessary for the development and function of Treg cells and is TF that defines the Treg cell lineage.

Treg cells are required for immune tolerance throughout life

In addition to suppressing lethal autoimmunity in neonates, Treg cells are also required during adulthood after most T cells have finished developing and taking residence in the periphery. This was demonstrated with the development of a mouse model whose *Foxp3* locus encodes a simian diphtheria toxin receptor (DTR)–GFP fusion protein, thus allowing for depletion of Treg cells upon diphtheria toxin (DT) treatment (22). Continuous DT treatment in $Foxp3^{DTR}$ males results in a lethal inflammatory phenotype indistinguishable from that of $Foxp3^{KO}$ mice. Importantly, treatment of adult $Foxp3^{DTR}$ mice with DT causes systemic inflammation featuring an even faster kinetic, with most mice dying in 2 weeks. By one week post-DT treatment, mice develop T cell activation, splenomegaly and lymphadenopathy, and lymphocytic infiltration in multiple non-lymphoid organs (22). Therefore, Treg cells are required for immune tolerance throughout life.

The immune activation in adult mice upon Treg cell ablation may be caused by de-inhibited autoreactive T cells or uncontrolled reactivity against the gut and skin microbiota. To differentiate between these two possibilities, $Foxp3^{DTR}$ mice are rederived and kept under germ-free (GF) condition (23). Upon DT treatment, GF $Foxp3^{DTR}$ mice developed immunopathology similar to specific pathogen free (SPF) mice, with the only exceptions being small intestine and pancreas having delayed and accelerated disease kinetics, respectively (23). In conclusion, Treg cells are required to prevent aberrant activation of autoreactive T cells during

adulthood, while T cells specific for the gut microbiota also contribute to the small intestine pathology in Treg cell-depleted mice. Thus, by inhibiting pro-inflammatory cell *in trans*, Treg cells represent a non-redundant mechanism of immune tolerance.

Potential function of Treg cells during established inflammation

Although it has been unequivocally established that Treg cells are indispensable for preventing onset of lethal autoimmunity, whether they can effectively exert their suppressive function under conditions of established or ongoing inflammation remains a topic of intense debate. Adoptive transfer of Treg cells into *Foxp3*^{KO} mice provides temporary symptom alleviation, but the suppressive ability wanes over time which ultimately precipitates the demise of the animals (24-30). Similarly, multiple efforts have been made to exploit the therapeutic potential of Treg cells for treating autoimmune diseases, but these clinical trials generate mostly negative results. These observations raise the possibility that Treg cells cannot suppress effectually when introduced into an established inflammatory environment. In fact, several studies have suggested that pro-inflammatory cytokines, such as IL-6 and IL-1, can cause Treg cells to lose suppressive function and even adopt pro-inflammatory characteristics, while others have shown that an inflammatory milieu can render Tconv cells resistant to Treg cell-mediated inhibition (24, 26, 28, 29, 31, 32). To corroborate these findings, Treg cells in patients with chronic inflammatory or autoimmune disorders are suspected to have compromised functionality because they expand at the inflammatory sites while the diseases persist, and when isolated these cells

express lower levels of suppressive molecules and demonstrate defective inhibitory function in *in vitro* assays (33-37).

However, the negative results could alternatively be interpreted as caveats intrinsic to adoptive transfer experiments: the transferred Treg cells may be trapped in the microvasculature in the lung and liver, thus leaving a small population of Treg cells with limited TCR repertoire to suppress diverse Tconv cell populations that vastly outnumber them. Besides, the transferred Treg cells, usually isolated from secondary lymphoid organs due to the large number of cell available, may not be able to migrate to the tissues where their function is required because they are not developed in the context of the specialized APCs that primed them for tissue homing. Likewise, interpretation of the clinical data can be tricky. Thanks to the complex genetic polymorphism that may play a role in the initiation of autoimmune diseases, it is difficult to elucidate if dysfunctional Treg cells are the cause or the result of chronic inflammation. Indeed, one study has shown that adoptively transferred Treg cells can offer prolonged remedy for T cell-induced colitis, but the cure might be owing to the specific etiology of the model—naïve T cell transfer—or unique physiology of the colon, such as constant epithelial turnover (38, 39). Others have demonstrated that Treg cells are capable of limiting the degree of immunopathology during active viral infection, thus improving prognosis (40-45).

To address these questions, we developed a novel mouse model that allows for installation of Treg cells into mice with established autoimmunity, which will be described in detail in Chapter Two (46).

Regulation of Treg cell differentiation in the thymus

As is other T cell subsets, Treg cell differentiation depends on an intricate interplay of TCR and cytokine signaling (47). Among these, TCR signaling strength and IL-2 play the most important role in Treg cell lineage commitment. While Foxp3 reporter expression can be detected in double-positive thymocytes (DPs) and in the thymic cortex, the majority of Foxp3 expression is observed in CD4SPs and in the medulla by using flow cytometry and immunofluorescence, respectively (48). The current model of Treg cell development follows a two-step mechanism proposed by Hsieh and Farrar and their colleagues: upon receiving TCR signaling of elevated strength, the developing thymocyte upregulates CD25, thus sensitizing the cell for IL-2. It is only after these CD4SP $CD25^{+}Foxp3^{-}$ immediate precursors of Treg cells encounter IL-2 do they start expressing Foxp3 and differentiating into mature Treg cells (49, 50). Molecularly, the signaling events activate the downstream TFs—AP-1, NFAT, and NFκB for TCR and STAT5 for IL-2—which cause global changes in chromatin accessibility, hence setting up the landscape for Foxp3-mediated transcriptional regulation, and bind to *cis*-regulatory elements in the *Foxp3* locus as *trans*-activators (51). The details of the involvement of these factors in Treg cell differentiation are described below.

Regulation of thymic Treg cell development: T cell receptor

TCR signaling strength is crucial for determining the fate of thymocytes: it ensures that the newly minted TCR has the appropriate affinity for self MHC molecules to pass positive and negative selection, instructs MHC class II or I restriction and CD4 or CD8 lineage choice, respectively, and directs higher affinity

TCR-expressing cells through agonist selection for differentiation into non-canonical T cell subsets, including CD8αα, NKT, and mucosal associated invariant T cells. Likewise, TCR signaling and its strength play a pivotal role in Treg cell lineage commitment and differentiation (52-55). The requirement for TCR signaling in the development of Treg cells is first noticed in TCR transgenic mice. Thymic differentiation into Treg cells by thymocytes expressing transgenic TCRs specific for foreign antigens, influenza A hemagglutinin or chicken egg ovalbumin (OVA), is greatly enhanced by the expression of a separate transgene in the thymus encoding the cognate antigens, which function as neo-self antigens (56-60). This finding not only elucidates the involvement of TCR signaling in thymic Treg (tTreg) cell development, but also suggests that tTreg cell differentiation is driven by autoreactive TCRs that evade negative selection. In agreement with this notion, expression of CD5, which is positively correlated with TCR signaling strength during thymic development, is higher on Treg cells compared to Tconv cells (61, 62). In addition, analysis of the TCRα usage of Treg and Tconv cells expressing a transgene-encoded β chain shows that their repertoires only partially overlap, suggesting that Treg cells develop in response to unique antigenic specificities (63).

The final piece of evidence proving that Treg cell TCR are more self-directed comes from experiments where Treg and Tconv cell derived TCRs are clone. Upon transfer of the into mice, bone marrow progenitor cells transduced with Treg cell TCRs readily give rise to Treg cells, whereas Tconv cell TCRs barely generated any (64). Meanwhile, Treg cell TCR-transduced T cells injected into T

cell-deficient mice rapidly proliferate and cause a wasting disease not seen for their Tconv cell counterparts (64). This experiment, together with previous observations, demonstrates that the distinct TCR usage by Treg cells is deterministic in their lineage commitment and is skewed towards recognizing self antigens. The autoreactive nature of Treg cell TCR likely signals stronger in the thymic medulla due to expression of peripheral tissue antigens on mTECs, which is consistent with their elevated CD5 expression, but not so strong as to trigger negative selection.

The complicated network of TCR signaling activates multiple TFs, many of which bind to the *Foxp3* locus and are implicated in the transcriptional regulation of Foxp3 expression and Treg cell development. The Foxp3 promoter is a binding site for NFAT and AP-1, downstream of PLCγ signaling, as well as Foxo1 and Foxo3 activated by CD28 costimulation (47, 51). CD28 signaling also participates in Treg cell differentiation by activating the PI3K-Akt pathway and downstream NFκB, as both CD28 and CD80/86 KO mice show substantial defect in the Treg cell compartment (65, 66). Like many other promoters of developmental genes, the basal *Foxp3* promoter has limited transcriptional initiation activity based on reporter assays (67, 68). Therefore, *Foxp3* transcription is mainly regulated by enhancers identified based on sequence conservation, hence named conserved non-coding sequences (CNS) (69). To date, four enhancers in and around the *Foxp3* locus have been identified to regulate its expression, whose numbering correspond to the order in which they appear on the X chromosome coordinate (69-74).

CNS3, an intronic enhancer located between the first and second coding exons of *Foxp3*, is another *cis*-regulatory element responsive to TCR/CD28 signaling in addition to the promoter by binding to the canonical NFκB family member c-Rel but not p50 or p65 (69). A c-Rel motif resembling that of the *Il2* CD28 response element is identified in CNS3, whose deletion abolishes c-Rel binding to CNS3 probes (69). The importance of c-Rel in tTreg development is illustrated by mice with T cell-specific deletion of c-Rel, which have drastically diminished Treg cell populations in the thymus (69, 75). CNS3 is decorated with histone H3 lysine 4 monomethylation (H3K4me1), the histone modification associated with permissive promoters and enhancers, in double-negative, DP, and CD4 SP thymocytes, naïve Tconv cells, as well as Treg cells (72). In contrast, H3K4me1 is only detected at the promoter in mature CD4 SP thymocytes and Tconv cells, which is later replaced in Treg cells with the active promoter mark H3K4me3 (72). Interestingly, CNS3 monomethylation is present in hematopoietic stem cells but absent in non-T cells, suggesting regulatory mechanisms leading to its silencing during differentiation of alternative cell fates. The sequential order in which CNS3 and the promoter are modified along Treg cell differentiation trajectory hints at the possibility that CNS3 functions as a pioneer factor to prime the promoter for activation upon receiving Treg cell-inducing signals. Indeed, CNS3 deletion causes a decrease in the H3K4me1 signal at the promoter in mature CD4SPs and naïve Tconv cells (72).

$CNS3^{KO}$ mice, like T cell-specific c-Rel-deficient mice, have vastly shrunken Treg cell compartment in the thymus (72). The peripheral Treg cell numerical

defect, however, is much less severe due to increase proliferation. Nonetheless, CNS3-sufficient and -deficient Treg cells are qualitatively different, the latter bearing a less diverse TCRα repertoire when expressing a transgenic β chain (72). This is because loss of CNS3 desensitizes the *Foxp3* locus to TCR stimulation and hence stronger TCR signaling is required for CNS3-deficient precursor cells to commit to the Treg cell lineage. In accordance with this notion, Treg cells in CNS3^{KO} mice express high levels of Nur77, a nuclear factor that reports TCR signaling strength. In addition, CNS3-deficient Treg cells divide more readily upon co-transfer with WT cells into lymphopenic mice, which is abolished by treatment with antibodies blocking MHC class II. This further indicates elevated TCR signaling strength in CNS3-deficient Treg cells. Due to the narrowed TCR repertoire, CNS3^{KO} mice have compromised immune tolerance, as demonstrated by spontaneous production of a diverse array of autoantibodies and mild T cell activation in the lung. Deletion of *Aire*, the transcriptional regulator that facilitates expression of peripheral tissue antigens in mTECs, drastically exacerbates the autoimmunity in CNS3^{KO} mice, which features T cell activation and expansion, tissue inflammation, and binding of autoantibodies to tissues (72). The worsened autoimmunity is not due to paucity of Treg cells in the periphery, but likely ascribed to an imbalance in the TCR repertoires of Treg cells and autoreactive Tconv cells further skewed by decreased peripheral tissue antigen expression in the thymus, which promotes negative selection of pathogenic T cells and agonist selection of Treg cells.

In conclusion, heightened TCR signaling recognizing self peptide in the thymus allows some thymocytes to develop into Treg cells, which serve a mechanism other than central tolerance to contain T cell-mediated autoimmunity. By binding to c-Rel activated by TCR/CD28 stimulation, intronic enhancer CNS3 primes the *Foxp3* promoter and increases its sensitivity to a wider range of TCR signaling strength during tTreg development, thus expanding the scope of protection afforded by tTreg cells. The molecular mechanisms of CNS3 activity regulation and CNS3-dependent promoter H3K4 monomethylation remain to be unveiled.

Beyond the *Foxp3* locus, TCR signaling in precursor cells causes changes in chromatin landscape that precede Foxp3 expression. One of such changes is the induction of CD25 expression, as shown by elevated Nur77 expression in CD4SP CD25^{+}Foxp3^{-} thymocytes (55, 76). Upregulation of CD25 sensitizes these precursor cells to IL-2, another pivotal factor in Treg cell development.

Regulation of thymic Treg cell development: Interleukin-2

Although indispensable for tTreg cell development, TCR signaling alone is not sufficient for generating the entire tTreg cell compartment, as suggested by the following observations. First, the overlapping TCR repertoire of Treg and Tconv cells indicates the presence of other signals that govern the fate choice of thymocytes of particular antigenic specificities (63). Second, while Treg cell-derived TCRs, when transduced into bone marrow progenitor cells, are better at giving rise to Treg over cells than Tconv cell-derived TCRs, some transgenic TCR-expressing cells differentiate into Tconv cells that later become anergic upon

migration to the periphery (57, 59). Third, thymocytes expressing the Treg cell-derived G113 transgenic TCRs cannot generate tTreg cells on the *Rag1*^{KO} background, which can be rescued when injected intrathymically into WT mice (77). Lastly, while tTreg cells do not emerge until day 3, the CD4SP CD25^{+}Foxp3^{-} immediate precursors of tTreg cells rapidly increase in number and plateau on P1 (49, 50, 78). All these data suggest signals other than TCR stimulation are required for tTreg development.

The missing link turned out to be a group of common γ chain cytokines, including IL-2, IL-7, and IL-15 (79-82). Of these, IL-2 has the most profound effect on tTreg cell differentiation. CD25^{+}Foxp3^{-} CD4SPs readily turn on Foxp3 *ex vivo* once treated with IL-2, and to a lesser extent with IL-7 and IL-15 (49, 50, 73, 76, 80). CD25^{-} mature CD4SPs upregulate CD25 upon *ex vivo* TCR stimulation, which then are susceptible to IL-2 treatment induced Foxp3 expression (50, 73, 76). Mice with germline deficiency of IL-2, CD25, or CD122 (encoding IL-2Rβ chain) have a severely diminished tTreg cell compartment with decreased Foxp3 expression level on a per-cell basis and profound immune activation in the periphery, while CD122 and IL-7Rα double KO or common γ chain KO mice completely lack tTreg cells and succumb to autoimmunity (79, 80, 82).

Despite the well appreciated importance of IL-2 on tTreg cell generation, its cellular source in the thymus remained elusive. While highly expressing IL-2 receptor, mature Treg cells fail to elaborate IL-2 upon stimulation and cannot support generation of additional Treg cells (83, 84). The candidates of thymic IL-2 production include thymocytes, thymic dendritic cells (DCs), and CD45^{-} stromal

cells (85, 86). Using genetic fate-mapping and conditional KO approaches, Hemmers et al. probed into the pattern and history of IL-2 expression among thymic cell populations (76). Conditional deletion of *Il2* in T cells using Lck-cre or CD4-cre result in compromised Treg cell generation and peripheral immune activation resembling those in germline $Il2^{KO}$ mice, while DC-specific IL-2 ablation using Zbtb46-cre do not impact Treg cell development. Of cells that have expressed IL-2 at some stage of their development, as illustrated by a recombination reporter induced by IL-2-cre, all are positive for CD45 and TCRβ, with the vast majority of them being CD4SP and the rest being CD8SP. While thymus is the only organ where IL-2 expression can be detected on P3, about 10% and 4% of Tconv and Treg cells in the spleen, respectively, have a history of IL-2 expression. Consistent with this, $CD25^{+}Foxp3^{-}$ CD4SPs, the immediate precursors of tTreg cells, as well as mature CD4SPs but not immature CD4SPs or Treg cells, produce IL-2 upon *ex vivo* stimulation with α-CD3/CD28. However, examination with ATAC-seq revealed that $CD25^{+}Foxp3^{-}$ CD4SPs are the only cell type whose Il2 locus is accessible. This seeming discrepancy is because the same signal that drives IL-2 production, TCR stimulation, also causes upregulation of CD25. IL-2 production by $CD25^{+}Foxp3^{-}$ CD4SPs promotes Foxp3 induction in a paracrine as well as autocrine manner, in that stimulating CD4SPs with staphylococcal enterotoxin B super-antigen, which strongly activates Vβ8-utilizing TCRs, also increased Foxp3 expression in Vβ5- and Vβ6-expressing thymocytes (76).

scRNA-seq experiments of thymocytes demonstrate that CD25^{+}Foxp3^{-} CD4SPs express the pro-apoptotic gene *Bcl2l11* (encoding Bim) highly and the anti-apoptotic gene *Bcl2* lowly, suggesting that these cells are autoreactive T cells undergoing negative selection. *Il2* transcript is captured in about 3% of cells and roughly equally distributed across Treg cells, mature CD4SPs, and CD25^{+}Foxp3^{-} CD4SPs. The Treg cells containing *Il2* transcript are likely cells that recently upregulated *Foxp3*. While most of IL-2 producers express NFκB pathway activation genes and *Bcl2* presumably as a result of TCR signaling, some, almost exclusively CD25^{+}Foxp3^{-} CD4SPs, express *Bcl2l11*. These results indicate that CD25^{+}Foxp3^{-} CD4SPs represent an interesting heterogenous population of cells with possibly non-mutually exclusive identities including apoptotic cells undergoing negative selection, IL-2 producers, and IL-2-sensitive immediate precursors of Treg cells. Although it is unclear whether the fate choice of these cells leading to drastically different terminal outcomes has been made at this point, one can imagine the possibility that intrinsic variation in TCR signaling, which at different strengths leads to IL-2 production, CD25 upregulation, and negative selection, and access to IL-2 could favor *Foxp3* induction, negative selection evasion, or apoptosis. Taken together, thymic IL-2 required for tTreg cell generation is produced by cells undergoing negative selection, which serves as a niche factor to scale the Treg cell compartment based on the number of apoptotic autoreactive cells (76).

Due to its pleiotropic function, it was unclear how IL-2 promote tTreg cell generation (87). As a major T cell survival cytokine, it can antagonize apoptosis so

that cells can withstand the elevated TCR signaling required for Foxp3 induction (88). Alternatively, it may directly act on the *Foxp3* locus and promote its transcription (71, 73). Lastly, it can serve as a T cell growth factor to expand a small number of newly generated tTreg cells (81). This question remained unresolved largely because the binding site for STAT5, the TF activated by IL-2, had not been found at the *Foxp3* locus in Treg cell precursors. Whereas binding of STAT5 can be detected at the CNS2 enhancer of *Foxp3* in *ex vivo* IL-2 stimulated Treg cells, it is neither accessible nor demethylated before Treg cell development has finished, hence unlikely to be responsible for IL-2 induced *Foxp3* induction (71). It was not until recently that a region located roughly 8.5 kb upstream of the promoter and in the intron of the *Ppp1r3f* gene, termed CNS0, was identified as the IL-2—STAT5 response element during tTreg cell development (73, 74).

CNS0 was first noticed as an open chromatin region and the binding site for Satb1 and the histone H3K4 monomethyltransferase MLL4 in Treg cells (89, 90). Germline ablation of CNS0 or Treg cell-specific deletion of Satb1 disrupts the chromatin landscape and modifications at the *Foxp3* locus, but how the activity of CNS0 is regulated by Treg cell-inducing signals was elusive (89, 90). Recently, two well-conserved STAT5 motifs were discovered within CNS0, and STAT5 binding was confirmed with ChIP-seq experiments performed on *ex vivo* IL-2 stimulated naturally occurring Treg (nTreg) cells isolated from secondary lymphoid organs and *in vitro* induced Treg (iTreg) cells generated by treating naïve Tconv cells with α-CD3/28, IL-2 and TGF-β (73). In contrast, STAT5 occupancy at CNS2

was only detected in nTreg but not iTreg cells, as it is not demethylated or accessible in the latter (71, 73). Like CNS3, CNS0 is accessible and primed prior to *Foxp3* induction, with accessibility and H3K4me1 modification first detected in CD4SPs and then increased in naïve Tconv and Treg cells (73). Deletion of CNS0 caused H3K4me1 signal to decrease at the promoter but not CNS3 and vice versa, suggesting that CNS0 and CNS3 deposit H3K4me1 at the promoter independently (73).

Implication of CNS0 in IL-2 responsiveness during tTreg cell development was further elucidated with functional and genetic experiments. While *Foxp3* induction in WT $CD25^{+}Foxp3^{-}$ CD4SPs become more efficient as IL-2 concentration increases, $CNS0^{KO}$ cells are irresponsive to IL-2 titration. As a result, $CNS0^{KO}$ mice have diminished Treg cell compartment in both the thymus and the spleen and a concomitant expanded thymic $CD25^{+}Foxp3^{-}$ CD4SP population (73, 74). The Treg cell defect is most conspicuous in neonates but compensated for as the animals age through increased proliferation of CNS0-deficient Treg cells upon exposure to excess IL-2 in the periphery. The TCR repertoire of $CNS0^{KO}$ Treg cells is less diverse and consist of fewer unique clones, suggesting that TCR and IL-2 signaling collectively contribute to the regulation of *Foxp3* induction. $CNS0^{KO}$ Treg cells display a more activated phenotype and gene expression signature, and ATAC-seq experiments reveal that their chromatin landscape is shaped by stronger TCR signaling, indicating that precursor cells expressing relatively weaker TCR fail to differentiate into Treg cells with an IL-2 irresponsive *Foxp3* locus. Despite reduced Treg cell numbers, $CNS0^{KO}$ mice are generally healthy and only

have mild peripheral T cell activation. When the Treg cell TCR repertoire is further narrowed by deleting *Aire*, however, CNS0^{KO}*Aire*$^{-/-}$ mice manifest more pronounced T cell activation and tissue immunopathology not seen in either single KO (73). In conclusion, by directly responding to IL-2—STAT5 signaling during *Foxp3* induction and priming the promoter, CNS0 promotes Treg cell lineage commitment for precursors expressing weaker TCR, thus further broaden the coverage of Treg cell-mediated tolerance on top of CNS3.

Generation of Treg cells in the periphery

It has been long appreciated that Treg cells can be generated in the periphery through conversion from naïve Tconv cells, in addition to thymic origin. Naïve DO11.10 transgenic T cells can differentiate into peripheral Treg (pTreg) cells upon intravenous OVA injection, but concomitant LPS treatment abolishes this conversion (91-93). It is thought that antigenic specificity promoting tTreg and pTreg cell generation follows a dichotomy: tTreg cells are reactive to self antigens, while pTreg cells develop at barrier sites in response to environmental antigens including allergens, dietary proteins, and the microbiota (57, 59, 63, 94-97). In support of this notion, Treg cells derived from naïve transgenic T cells are detected in the mesenteric lymph nodes upon oral delivery of the cognate dietary antigen OVA or the commensal species *Helicobacter hepaticus*, respectively (93, 98, 99). However, exceptions to the dichotomy are possible in theory. The recent discovery of enteric DCs migrating to and presenting antigens in the thymus provides the theoretical basis for thymic generation of microbiota-reactive Treg cells (100). In addition, it is likely that some autoreactive Tconv cells can differentiate into Treg

cells upon recognition of self peptide presented by APCs that specialized in presenting mucosal antigens. Markers for identifying tTreg (Helios, Nrp-1) and pTreg (RORγt) cells have been proposed, but their utility is limited because expression of these markers are correlational and can vary due to cellular activation, tissue microenvironment, and presence of microbiota (98, 101-103). Whether tTreg and pTreg cells represent separate lineages with distinct function and phenotype requires further investigating using novel strategies, including complex genetic models, lineage-tracing approaches, and single-cell multi-omic techniques. In Chapter Three, we will describe a novel mouse model we developed that allows for specific ablation of pTreg cells and the resulting biological sequela.

The importance of TCR specificity in pTreg cell generation is illustrated by studies using TCR transgenic mice, but tolerogenic cytokines, including TGF-β and retinoic acid (RA), enable pTreg cell differentiation over a wide range of TCR signaling strength (104-109). TGF-β was first shown to support pTreg development with an *in vitro* assay that mimics the *in vivo* process. Naïve Tconv cells upregulate Foxp3 in 24–48 h when stimulated with α-CD3/28, TGF-β, and IL-2, which is further boosted with RA (104, 110, 111). The resulting iTreg cells possess suppressive function but are different from nTreg cells in that their Foxp3 expression is unable and is gradually lost upon division (69, 71). In the small and large intestine, TGF-β produced by stromal cells promotes two alternative cell fates in Tconv cells upon activation, depending on the presence of other APC-derived cytokines: IL-6, IL-21, and IL-23 support Th17 cell polarization, while RA facilitates pTreg cell generation (105-109, 112-114). TGF-β also regulates Tconv cell fate choice in a quantitative

manner: high concentration of TGF-β inhibits IL-23 receptor expression, thus favoring pTreg cells (115).

CNS1 is the *Foxp3* enhancer responsive to signals promoting pTreg cells development. Located with the first intron, CNS1 contains conserved binding sites for Smad3 and RAR/RXR, the TF and nuclear receptor activated by TGF-β and RA, respectively, as well as NFAT, a known component of the TGF-β-induced *Foxp3* enhanceosome (69, 116, 117). $CNS1^{KO}$ Tconv cells are less efficient at expressing Foxp3 in *in vitro* induction assays and are not sensitive to RA titration (70). In contrast, decreasing TGF-β concentration reduces the induction efficiency for both $CNS1^{WT}$ and $CNS1^{KO}$ cells because of CNS1-independent mechanisms of TGF-β signaling-induced pTreg cells differentiation (70). Such mechanisms include promoting the survival and fitness of Treg or precursor cells and antagonizing Dnmt1 activity which silences *Foxp3* through maintenance DNA methylation (118). While dispensable for tTreg development, CNS1 is required for optimal peripheral induction, as $CNS1^{KO}$ OTII cells failed to become Treg cells upon oral gavage with OVA (70).

A pivotal function of pTreg cells is to prevent pathological immunity towards the microbiota (23). SPF CNS1-deficient mice have diminished Treg cell compartment in the small and large intestine lamina propria (70, 119). Although dependent most likely on the exact composition of the commensal flora, the extent of the *in vivo* defect is less severe than *in vitro*, suggesting compensatory mechanisms such as enhanced proliferation. The compromised pTreg cell generation leads to mastocytosis, goblet cell activation, and elevated production

of type 2 cytokines by T cells and innate lymphoid cells (ILCs) upon exposure to microbiota, which in turn perturbs the colonization of border-dwelling species in the large intestine, notably *Mucispirillum schaedleri* (119). Changes in the commensal flora then cause decreased richness of bacterial metabolic pathways and disrupted metabolite profile in the host, rending $CNS1^{KO}$ mice to weigh less despite normal food intake (119). At 12 months, $CNS1^{KO}$ mice spontaneously develop type 2 inflammation in the gut and asthma-like pathology in the airway, consistent with the heightened type 2 immunity during early life (70). Therefore, by restraining immunity against border-dwelling species, CNS1-dependent pTreg cells ensure microbial diversity and metabolic fitness of the host.

The interaction between pTreg cells and commensal flora is bi-directional, with microbiota-derived metabolites modulating pTreg cell differentiation. Fecal slurry from SPF but not antibiotic-treated or germ-free mice increase Treg cell induction efficiency in a DC–Tconv cell co-culture (120). Germ-free feces is depleted of short-chain fatty acids including butyrate and propionate, produced during microbial fermentation of starch, which promote pTreg cell generation both *in vitro* and systemically in abiotic mice in a CNS1-dependent manner. By functioning as a histone deacetylase inhibitor, butyrate facilitates pTreg cell induction by both acting in DC and T cells: on the one hand, it decreases DC activation and proinflammatory cytokine (IL-12, IL-6) production; on the other hand, it enhances priming of *Foxp3 cis*-regulatory elements and Foxp3 protein stability by increasing acetylation of histone at the *Foxp3* locus and Foxp3 itself,

respectively (120). In contrast, acetate and propionate promote colonic Treg cell proliferation and accumulation by binding to their receptor, Gpr43 (121).

Apart from fermenting dietary molecules, the gut microbiota also generates immunoactive agents by metabolizing host-derived molecules. Bile acids, which are produced in the liver and deconjugated and modified extensively by commensal species to give rise to secondary bile acids, are a class of such substances (122). Recently, three groups identified various bile acid regimens that promote Treg cell homeostasis *in vitro* and in the colonic lamina propria, and proposed three vastly different molecular mechanisms (123-125). By screening multiple primary and secondary bile acids on a DC–T cell co-culture, we discovered that 3β-hydroxydeoxycholic acid (isoDCA) and ω-muricholic acid enhanced Treg cell induction (123). We further pursued isoDCA due to its better understood biosynthesis, and demonstrated that it functioned by inhibiting Farnesoid X receptor activity in DCs, with no effect on a T cell-only culture. The biosynthetic pathway of isoDCA can be reconstructed by combining *Clostridium scindens* and an engineered *Bacteroides thetaiotaomicron*. When given to germ-free WT but not CNS1^{KO} mice, the two-bug cocktail increased RORγt^{+} Treg cells in the colon that are enriched for microbiota-dependent pTreg cells (123). In another study, Hang and colleagues showed that isoallolithocholic acid (isoalloLCA) promoted Treg cell differentiation in T cell polarization assays and in the colon when fed to mice (125). Surprisingly, isoalloLCS seemed to favor Treg cell induction by stimulating the production of mitochondrial reactive oxygen species and required CNS3 to take action. Lastly, Song et al. demonstrated that a

concoction of three primary or eight secondary bile acids could increase the proportion of colonic Treg cells expressing RORγt in mice feeding on a minimal diet and provide protection in a DSS colitis model (124). This effect was dependent on the ability of commensals to deconjugate primary bile acids and vitamin D receptor expression in Treg cells. Together, bile acids represent a biochemically and functionally complex class of molecules possessing immunomodulating activities, with a diverse range of mechanisms of action likely dependent on concentration, microbial composition, and expression pattern of host factors (123-125).

In conclusion, pTreg cells and microbiota have established a mutually beneficial relationship, with the former maintaining immune tolerance towards the commensal flora as well as environmental antigens and microbial metabolites favoring pTreg cell induction of homeostasis. Disrupted pTreg cell generation in the gut, skin, and placenta has been shown be implicated in multiple disorders, including inflammatory bowel disease, atopy, psoriasis, and miscarriage during allogenic pregnancy (126-129).

Synergistic regulation of Foxp3 expression and its maintenance by enhancers

Many biochemical and functional features are shared among Foxp3 enhancers. For example, both CNS0 and CNS3 are implicated in tTreg cell development and contribute to promoter H3K4 monomethylation (73, 74). Besides, STAT5 occupancy is detected at CNS0 and CNS2 in IL-2 stimulated Treg cells (71, 73). Lastly, CNS1, CNS2, and CNS3 are all binding sites of TCR-activated TFs (47, 51, 69). Therefore, it is possible that these enhancers regulate *Foxp3*

transcription in a combinatorial fashion and compensate for the loss of one another. Indeed, both CNS0/3 and CNS0/2 double KO (DKO) mice are lethal due to compounded exacerbation of Treg cell defect compared to the respective single KO's (74, 130). Treg cells are barely detected in CNS0/3 DKO mice in either the thymus or peripheral due to severely compromised tTreg cell generation, and their autoimmune phenotype is indistinguishable from that of *Foxp3*^{KO} mice(74). In contrast, tTreg cell frequency in CNS0/2 DKO mice is not worse than CNS0^{KO} mice. While CNS0 is not required for Foxp3 expression maintenance in the presence of CNS2, loss of Foxp3 protein is more pronounced when CNS0 is deletion in CNS2-deficient nTreg cells or CNS2-inactive iTreg cells (130). Ascorbate treatment, an activator of TET enzymes, rescues the unstable Foxp3 expression in CNS0-deficient CNS2-replete iTreg cells (73, 131, 132). The *Foxp3* locus in CNS0/2 DKO mice, however, cannot respond to IL-2 signaling and hence is incapable of sustaining its own transcription, causing mice to succumb to autoimmunity within 5 months (130). In addition to Treg cell stability and tTreg cell generation, *Foxp3* enhancers, specifically CNS1 and CNS0, also synergize to regulate pTreg cell induction, which we will discuss in Chapter Three.

CHAPTER TWO:

Regulatory T cells function in established systemic inflammation and reverse fatal autoimmunity*

*Published as: Hu W, Wang ZM, Feng Y, Schizas M, Hoyos BE, van der Veeken J, Verter JG, Bou-Puerto R, Rudensky AY. Regulatory T cells function in established systemic inflammation and reverse fatal autoimmunity. Nature Immunology. 2021 Sep;22(9):1163-74.

Introduction

Regulatory T (Treg) cells expressing the X-linked transcription factor Foxp3 have been implicated in the control of inflammation in diverse settings (15-17, 19, 133-137). Mice and humans lacking functional *Foxp3* gene develop fatal multi-organ autoimmune and inflammatory disease featuring lymphadenopathy and splenomegaly, eosinophilia, hyper IgE syndrome, and markedly increased systemic levels of a wide range of pro-inflammatory cytokines (133-135). Foxp3 protein expression is required for Treg cell differentiation and function (15-17, 19). Analyses of mice harboring a *Foxp3*^{GFPKO} reporter-null allele showed that Foxp3-deficient GFP^{+} Treg "wannabes" lack suppressor capacity, which can be restored by expression of a *Foxp3* transgene (136-138). Foxp3-deficient mice display autoimmune pathology by day 10 of life with most mice dying within 3-4 weeks (17, 22, 139). Likewise, Treg cell ablation induced upon diphtheria toxin (DT) treatment of healthy adult *Foxp3*$^{DTR-GFP}$ mice, whose endogenous *Foxp3* locus encodes a simian DT receptor (DTR)-GFP fusion protein, leads to similar widespread autoimmune inflammation to which they succumb within 2 weeks (22). Adoptive transfer of wild-type Treg cells into *Foxp3*$^{DTR-GFP}$ mice at the time of DT administration or into 1-day-old *Foxp3* mutant mice prevents the disease (17, 22). These studies have unequivocally demonstrated a critical role of Treg cells in preventing autoimmune inflammation and associated pathologies.

However, a major outstanding issue is whether Treg cells can effectively function in settings of established systemic inflammation and reverse and restrain severe autoimmune diseases. In fact, a large body of work in experimental animal

models of infection, inflammation, and cancer suggests that major immune effector cytokines, including IL-6, IL-1, type I and II IFNs, IL-23, and IL-4, can cause Treg cells to lose Foxp3 expression, become functionally inactivated, and acquire pro-inflammatory features, or render immune effector cells refractory to Treg cell-mediated suppression (24, 26-30). Accordingly, numerous analyses of Treg cells present at inflammatory sites of autoimmune patients suggested their function was impaired (33-37). Additional uncertainty stems from the possibility that the three archetypal inflammatory immune responses (types 1, 2, and 3), featuring distinct spectra of secreted and cellular effectors, may differ in their ability to compromise Treg cell functionality or sensitivity to Treg cell-mediated suppression. In this regard, variation in Treg cell frequencies was reported to result in a disproportionate dysregulation of type 2 vs. type 1 autoimmunity (140). Thus, to address the major outstanding question above, we sought to employ an experimental animal model which would: 1) exhibit systemic mixed type 1, 2, and 3 autoimmunity and tissue inflammation; 2) enable temporal control and efficient switching of Treg cell suppressor function in an established disease; 3) eschew adoptive Treg cell transfer, which does not guarantee their sufficient migration to and accumulation at the inflammatory sites; and 4) allow for extended longitudinal observation.

We reason that the cardinal features of the aforementioned archetypal inflammatory responses are shared by a broad spectrum of autoimmune and inflammatory diseases. The breadth and severity of the autoimmune inflammation resulting from Foxp3 deficiency, characterized by activation and expansion of all

major adaptive and innate immune cell types and rampant cytokine storm, make it an ideal experimental setting for testing the ability of Treg cells to operate in established inflammation. By engineering mice where an inducible Cre recombinase allowed for the installation of Treg cells in severely diseased animals, we found that Treg cells were functional in settings of established systemic mixed-type inflammation and capable of restoring health. Upon sensing the inflammatory environment, Treg cells became activated, rapidly expanded, exhibited heightened suppressive capacity, and persisted for an extended period of time with no signs of dysfunction.

Restoration of Foxp3 expression in Treg "wannabes"

To investigate the ability of Treg cells to function in settings of established severe inflammation, we generated mice harboring a reversible *Foxp3* $^{\text{loxP-Thy1.1-STOP-loxP-GFP}}$ reporter-null allele (*Foxp3*^{LSL}). In these mice, a loxP site-flanked Thy1.1 reporter followed by a STOP cassette was inserted into the *Foxp3* locus upstream of the *Foxp3*^{GFP} reporter allele with Thy1.1 expression marking a population of Treg "wannabes" (Fig. 2.1, Fig. 2.2a-c). These cells were phenotypically similar to those expressing the *Foxp3*^{GFPKO} allele, and distinct from either naïve or activated conventional CD4 T cells, or Foxp3-sufficient Treg cells (Fig. 2.2d). To ascertain that Treg "wannabes" bare a similarly self-reactive TCR repertoire as Treg cells, we assessed their TCR Vβ5 usage. C57BL/6 mice express viral superantigens vSAG8 and vSAG9, whose recognition by Vβ5 utilizing TCRs leads to partial deletion of Vβ5^{+} conventional CD4 T cells and promotes the generation of Vβ5^{+} Treg cells (141-143). We observed that Treg and "wannabe" cells showed

comparably elevated Vβ5 usage relative to conventional CD4 T cells. This result suggests Treg and “wannabe” cells were similarly “self-focused” and that lack of Foxp3 did not result in shifted self-reactivity of the TCR repertoire of Treg “wannabes” (Fig. 2.2e). Combining *Foxp3*^{LSL} allele with *Cd4*^{creERT2} allele encoding a tamoxifen-activatable Cre-ERT2 fusion protein enabled excision of the STOP cassette upon 4-hydroxytamoxifen (4-OHT) treatment and conversion of Foxp3-deficient Thy1.1^{+} “wannabes” into Foxp3-sufficient GFP^{+} Treg cells (Fig. 2.3a-b). The latter, when co-transferred with Foxp3^{-} CD4 T cells into lymphopenic recipients, suppressed the wasting disease similar to those isolated from control *Foxp3*^{GFP} mice (Fig. 2.3c). Thus, rescued expression of endogenous Foxp3 in Treg “wannabes” conferred suppressor function and fitness in accordance with previous findings.

Figure 2.1 Generation and characterization of *Foxp3*^{LSL} mice.
Schematics of the targeting construct and the *Foxp3*^{LSL} allele before and after Flp recombinase-mediated removal of the neo cassette. Homologous regions between the targeting construct and the WT allele are demarcated with dashed gray lines. Gene map is based on RefSeq record NM_001199347.1. pA, bovine growth hormone polyadenylation signal; neo, neomycin resistance gene; PGK, mouse phosphoglycerate kinase 1 promoter; 3xSV40pA, triple-tandem SV40 early polyadenylation signals (STOP cassette); DTA, diphtheria toxin A.

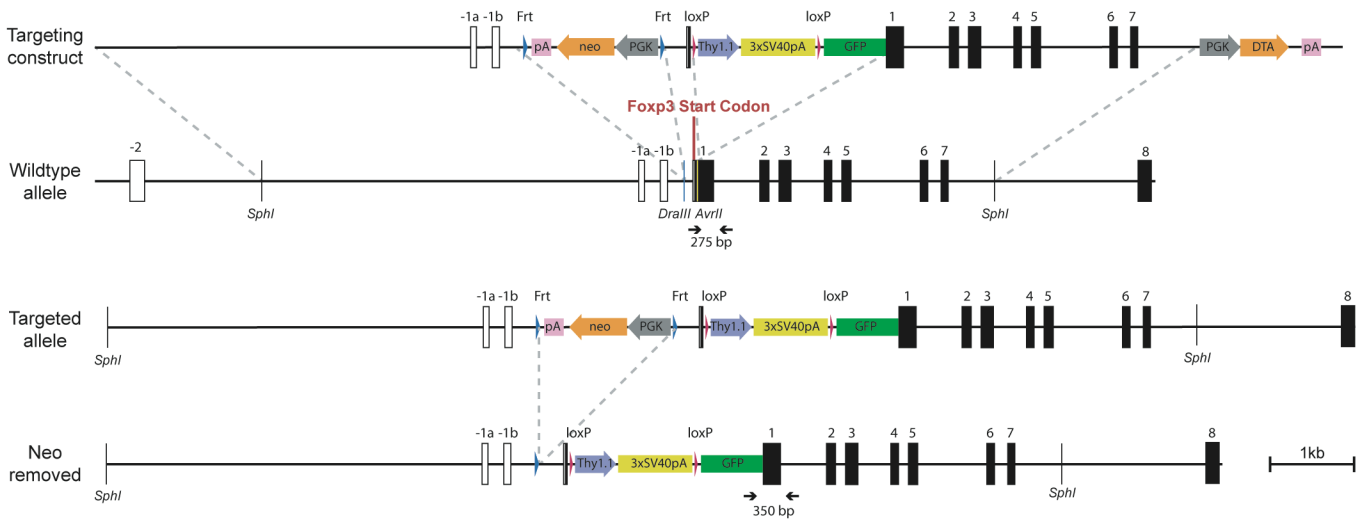
Targeting construct
-1a -1b
Frt
pA
neo
PGK
Frt
loxP
Thy1.1
3xSV40pA
loxP
GFP
1
2 3
4 5
6 7
PGK
DTA
pA
Foxp3 Start Codon
Wildtype allele
-2
SphI
-1a -1b
1
2 3
4 5
6 7
8
DraIII AvrII
275 bp
SphI
Targeted allele
-1a -1b
Frt
pA
neo
PGK
Frt
loxP
Thy1.1
3xSV40pA
loxP
GFP
1
2 3
4 5
6 7
8
SphI
SphI
Neo removed
-1a -1b
loxP
Thy1.1
3xSV40pA
loxP
GFP
1
2 3
4 5
6 7
8
1kb
SphI
350 bp
SphI

Figure 2.2 Related to Figure 2.1.

a, Genotyping PCR showing the WT (275 bp) and knock-in-specific (350 bp) bands using primers labeled in Fig. 2.1.

b, c, Flow cytometric analysis of T cells and TCRβ^{hi} single positive thymocytes from 3-wk-old male *Foxp3*$^{LSL/y}$ (c) and 8-10-wk-old female *Foxp3*$^{LSL/WT}$ (d) mice. LN, lymph nodes.

d, Expression of molecules associated with T cell activation in splenic Foxp3^{+} Treg and Thy1.1^{+} Treg "wannabes", and naïve (CD44^{lo}CD62L^{hi}) and activated (CD44^{hi}CD62L^{lo}) conventional CD4 T cells shown in d.

e, Percentages of TCRVβ5^{+}, Vβ6^{+} and Vβ8^{+} cells among the indicated splenic CD4 T cell populations from 8-10-wk-old female *Foxp3*$^{LSL/DTR-GFP}$ mice. Cells are gated on the CD44^{lo}CD62L^{hi} subset to avoid potential clonal expansion during activation. One way ANOVA.

All error bars denote mean $\pm$ s.e.m. ns, non-significant; *, $p<0.05$; **, $p<0.01$; ***, $p<0.001$; ****, $p<0.0001$.

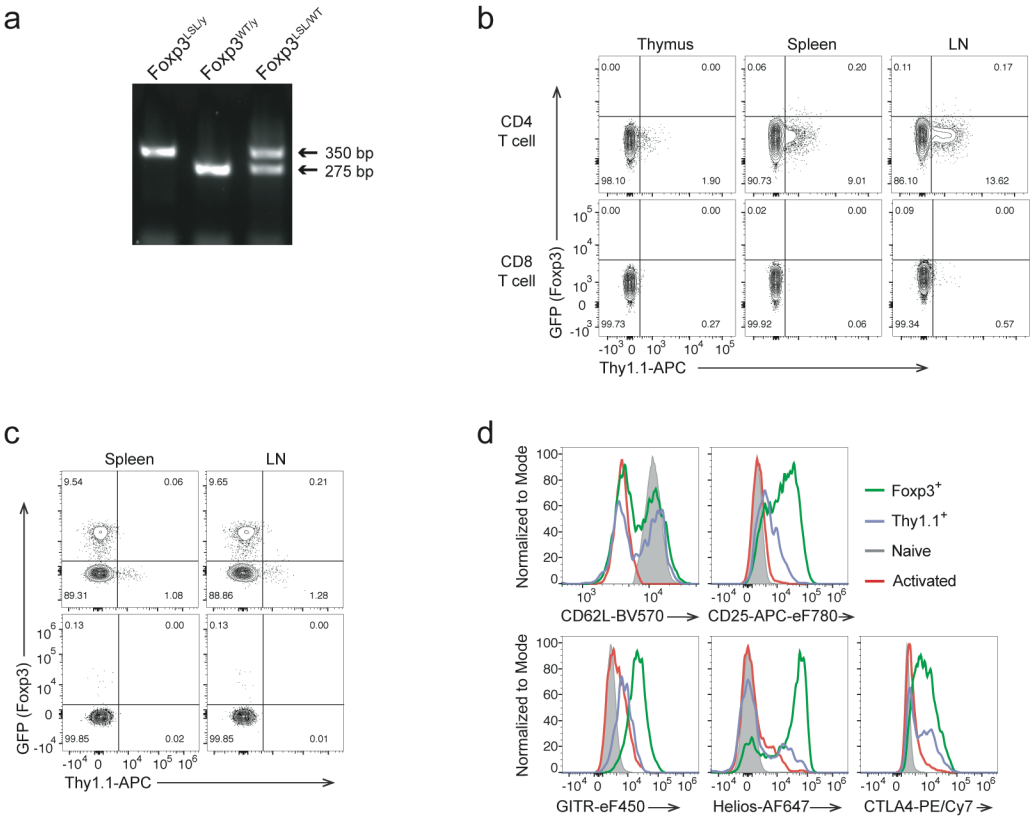
a
Foxp3LSL/y
Foxp3WT/y
Foxp3LSL/WT
350 bp
275 bp
b
Thymus
Spleen
LN
CD4 T cell
CD8 T cell
GFP (Foxp3)
Thy1.1-APC
c
Spleen
LN
GFP (Foxp3)
Thy1.1-APC
d
Normalized to Mode
CD62L-BV570
CD25-APC-eF780
GITR-eF450
Helios-AF647
CTLA4-PE/Cy7
Foxp3+
Thy1.1+
Naive
Activated
e
Vβ5+ (%CD62Lhi)
Vβ6+ (%CD62Lhi)
Vβ8+ (%CD62Lhi)
ns
****
*
**
Foxp3+
Thy1.1+
Foxp3−Thy1.1−

Figure 2.3 Related to Figure 2.1.

a, Schematic of the *Foxp3*^{LSL} allele.

b, Flow cytometric analysis of splenic CD4 T cells 1 week post 4-OHT treatment.

c, 2x10^6 CD45.1$^+$Foxp3$^–$ conventional CD4 T cells were co-transferred with 2x10^5 CD45.2$^+$ Treg "wannabes" from 2-3-wk-old *Foxp3*$^{LSL/y}$ mice or Treg cells from 6-8-wk-old *Foxp3*^{GFP} mice into *Tcrb*$^{–/–}$*Tcrd*$^{–/–}$ mice. Recipients were orally gavaged with tamoxifen and injected i.p. with diphtheria toxin (DT) at the indicated time points (top). DT was administered to deplete the few contaminating DTR-expressing Treg cells in the transferred FACS-purified conventional T cells or those induced to express Foxp3 after transfer. Cellularity and proliferation of CD45.1$^+$ responder cells from lymph nodes were analyzed using flow cytometry (bottom). Data are representative of two independent experiments.

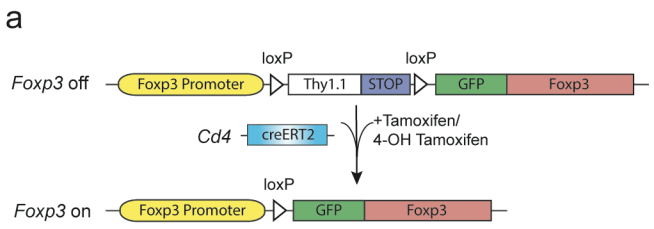
a
loxP
loxP
Foxp3 off
Foxp3 Promoter
Thy1.1
STOP
GFP
Foxp3
Cd4
creERT2
+Tamoxifen/
4-OH Tamoxifen
loxP
Foxp3 on
Foxp3 Promoter
GFP
Foxp3

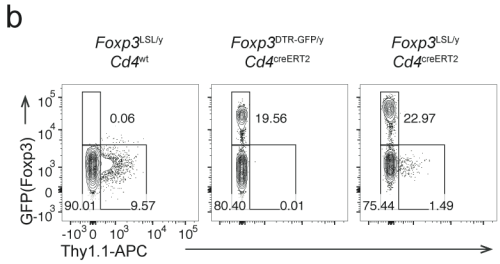
b
Foxp3LSL/y
Cd4wt
Foxp3DTR-GFP/y
Cd4creERT2
Foxp3LSL/y
Cd4creERT2
GFP(Foxp3)
0.06
90.01
9.57
19.56
80.40
0.01
22.97
75.44
1.49
Thy1.1-APC

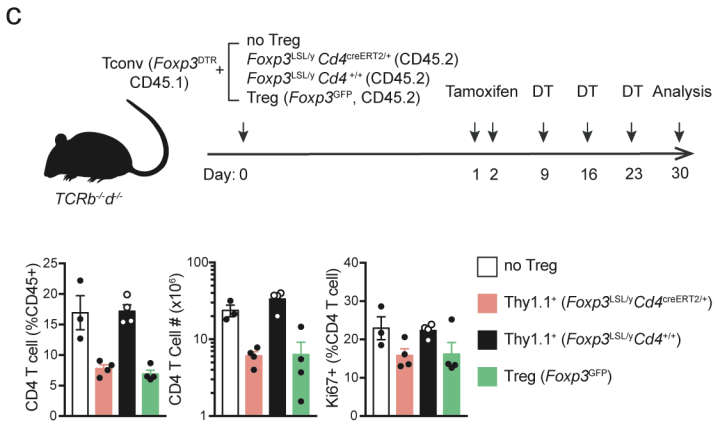
c
Tconv (Foxp3DTR
CD45.1)
+
no Treg
Foxp3LSL/y Cd4creERT2/+ (CD45.2)
Foxp3LSL/y Cd4+/+ (CD45.2)
Treg (Foxp3GFP, CD45.2)
Tamoxifen
DT
DT
DT
Analysis
TCRb-/-d-/-
Day: 0
1 2
9
16
23
30
CD4 T cell (%CD45+)
CD4 T Cell # (x10^6)
Ki67+ (%CD4 T cell)
no Treg
Thy1.1+ (Foxp3LSL/yCd4creERT2/+)
Thy1.1+ (Foxp3LSL/yCd4+/+)
Treg (Foxp3GFP)

Treg cells reverse established disease in young and adult mice

Hemizygous male *Foxp3*^{LSL} mice developed multi-organ autoimmune inflammation indistinguishable from that of Foxp3-deficient mice, to which they succumbed within 3-4 weeks with few surviving for up to 6 weeks after birth. To test whether Treg cells can suppress ongoing inflammation, male *Foxp3*^{LSL}*Cd4*^{creERT2} or *Foxp3*^{LSL}*Cd4*^{wt} mice were administered with a single dose of 4-OHT at 2 weeks of age, by which time they exhibited pronounced autoimmune syndrome with conspicuous clinical manifestations including blepharitis and macroscopic skin lesions. The recombination efficiency was comparable in lymphoid and non-lymphoid organs on day 3 following 4-OHT administration (Fig. 2.4a). Within 4 weeks, the disease in 4-OHT-treated *Foxp3*^{LSL}*Cd4*^{creERT2} mice was greatly alleviated with the extent of activation of innate and adaptive immune cells approaching the level of healthy *Foxp3*$^{DTR\text{-}GFP}$*Cd4*^{creERT2} controls. In contrast, the disease in 4-OHT-treated *Foxp3*^{LSL}*Cd4*^{wt} mice rapidly progressed with no mice surviving beyond 6 weeks of age (Fig. 2.4b-d; Fig. 2.5; Fig. 2.6).

Since the observed reversal of inflammation could be due to restoration of Foxp3 expression in thymocytes or peripheral Treg “wannabes”, we combined 4-OHT treatment with continuous FTY720-induced blockade of thymic output. Accordingly, we observed increased numbers of thymic Treg cells and the percentages of *Rosa26*$^{loxP\text{-}STOP\text{-}loxP\text{-}tdTomato}$ (*R26*^{Tom}) recombination reporter-expressing thymocytes labeled upon 4-OHT treatment (Fig. 2.7a-b). Diminished immune activation and inflammation in *Foxp3*^{LSL}*Cd4*^{creERT2} mice, compared to *Foxp3*^{LSL}*Cd4*^{wt} controls, on day 14 following combined 4-OHT and FTY720

treatment suggested that Treg cells rescued in the periphery were effective at controlling inflammation in the absence of thymic output (Fig. 2.7c-d). CD4 (Foxp3^{-} Thy1.1^{-}) and CD8 T cell activation was suppressed within a week after 4-OHT-induced restoration of Treg cell function, as evidenced by reduced expression of Ki67, CD44, CD25, IFNγ, and IL-4 (Fig. 2.4c; Fig. 2.6). Likewise, myelo-proliferation marked by expansion of neutrophils, monocytes, and eosinophils (Fig. 2.4d; Fig. 2.8a) and severe acute phase response reflected in high level of serum amyloid P (SAP) were ameliorated in rescued *Foxp3*^{LSL}*Cd4*^{creERT2} mice (Fig. 2.8b). In addition, levels of IgE, IgG1 and IgM were brought down by newly generated Treg cells in *Foxp3*^{LSL}*Cd4*^{creERT2} mice in comparison to control *Foxp3*^{LSL}*Cd4*^{wt} mice (Fig. 2.8c-d). Manifest tissue immune infiltration and inflammation disappeared in *Foxp3*^{LSL}*Cd4*^{creERT2} mice but not *Foxp3*^{LSL}*Cd4*^{wt} controls within 4 weeks of 4-OHT administration (Fig. 2.8 e-f). A closer examination of the skin pathology in pre-treatment *Foxp3*^{LSL}*Cd4*^{creERT2} and *Foxp3*^{LSL}*Cd4*^{wt} mice revealed lichenoid interface dermatitis, which was resolved in treated *Foxp3*^{LSL}*Cd4*^{creERT2} mice but continued to worsen in *Foxp3*^{LSL}*Cd4*^{wt} mice (Fig. 2.9a-b). Additionally, liver damage evident by apoptotic hepatocytes and decreased serum albumin concentrations in *Foxp3*^{LSL}*Cd4*^{creERT2} mice normalized within 4 weeks after 4-OHT treatment (Fig. 2.9c-e). The disease reversal was not a mere consequence of subtracting the Treg "wannabes" from the CD4 T cell pool, considering that the disease severity in Foxp3-deficient mice harboring Treg "wannabes" was identical to that of neonates subjected to chronic Treg cell ablation (22). Thus, Treg cells are capable of

effectively suppressing multiple arms of the inflammatory immune response in young mice under conditions of established autoimmunity, causing its reversal.

To assess whether Treg cells can restrain ongoing inflammation in adulthood, we generated healthy mosaic heterozygous female *Foxp3*$^{\text{DTR-GFP/LSL}}$*Cd4*$^{\text{creERT2}}$ mice, which harbor both a functional Treg and a non-functional "wannabe" population expressing the *Foxp3*$^{\text{DTR-GFP}}$ and *Foxp3*$^{\text{LSL}}$ allele, respectively. Recurrent DT administration causes widespread autoimmunity in *Foxp3*$^{\text{DTR-GFP}}$ mice to which they succumb within 10-14 days(22). Similarly, DT-treated adult (8-10-week-old) *Foxp3*$^{\text{DTR-GFP/LSL}}$ heterozygous females exhibited massive immune activation by day 7, at which point the diseased *Foxp3*$^{\text{DTR-GFP/LSL}}$*Cd4*$^{\text{creERT2}}$ and *Foxp3*$^{\text{DTR-GFP/LSL}}$*Cd4*$^{\text{wt}}$ mice were administered tamoxifen to convert Treg "wannabes" to Treg cells (Fig. 2.10a). The rehabilitated Treg cells efficiently suppressed T cell activation within 2 weeks and ameliorated the inflammatory lesions in the skin, lung, and liver by week 5, whereas in control *Foxp3*$^{\text{DTR-GFP/LSL}}$*Cd4*$^{\text{wt}}$ mice the fatal disease rapidly progressed (Fig. 2.10b; Fig. 2.11; Fig. 2.12). The 5 week endpoint was chosen as it was the longest period we were confident the mice were not developing neutralizing DT-specific antibodies. Thus, Treg cells can function under inflammatory settings and suppress established lethal autoimmunity in both neonates and adults.

Figure 2.4 Restoration of *Foxp3* expression in Treg "wannabes" cures fulminant autoimmunity in male *Foxp3*^{LSL} mice.

Mice were treated with 4-hydroxytamoxifen (4-OHT) on postnatal day 14.

a, 4-OHT mediated recombination efficiency in lymphoid and non-lymphoid organs. Experimental scheme (left) and recombination efficiency of *Rosa26*^{Tom} in Treg cells from indicated organs (right). One-way ANOVA.

b, Lymph nodes (top), spleens (middle), and thymi (bottom) of mice of indicated genotypes 4 weeks after 4-OHT treatment.

c,d, Percentages of activated, proliferating, and cytokine-producing splenic T cells (d) and frequencies of splenic myeloid cell populations (e) at indicated time points after 4-OHT treatment.

All error bars denote mean ± s.e.m. ns, non-significant; *, $p<0.05$; **, $p<0.01$; ***, $p<0.001$; ****, $p<0.0001$

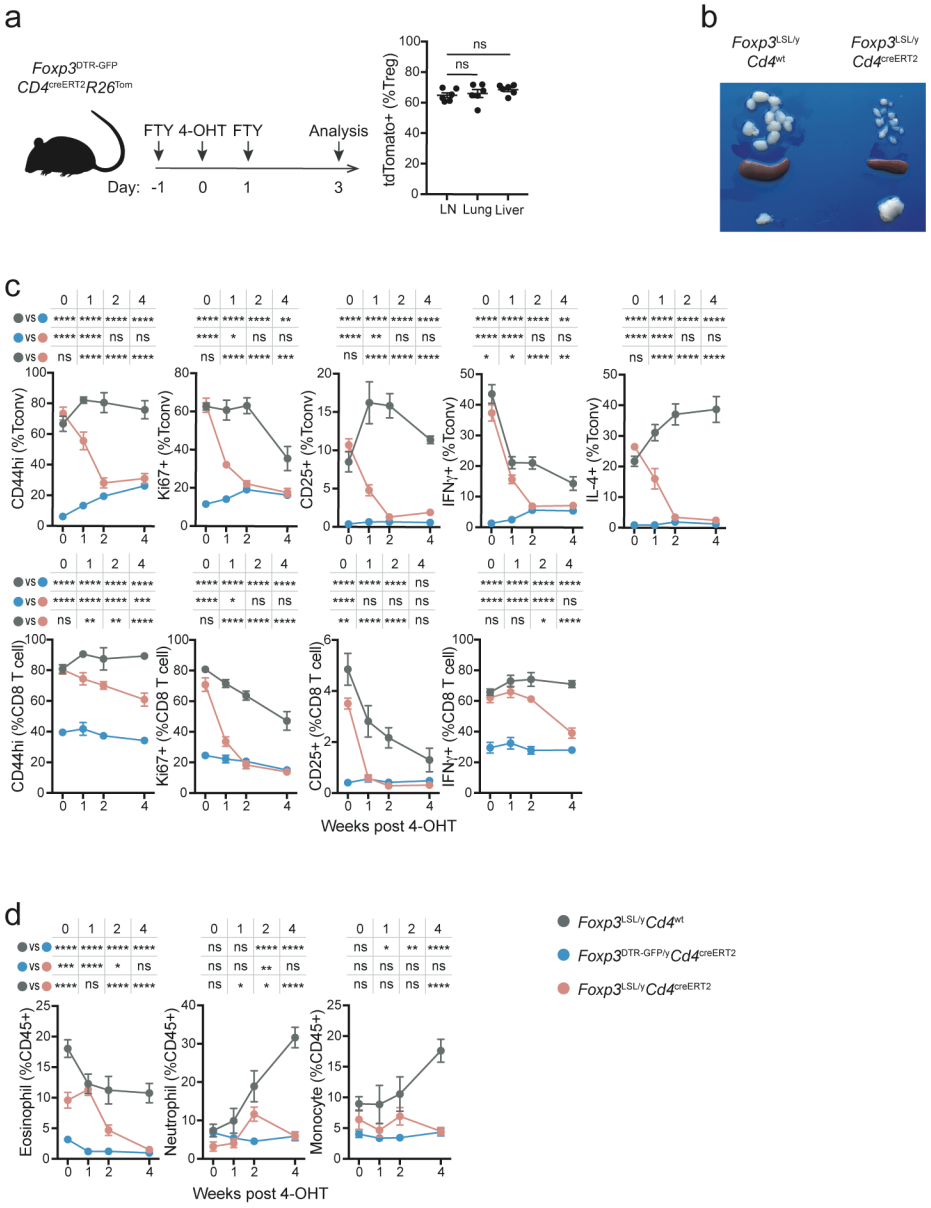
a
Foxp3DTR-GFP
CD4creERT2R26Tom
FTY 4-OHT FTY
Analysis
Day: -1 0 1 3
tdTomato+ (%Treg)
ns
LN Lung Liver
b
Foxp3LSL/y
Cd4wt
Foxp3LSL/y
Cd4creERT2
c
CD44hi (%Tconv)
Ki67+ (%Tconv)
CD25+ (%Tconv)
IFN-γ+ (%Tconv)
IL-4+ (%Tconv)
CD44hi (%CD8 T cell)
Ki67+ (%CD8 T cell)
CD25+ (%CD8 T cell)
IFN-γ+ (%CD8 T cell)
Weeks post 4-OHT
d
Eosinophil (%CD45+)
Neutrophil (%CD45+)
Monocyte (%CD45+)
Weeks post 4-OHT
Foxp3LSL/yCd4wt
Foxp3DTR-GFP/yCd4creERT2
Foxp3LSL/yCd4creERT2

Figure 2.5 Related to Figure 2.4.

Male *Foxp3*^{LSL} mice were treated with 4-OHT on postnatal day 14 and analyzed throughout the following 4 weeks.

a, Representative histograms showing expression of proliferation and activation markers by splenic conventional CD4 and CD8 T cells at the indicated time points.

b, Representative contour plots of flow cytometric analyses of activated and cytokine-producing splenic conventional CD4 and CD8 T cell populations.

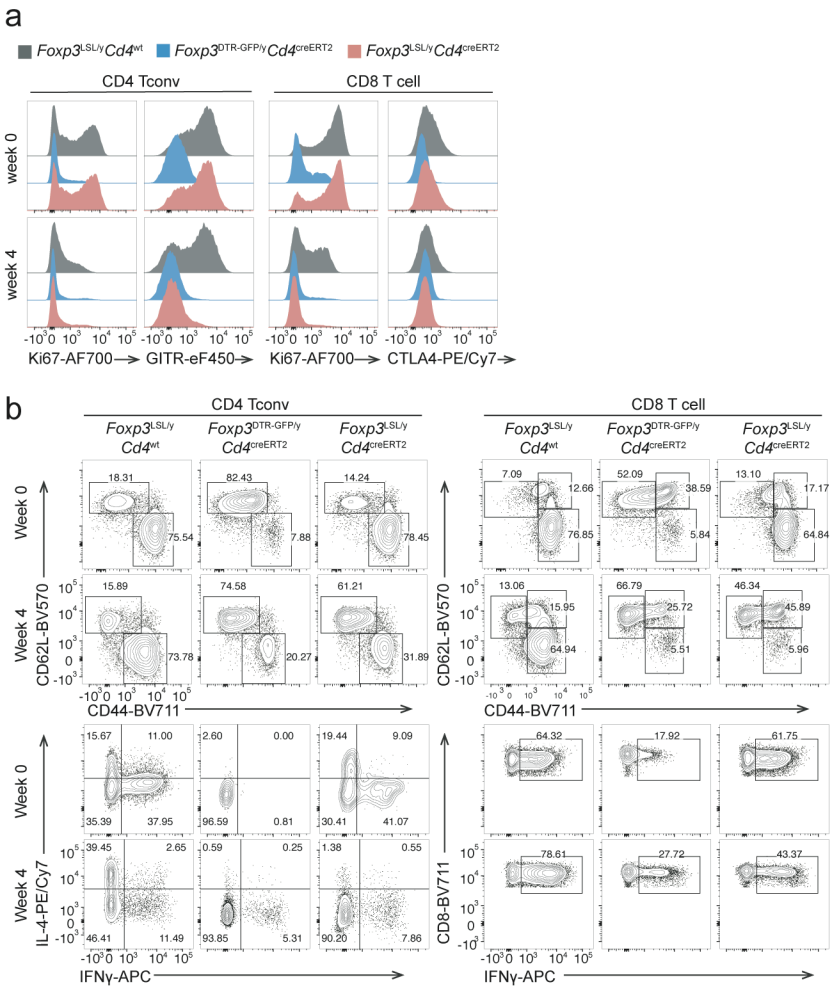
a
Foxp3LSL/yCd4wt
Foxp3DTR-GFP/yCd4creERT2
Foxp3LSL/yCd4creERT2
CD4 Tconv
CD8 T cell
week 0
week 4
Ki67-AF700
GITR-eF450
Ki67-AF700
CTLA4-PE/Cy7
b
CD4 Tconv
CD8 T cell
Foxp3LSL/y Cd4wt
Foxp3DTR-GFP/y Cd4creERT2
Foxp3LSL/y Cd4creERT2
Week 0
Week 4
CD62L-BV570
CD44-BV711
IL-4-PE/Cy7
IFNγ-APC
CD8-BV711
18.31
75.54
82.43
7.88
14.24
78.45
7.09
12.66
76.85
52.09
38.59
5.84
13.10
17.17
64.84
15.89
73.78
74.58
20.27
61.21
31.89
13.06
15.95
64.94
66.79
25.72
5.51
46.34
45.89
5.96
15.67
11.00
35.39
37.95
2.60
0.00
96.59
0.81
19.44
9.09
30.41
41.07
64.32
17.92
61.75
39.45
2.65
46.41
11.49
0.59
0.25
93.85
5.31
1.38
0.55
90.20
7.86
78.61
27.72
43.37

Figure 2.6 Related to Figure 2.4.

a, b, frequencies (a) and numbers (b) of activated, proliferating and cytokine-producing conventional CD4 and CD8 T cells from lymph nodes of mice of indicated genotypes at designated time points after 4-OHT treatment. Two-way ANOVA with Tukey's multiple comparison correction.

All error bars denote mean ± s.e.m. ns, non-significant; *, $p<0.05$; **, $p<0.01$; ***, $p<0.001$; ****, $p<0.0001$.

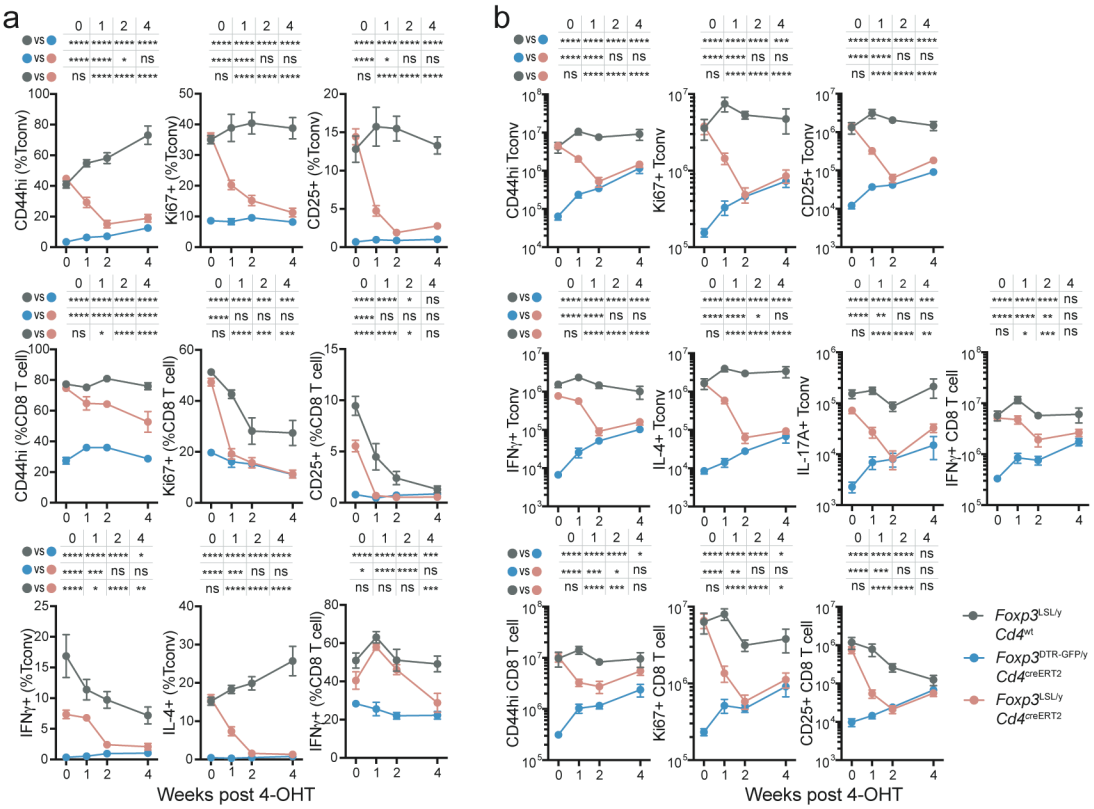
a
b
CD44hi (%Tconv)
Ki67+ (%Tconv)
CD25+ (%Tconv)
CD44hi (%CD8 T cell)
Ki67+ (%CD8 T cell)
CD25+ (%CD8 T cell)
IFNγ+ (%Tconv)
IL-4+ (%Tconv)
IFNγ+ (%CD8 T cell)
CD44hi Tconv
Ki67+ Tconv
CD25+ Tconv
IFNγ+ Tconv
IL-4+ Tconv
IL-17A+ Tconv
IFNγ+ CD8 T cell
CD44hi CD8 T cell
Ki67+ CD8 T cell
CD25+ CD8 T cell
Weeks post 4-OHT
Foxp3LSL/y Cd4wt
Foxp3DTR-GFP/y Cd4creERT2
Foxp3LSL/y Cd4creERT2

Figure 2.7 Restoration of *Foxp3* expression in peripheral Treg "wannabes" rescues immune activation in male *Foxp3*^{LSL} mice.

a, Experimental Design. 2-wk-old mice were treated with 4-hydroxytamoxifen (4-OHT) while being continuously treated with FTY720 to block thymic output. A *Rosa26*$^{loxP\text{-}STOP\text{-}loxP\text{-}td\text{Tomato}}$ (*R26*$^{\text{LSL-}td\text{Tomato}}$) recombination reporter allele was introduced to the mice to enable labeling of all CD4 T cells undergoing Cre-mediated recombination induced by 4-OHT.

b, Number of Treg cells in the thymus (left), and percentage of tdTomato^{+} cells among Foxp3^{-}Thy1.1^{-} CD4SP thymocytes (right), from FTY720-treated mice and untreated controls on day 14. Two-tailed unpaired *t*-tests with multiple hypothesis testing correction using the Holm-Sidak method.

c, d, Numbers of activated, proliferating, and cytokine-producing conventional CD4 and CD8 T cells in the spleen (c) and lymph nodes (d). One-way ANOVA with Tukey's multiple comparison test.

All error bars denote mean ± s.e.m. ns, non-significant; *, $p<0.05$; **, $p<0.01$; ***, $p<0.001$; ****, $p<0.0001$.

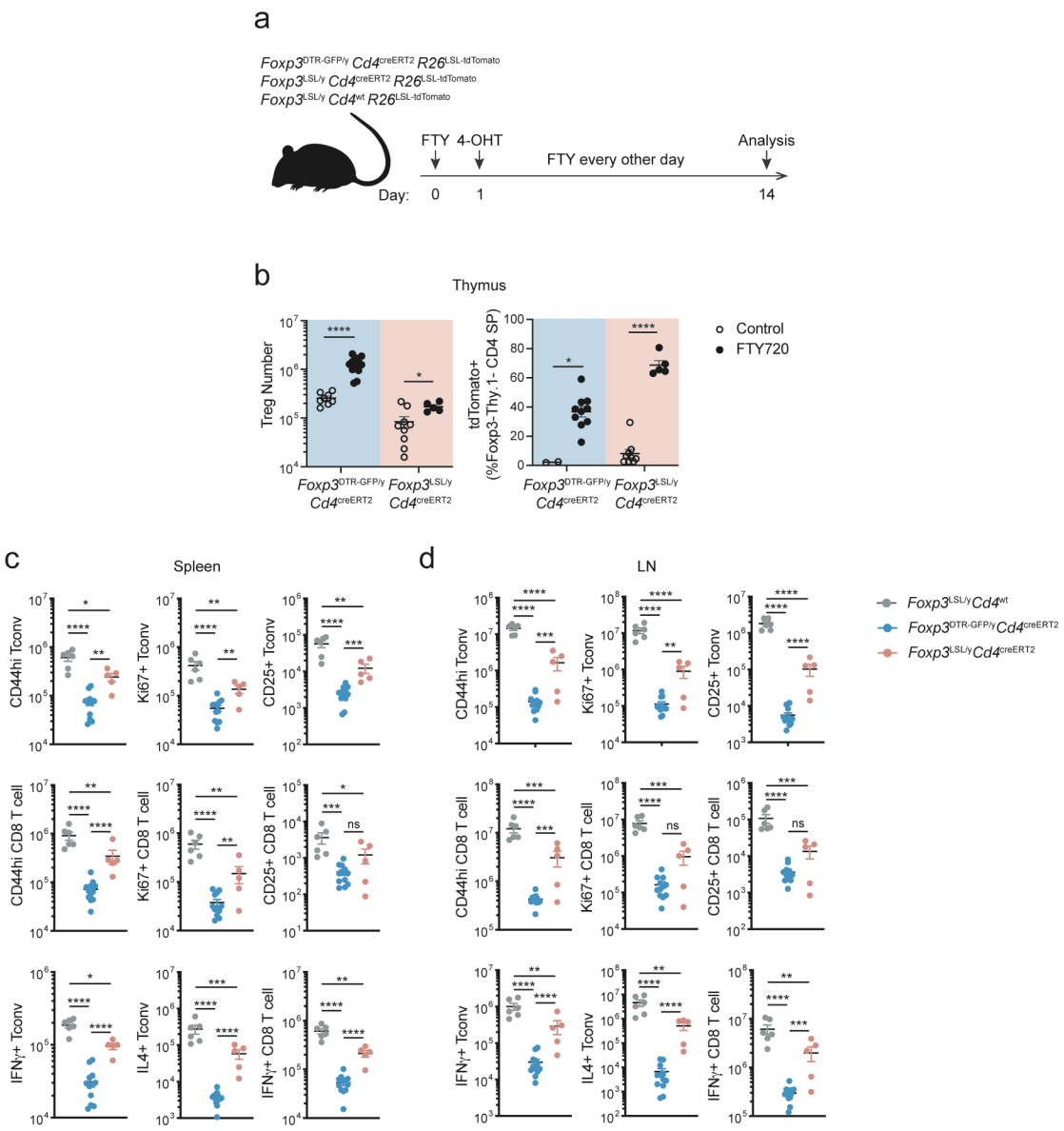
a
Foxp3DTR-GFP/y Cd4creERT2 R26LSL-tdTomato
Foxp3LSL/y Cd4creERT2 R26LSL-tdTomato
Foxp3LSL/y Cd4wt R26LSL-tdTomato
FTY
4-OHT
FTY every other day
Analysis
Day: 0 1 14
b
Thymus
Treg Number
tdTomato+ (%Foxp3-Thy.1- CD4 SP)
Control
FTY720
c
Spleen
CD44hi Tconv
Ki67+ Tconv
CD25+ Tconv
CD44hi CD8 T cell
Ki67+ CD8 T cell
CD25+ CD8 T cell
IFNγ+ Tconv
IL4+ Tconv
IFNγ+ CD8 T cell
d
LN
Foxp3LSL/yCd4wt
Foxp3DTR-GFP/yCd4creERT2
Foxp3LSL/yCd4creERT2

Figure 2.8 Related to Figure 2.4.

a, Numbers of splenic myeloid cell populations at indicated time points after 4-OHT treatment. Two-way ANOVA with Tukey's multiple comparison correction.

b, Serum amyloid P (SAP) levels (f) at indicated time points after 4-OHT treatment.

c, d, Levels of antibodies in the serum 4 weeks post-4-OHT treatment.

e, Haematoxylin and eosin staining of indicated tissues before and 4 weeks after 4-OHT treatment.

f, Histology scores of indicated tissues before and 4 weeks after 4-OHT treatment.

Two-way (a, b, f) or one-way (c, d) ANOVA with Tukey's multiple comparison test. All error bars denote mean ± s.e.m. ns, non-significant; *, $p<0.05$; **, $p<0.01$; ***, $p<0.001$; ****, $p<0.0001$.

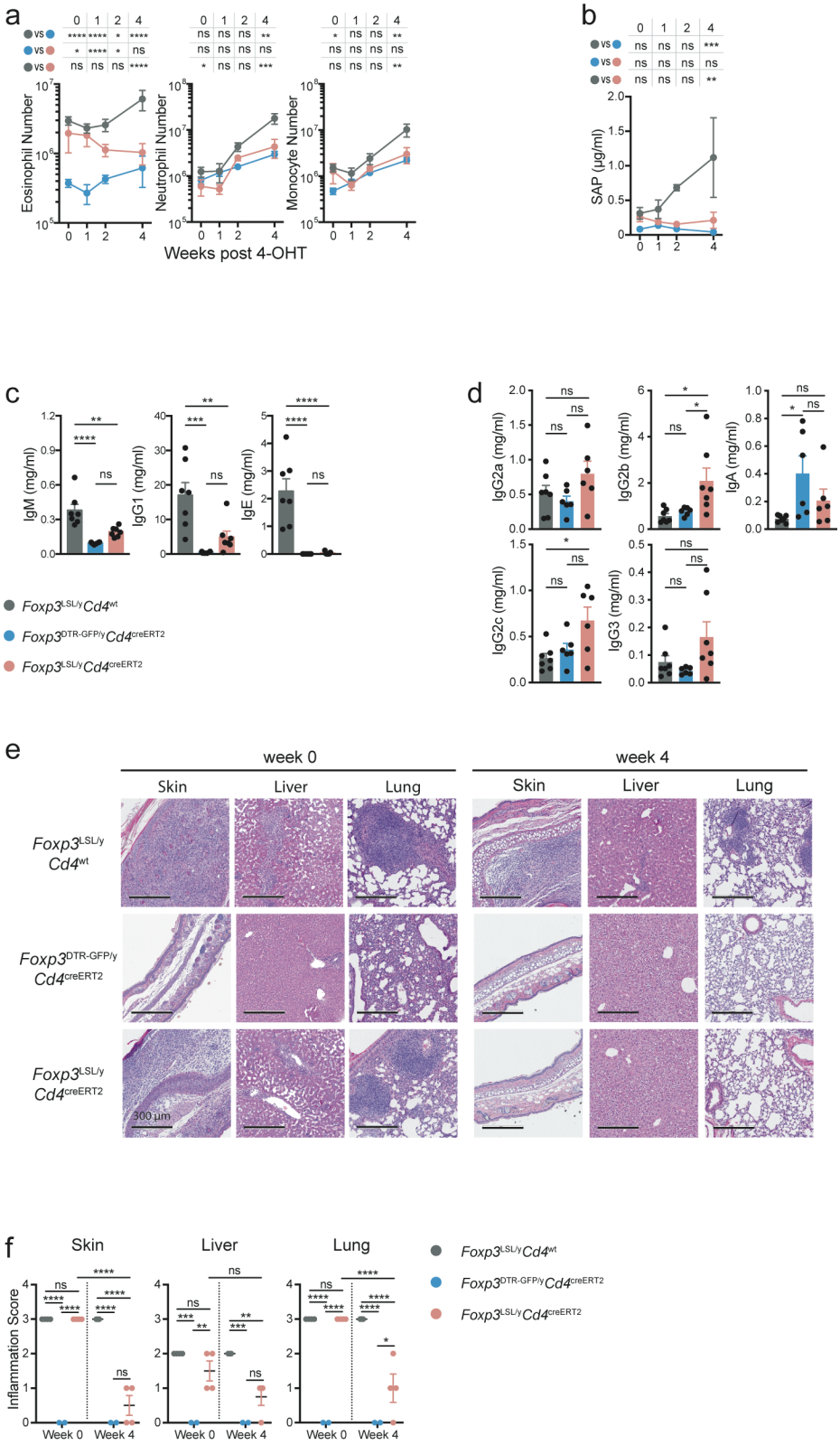
a
b
c
d
e
f
Eosinophil Number
Neutrophil Number
Monocyte Number
Weeks post 4-OHT
SAP (µg/ml)
IgM (mg/ml)
IgG1 (mg/ml)
IgE (mg/ml)
IgG2a (mg/ml)
IgG2b (mg/ml)
IgA (mg/ml)
IgG2c (mg/ml)
IgG3 (mg/ml)
Foxp3LSL/yCd4wt
Foxp3DTR-GFP/yCd4creERT2
Foxp3LSL/yCd4creERT2
week 0
week 4
Skin
Liver
Lung
300 µm
Inflammation Score
Week 0
Week 4

Figure 2.9 Restoration of *Foxp3* expression in Treg “wannabes” rescues tissue damage in the skin and liver of male *Foxp3*^{LSL} mice.

Mice were treated with 4-OHT on postnatal day 14 and examined at the indicated time points post-treatment.

a, b, H&E staining of skin sections showing epidermal hyperplasia and formation of serocellular crust (arrow heads). Dashed lines demarcate the boundary between epidermis and dermis.

c, TUNEL (terminal deoxynucleotidyl transferase dUTP nick end labeling) assay followed by immunohistochemistry to visualize apoptotic cells (arrow heads) in H&E counter-stained liver sections from mice of indicated genotypes.

d, Quantification of TUNEL^{+} cells. e, Measurement of serum albumin levels.

All error bars denote mean ± s.e.m. ns, non-significant; *, $p<0.05$; **, $p<0.01$; ***, $p<0.001$; ****, $p<0.0001$.

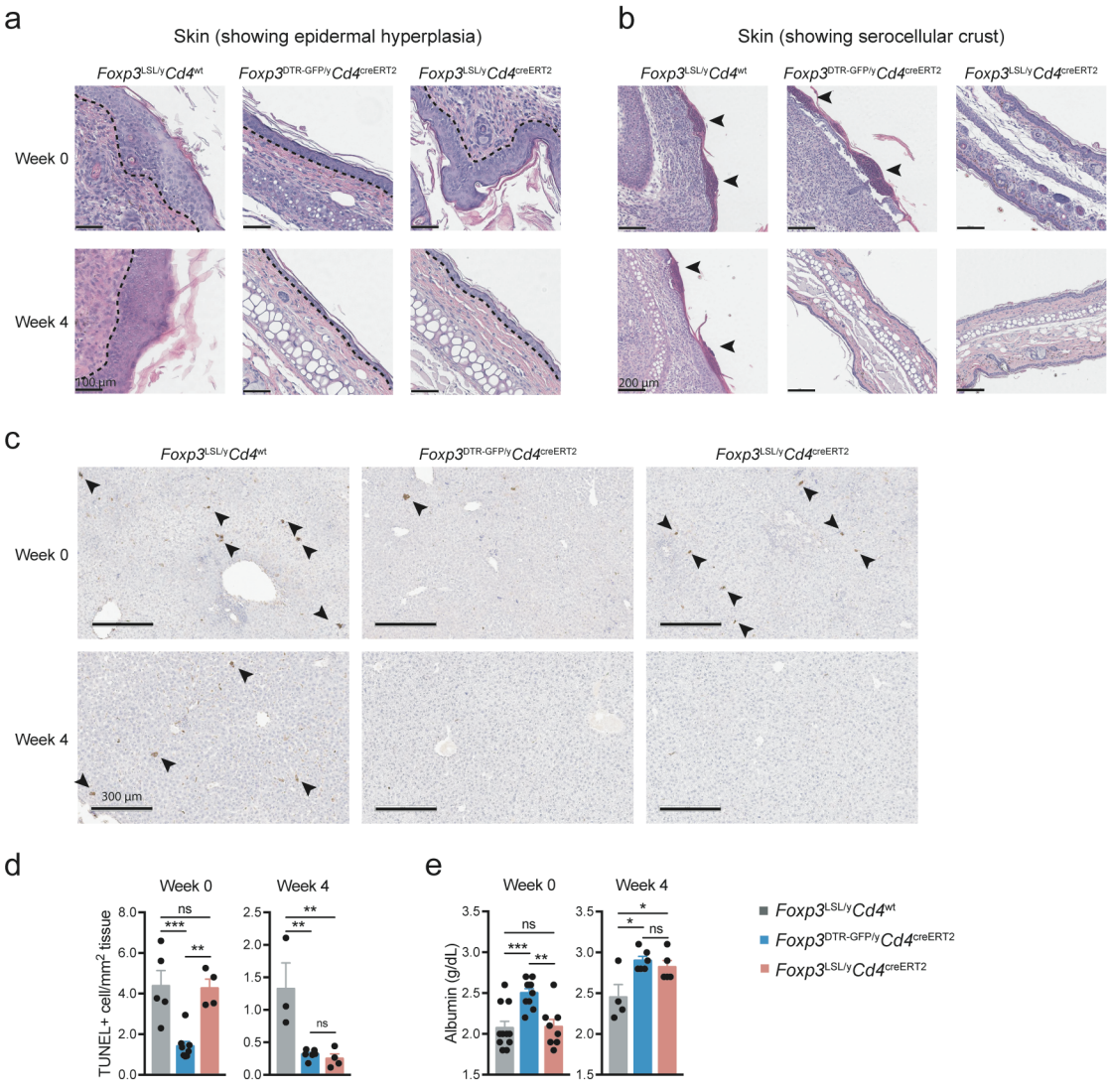
a
Skin (showing epidermal hyperplasia)
Foxp3LSL/yCd4wt
Foxp3DTR-GFP/yCd4creERT2
Foxp3LSL/yCd4creERT2
Week 0
Week 4
100 µm
b
Skin (showing serocellular crust)
Foxp3LSL/yCd4wt
Foxp3DTR-GFP/yCd4creERT2
Foxp3LSL/yCd4creERT2
200 µm
c
Foxp3LSL/yCd4wt
Foxp3DTR-GFP/yCd4creERT2
Foxp3LSL/yCd4creERT2
Week 0
Week 4
300 µm
d
Week 0
Week 4
TUNEL+ cell/mm2 tissue
ns
***
**
**
**
ns
e
Week 0
Week 4
Albumin (g/dL)
ns
***
**
*
*
ns
Foxp3LSL/yCd4wt
Foxp3DTR-GFP/yCd4creERT2
Foxp3LSL/yCd4creERT2

Figure 2.10 Restoration of *Foxp3* expression in Treg "wannabes" in mosaic adult female *Foxp3*$^{LSL/DTR\text{-}GFP}$ mice suppresses immune activation caused by diphtheria toxin-mediated Treg cell ablation.

a, Experimental scheme. 8-10-week-old female mice were injected with diphtheria toxin (DT) intraperitoneally and given oral gavage of tamoxifen (Tam) on designated days.

b, Frequencies of activated, proliferating, and cytokine producing splenic conventional CD4 and CD8 T cells at the indicated time points.

Data are pooled from two independent experiments with 3 to 5 mice per group per time point. Two-way ANOVA with Tukey's multiple comparison test. All error bars denote mean ± s.e.m. ns, non-significant; *, $p<0.05$; **, $p<0.01$; ***, $p<0.001$; ****, $p<0.0001$.

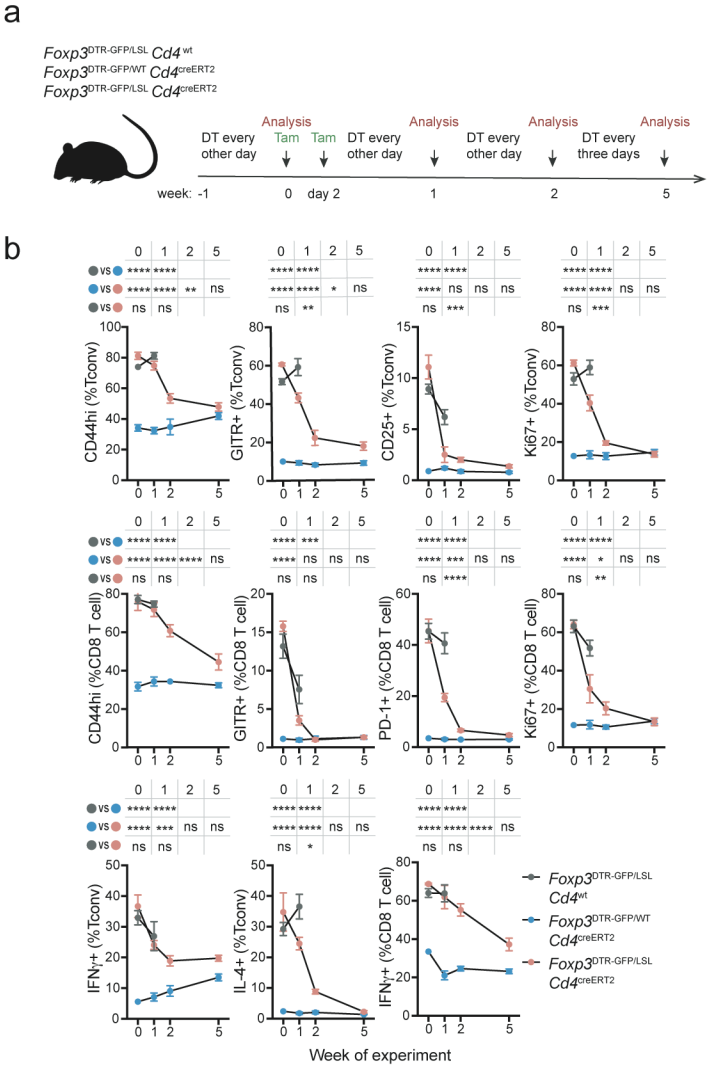
a
Foxp3DTR-GFP/LSL Cd4wt
Foxp3DTR-GFP/WT Cd4creERT2
Foxp3DTR-GFP/LSL Cd4creERT2
Analysis
Tam
Tam
DT every other day
DT every other day
DT every other day
DT every three days
week: -1
0
day 2
1
2
5
b
CD44hi (%Tconv)
GITR+ (%Tconv)
CD25+ (%Tconv)
Ki67+ (%Tconv)
CD44hi (%CD8 T cell)
GITR+ (%CD8 T cell)
PD-1+ (%CD8 T cell)
Ki67+ (%CD8 T cell)
IFNγ+ (%Tconv)
IL-4+ (%Tconv)
IFNγ+ (%CD8 T cell)
Foxp3DTR-GFP/LSL Cd4wt
Foxp3DTR-GFP/WT Cd4creERT2
Foxp3DTR-GFP/LSL Cd4creERT2
Week of experiment

Figure 2.11 Related to Figure 2.10.

a-c, Haematoxylin and eosin staining of sections of skin (a), lung (b), and liver (c) from mice of indicated genotypes at denoted time points post tamoxifen treatment (left), and their respective inflammation scores (right). One-way ANOVA with Tukey's multiple comparison test.

All error bars denote mean ± s.e.m. ns, non-significant; *, $p<0.05$; **, $p<0.01$; ***, $p<0.001$; ****, $p<0.0001$.

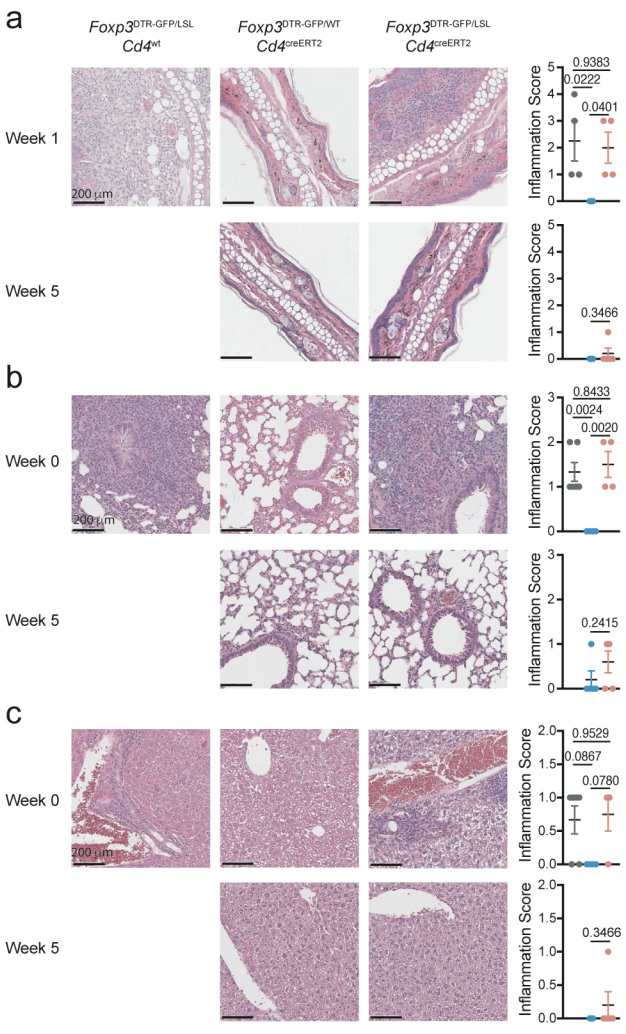
a
Foxp3DTR-GFP/LSL Cd4wt
Foxp3DTR-GFP/WT Cd4creERT2
Foxp3DTR-GFP/LSL Cd4creERT2
Week 1
Week 5
200 μm
Inflammation Score
0.9383
0.0222
0.0401
0.3466
b
Week 0
Week 5
0.8433
0.0024
0.0020
0.2415
c
Week 0
Week 5
0.9529
0.0867
0.0780
0.3466

Figure 2.12 Restoration of *Foxp3* expression in Treg "wannabes" in mosaic adult female *Foxp3*$^{LSL/DTR\text{-}GFP}$ mice suppresses immune activation caused by diphtheria toxin-mediated Treg cell ablation.

Experimental scheme shown in Figure 2.10.

a, Representative histograms showing expression of activation and proliferation markers in splenic conventional T cell populations.

b, Representative contour plots of splenic conventional CD4 and CD8 T cells showing cytokine production.

c, Percentages (left) and numbers (right) of Treg and Treg "wannabes" from indicated tissues 5 wks post 4-OHT administration. Two-way ANOVA with Tukey's multiple comparison test.

All error bars denote mean ± s.e.m. ns, non-significant; *, $p<0.05$; **, $p<0.01$; ***, $p<0.001$; ****, $p<0.0001$.

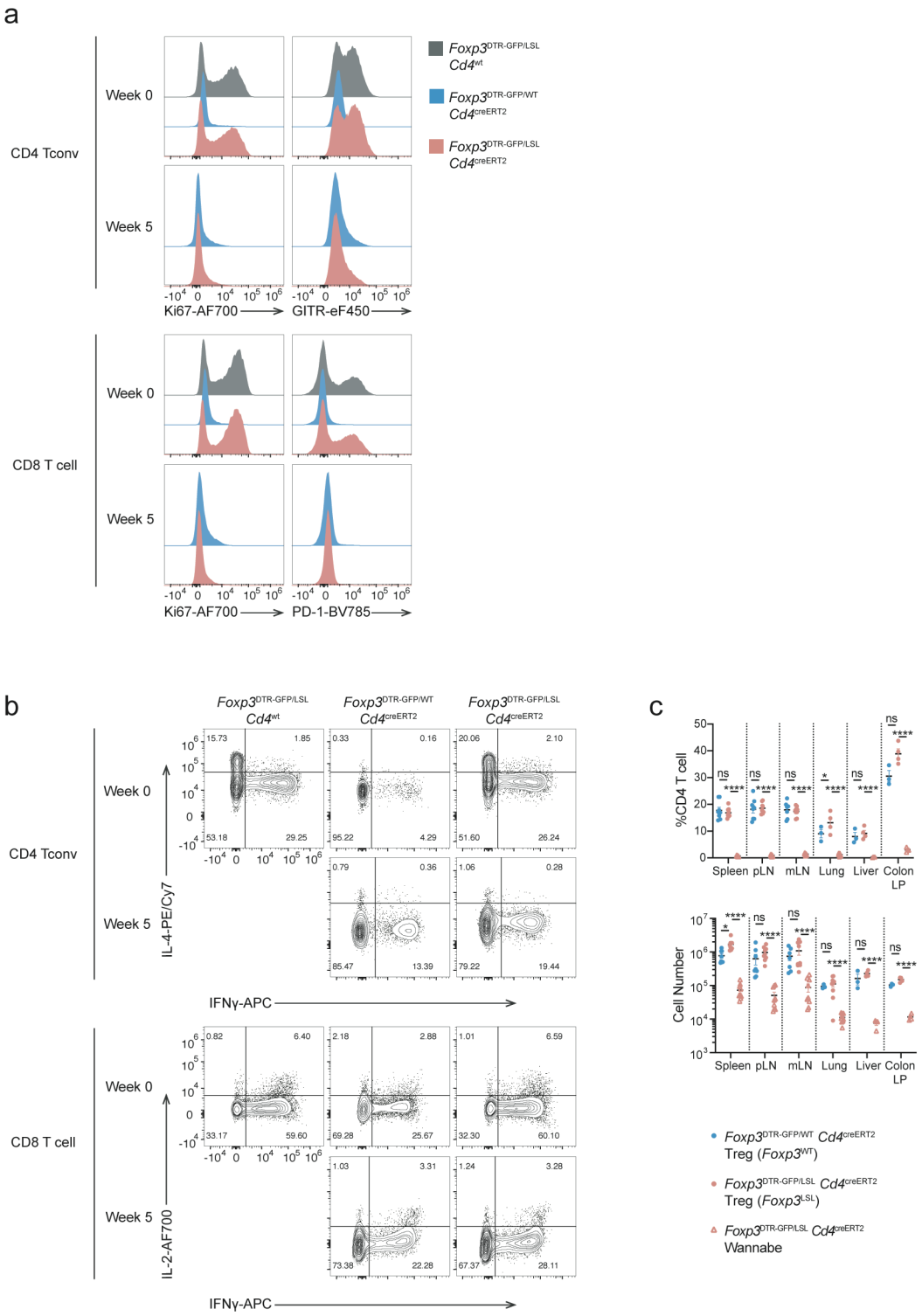
a
CD4 Tconv
Week 0
Week 5
Foxp3DTR-GFP/LSL Cd4wt
Foxp3DTR-GFP/WT Cd4creERT2
Foxp3DTR-GFP/LSL Cd4creERT2
Ki67-AF700
GITR-eF450
CD8 T cell
PD-1-BV785
b
IL-4-PE/Cy7
IFNγ-APC
IL-2-AF700
c
%CD4 T cell
Cell Number
Spleen
pLN
mLN
Lung
Liver
Colon LP
Foxp3DTR-GFP/WT Cd4creERT2 Treg (Foxp3WT)
Foxp3DTR-GFP/LSL Cd4creERT2 Treg (Foxp3LSL)
Foxp3DTR-GFP/LSL Cd4creERT2 Wannabe

Foxp3 imparts Treg cell functionality in inflammatory milieu

Next, we explored the intrinsic and extrinsic phenotypic shifts Foxp3 expression afforded to Treg "wannabes" in inflammatory vs. non-inflammatory settings. Compared to healthy *Foxp3*$^{DTR\text{-}GFP}$*Cd4*^{creERT2} littermates, we observed a transient increase in Treg proportion in male *Foxp3*^{LSL}*Cd4*^{creERT2} mice, which peaked on day 7 post 4-OHT treatment and normalized after 4 weeks when the autoimmune disease was largely eradicated (Fig. 2.13a). On day 7, the Thy1.1^{-} GFP^{+} Treg cells in rescued *Foxp3*^{LSL}*Cd4*^{creERT2} mice were more proliferative and expressed higher amounts of GITR and CTLA4 than those in healthy *Foxp3*$^{DTR\text{-}GFP}$*Cd4*^{creERT2} controls (Fig. 2.13b-c). RNA-seq analysis of Thy1.1^{-}GFP^{+} Treg cells and Thy1.1^{+}GFP^{-} "wannabes" isolated from *Foxp3*^{LSL} males on day 7 following 4-OHT treatment, and of Treg cells isolated from similarly treated *Foxp3*$^{DTR\text{-}GFP}$*Cd4*^{creERT2} controls showed that Treg cells from diseased and control mice were considerably different (PC2; 30% variance), with differentially regulated genes in the former enriched for previously reported Treg cell (144) and STAT5 (87) activation gene signatures (Fig. 2.13d). Notably, the transcriptomes of both Treg populations were markedly different—equidistant in PCA—from Thy1.1^{+}GFP^{-} Treg "wannabes" (Fig. 2.13d). Treg cells in *Foxp3*^{LSL}*Cd4*^{creERT2} mice downregulated *Tcf7*, *Sell*, and *Ccr7* transcripts and upregulated cell cycle, anabolism, and Treg suppressor function-related genes (*Gzma*, *Gzmb*, *Lgals1*, *Lgals3*, *Il10*, *Fgl2*, *Ctla4*, *Entpd1*, *Icos*, and *Tigit*) (145, 146), suggesting that they were more metabolically active and suppressive than control Treg cells (Fig. 2.13e). Indeed, Treg cells isolated on day 7 post 4-OHT administration from

Foxp3^{LSL}*Cd4*^{creERT2} mice were significantly more potent at suppressing T cell proliferation *in vitro* than their counterparts from *Foxp3*$^{DTR\text{-}GFP}$*Cd4*^{creERT2} mice (Fig. 2.14b).

Notably, activated Treg "wannabes" from DT-treated *Foxp3*$^{LSL/DTR\text{-}GFP}$ sick female mice shared some gene expression changes with those of activated Treg cells in rescued *Foxp3*$^{LSL/y}$ mice (Fig. 2.13d, Fig. 2.15). However, this acquisition of activated phenotype by Treg "wannabes" did not confer any appreciable suppressive capacity, as *Foxp3*$^{LSL/DTR}$*Cd4*^{wt} mice, in which tamoxifen treatment could not restore Foxp3 expression, died of similar systemic multi-organ inflammation seen in *Foxp3*$^{LSL/y}$ mice. Thus, the heightened suppressor capacity of rehabilitated Treg cells in *Foxp3*^{LSL}*Cd4*^{creERT2} mice could be due to exposure to an inflammatory environment upon *Foxp3* induction or a cell-intrinsic effect of delayed Foxp3 expression regardless of the environment. To distinguish between these two possibilities, we analyzed the "wannabe"-converted and control Treg cells under basal non-inflammatory conditions in healthy heterozygous female *Foxp3*$^{LSL/WT}$*Cd4*^{creERT2} and *Foxp3*$^{DTR\text{-}GFP/WT}$*Cd4*^{creERT2} mice, respectively, on day 7 post 4-OHT treatment. In contrast to Treg cells exposed to the inflammatory environment in male mice, Thy1.1^{-}GFP^{+} Treg cells in 4-OHT-treated mosaic *Foxp3*$^{LSL/WT}$*Cd4*^{creERT2} females failed to exhibit increased proliferative activity or enhanced CTLA4 and GITR expression, compared to GFP^{-}Foxp3^{+} Treg cells expressing the *Foxp3*^{WT} allele in the same mice (Fig. 2.14a). Likewise, comparable suppressor activity was observed for Thy1.1^{-}GFP^{+} Treg cells and control GFP^{+} counterparts isolated from 4-OHT-treated healthy *Foxp3*$^{LSL/WT}$*Cd4*^{creERT2} and

Foxp3$^{DTR\text{-}GFP/WT}$*Cd4*^{creERT2} female mice, respectively (Fig. 2.14b). To the contrary, sick *Foxp3*$^{DTR\text{-}GFP/LSL}$*Cd4*^{creERT2} mosaic female mice, subjected to DT-induced ablation of *Foxp3*$^{DTR\text{-}GFP}$ Treg cells and tamoxifen-induced Foxp3 restoration in *Foxp3*^{LSL} cells, showed a transient increase in Treg percentages at 1 and 2 weeks post tamoxifen-mediated rescue, which disappeared by week 5 (Fig. 2.14c). These Treg cells also exhibited enhanced proliferation and heightened activation as evidenced by elevated expression of Ki67, CTLA4, GITR and ICOS (Fig. 2.14d-e). Thus, the enhanced proliferative potential and suppressive capacity of Treg cells in diseased *Foxp3*^{LSL}*Cd4*^{creERT2} male and DT-treated *Foxp3*$^{DTR\text{-}GFP/LSL}$*Cd4*^{creERT2} female mice were likely due to sensing of inflammation assisted by restored Foxp3 expression.

Figure 2.13 Rescued Treg cells in inflamed mice are activated and potently suppressive in inflammatory settings.

a-c, Male *Foxp3*$^{\text{DTR-GFP}}$*Cd4*$^{\text{creERT2}}$ and *Foxp3*$^{\text{LSL}}$*Cd4*$^{\text{creERT2}}$ mice were treated with 4-OHT on postnatal day 14. Data are pooled from three independent experiments.

a, Percentages of splenic Treg cells at indicated time points following 4-OHT treatment. Two-tailed unpaired *t*-tests with Holm-Sidak multiple comparison.

b, c, representative histograms (b) and combined data (c) showing expression of Ki67, CTLA4 and GITR by rescued and control splenic Treg cells on day 7 post 4-OHT treatment. Two-tailed unpaired *t*-tests.

d, e, RNA-seq analysis of rescued Treg cells, control Treg cells, and Treg "wannabes" from male mice of indicated genotypes treated with 4-OHT on postnatal day 14 and analyzed 7 days afterwards.

d, Principal component analysis of gene expression in the three indicated cell populations (top), and empirical cumulative distribution function plots showing gene signatures of activated Treg cells (bottom left) and Treg cells expressing a constitutively active form of STAT5b (bottom right). Two-sided Kolmogorov-Smirnov test.

e, Heatmaps showing expression of curated genes in rescued and control Treg cells from mice of indicated genotypes.

All error bars denote mean ± s.e.m. ns, non-significant; *, $p<0.05$; **, $p<0.01$; ***, $p<0.001$; ****, $p<0.0001$.

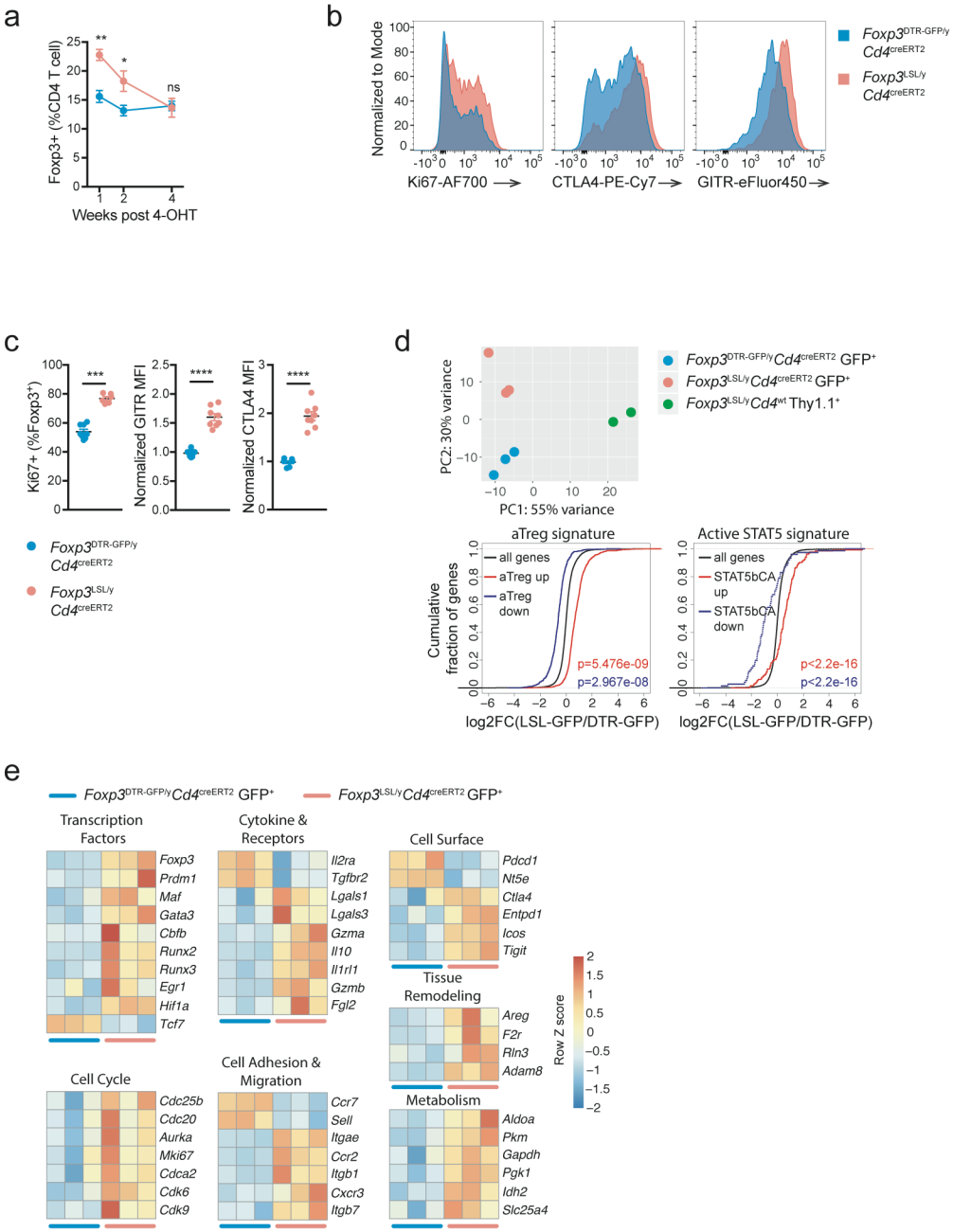
a
Foxp3+ (%CD4 T cell)
Weeks post 4-OHT
**
*
ns
b
Normalized to Mode
Ki67-AF700
CTLA4-PE-Cy7
GITR-eFluor450
Foxp3DTR-GFP/y Cd4creERT2
Foxp3LSL/y Cd4creERT2
c
Ki67+ (%Foxp3+)
Normalized GITR MFI
Normalized CTLA4 MFI
***
****
****
Foxp3DTR-GFP/y Cd4creERT2
Foxp3LSL/y Cd4creERT2
d
PC2: 30% variance
PC1: 55% variance
Foxp3DTR-GFP/y Cd4creERT2 GFP+
Foxp3LSL/y Cd4creERT2 GFP+
Foxp3LSL/y Cd4wt Thy1.1+
aTreg signature
Active STAT5 signature
Cumulative fraction of genes
all genes
aTreg up
aTreg down
STAT5bCA up
STAT5bCA down
p=5.476e-09
p=2.967e-08
p<2.2e-16
p<2.2e-16
log2FC(LSL-GFP/DTR-GFP)
e
Foxp3DTR-GFP/y Cd4creERT2 GFP+
Foxp3LSL/y Cd4creERT2 GFP+
Transcription Factors
Foxp3
Prdm1
Maf
Gata3
Cbfb
Runx2
Runx3
Egr1
Hif1a
Tcf7
Cytokine & Receptors
Il2ra
Tgfbr2
Lgals1
Lgals3
Gzma
Il10
Il1rl1
Gzmb
Fgl2
Cell Surface
Pdcd1
Nt5e
Ctla4
Entpd1
Icos
Tigit
Tissue Remodeling
Areg
F2r
Rln3
Adam8
Metabolism
Aldoa
Pkm
Gapdh
Pgk1
Idh2
Slc25a4
Cell Cycle
Cdc25b
Cdc20
Aurka
Mki67
Cdca2
Cdk6
Cdk9
Cell Adhesion & Migration
Ccr7
Sell
Itgae
Ccr2
Itgb1
Cxcr3
Itgb7
Row Z score

Figure 2.14 Related to Figure 2.13.

a, Expression of Ki67, CTLA4 and GITR by indicated splenic Treg cell subsets from mosaic heterozygous *Foxp3*$^{\text{DTR-GFP/WT}}$*Cd4*$^{\text{creERT2}}$ and *Foxp3*$^{\text{LSL/WT}}$*Cd4*$^{\text{creERT2}}$ female mice treated with 4-OHT on postnatal day 14 and analyzed after 7 days. One-way ANOVA with Tukey's multiple comparison test.

b, Suppression of *in vitro* proliferation of conventional CD4 T cells induced by α-CD3 antibody and antigen-presenting cells by control or rescued Treg cells (GFP^{+}) or Treg "wannabes" (Thy1.1^{+}) from indicated strains of mice on day 7 post 4-OHT treatment. Two-way ANOVA with Tukey's multiple comparison test.

c-e, Adult mosaic heterozygous female *Foxp3*$^{\text{DTR-GFP/WT}}$*Cd4*$^{\text{creERT2}}$ and *Foxp3*$^{\text{DTR-GFP/LSL}}$*Cd4*$^{\text{creERT2}}$ mice were treated as in Figure 2.10a.

c, Percentages of splenic Treg cells at indicated time points following tamoxifen treatment. Multiple *t*-tests with Holm-Sidak multiple comparison.

d, e, Representative histograms (d) and combined data (e) showing expression of indicated markers by Treg cells at week 1. Two-tailed unpaired *t*-tests.

All error bars denote mean $\pm$ s.e.m. ns, non-significant; *, p<0.05; **, p<0.01; ***, p<0.001; ****, p<0.0001.

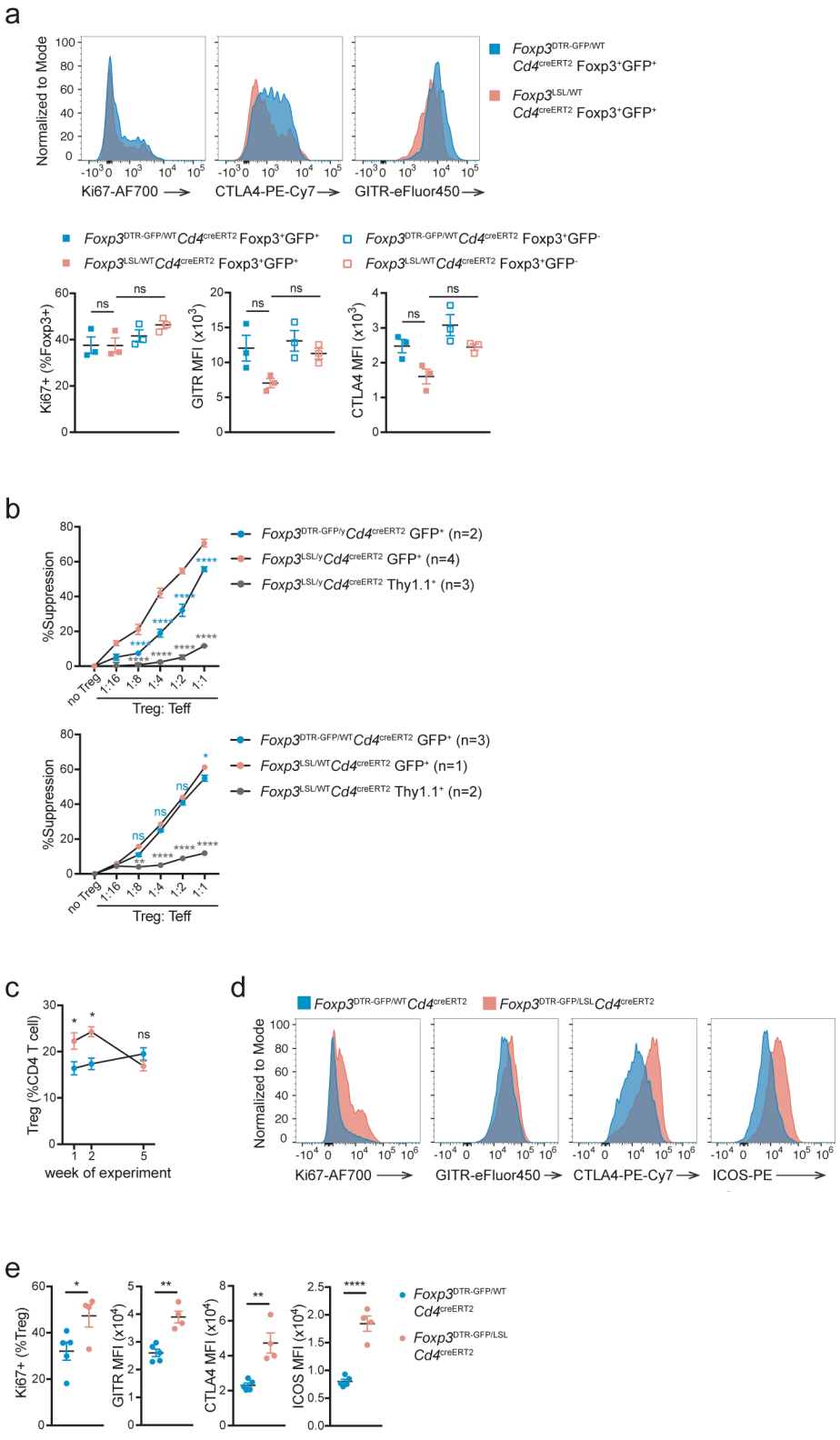
a
Normalized to Mode
Ki67-AF700
CTLA4-PE-Cy7
GITR-eFluor450
Foxp3DTR-GFP/WT Cd4creERT2 Foxp3+GFP+
Foxp3LSL/WT Cd4creERT2 Foxp3+GFP+
Foxp3DTR-GFP/WT Cd4creERT2 Foxp3+GFP-
Foxp3LSL/WT Cd4creERT2 Foxp3+GFP-
Ki67+ (%Foxp3+)
GITR MFI (x10^3)
CTLA4 MFI (x10^3)
ns
b
%Suppression
Treg: Teff
no Treg
1:16
1:8
1:4
1:2
1:1
Foxp3DTR-GFP/Y Cd4creERT2 GFP+ (n=2)
Foxp3LSL/Y Cd4creERT2 GFP+ (n=4)
Foxp3LSL/Y Cd4creERT2 Thy1.1+ (n=3)
Foxp3DTR-GFP/WT Cd4creERT2 GFP+ (n=3)
Foxp3LSL/WT Cd4creERT2 GFP+ (n=1)
Foxp3LSL/WT Cd4creERT2 Thy1.1+ (n=2)
c
Treg (%CD4 T cell)
week of experiment
d
Foxp3DTR-GFP/WT Cd4creERT2
Foxp3DTR-GFP/LSL Cd4creERT2
Normalized to Mode
Ki67-AF700
GITR-eFluor450
CTLA4-PE-Cy7
ICOS-PE
e
Ki67+ (%Treg)
GITR MFI (x10^4)
CTLA4 MFI (x10^4)
ICOS MFI (x10^4)
Foxp3DTR-GFP/WT Cd4creERT2
Foxp3DTR-GFP/LSL Cd4creERT2

Figure 2.15 Analysis of gene expression changes in Treg “wannabes” induced upon activation.

a, Experimental scheme. 8-10-wk-old heterozygous female *Foxp3*$^{LSL/DTR\text{-}GFP}$*Cd4*^{wt} mice were treated with diphtheria toxin (DT) on designated days to deplete *Foxp3*$^{DTR\text{-}GFP}$-expressing Treg cells and induce activation of *Foxp3*^{LSL}-expressing Treg “wannabes” which were sorted and analyzed by RNA-seq.

b, FC-FC plot of activation-induced gene expression changes in Treg cells and “wannabes”. Genes with mean normalized counts of >100 are shown. Differentially expressed genes (p<0.05) are colored based on the direction of the change in either or both cell types.

c, Venn diagram showing the numbers of genes with larger than a 2-fold change in activated Treg cells and “wannabes”.

d, eCDF plots showing expression changes in activated Treg “wannabes” for all genes (black) and Treg activation signature genes that are up- (red) or down- (blue) regulated. Two-sided Kolmogorov-Smirnov test.

e, FC-FC plots showing gene expression changes in Treg cells vs. “wannabes” isolated from sick and healthy mice. Signature genes that are up- or down-regulated in activated Treg and conventional CD4 T cells are highlighted in different colors.

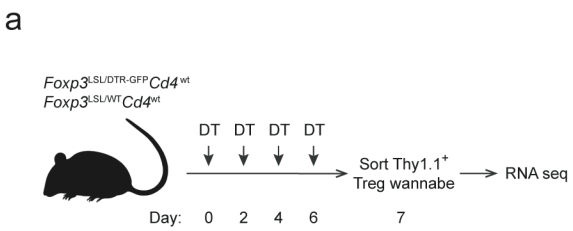
a
Foxp3LSL/DTR-GFP Cd4wt
Foxp3LSL/WT Cd4wt
DT DT DT DT
Sort Thy1.1+
Treg wannabe
RNA seq
Day: 0 2 4 6 7

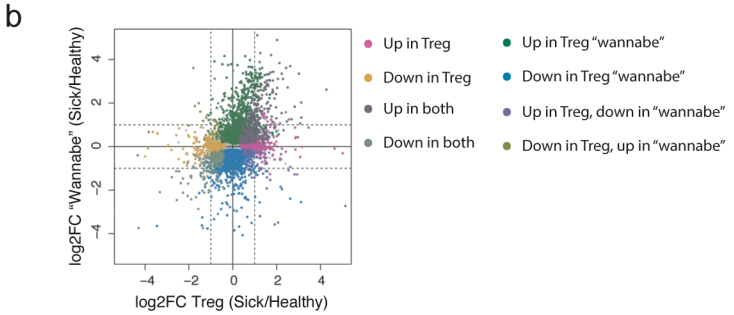
b
log2FC "Wannabe" (Sick/Healthy)
log2FC Treg (Sick/Healthy)
Up in Treg
Down in Treg
Up in both
Down in both
Up in Treg "wannabe"
Down in Treg "wannabe"
Up in Treg, down in "wannabe"
Down in Treg, up in "wannabe"

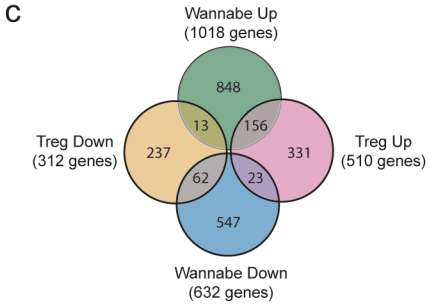
c
Wannabe Up
(1018 genes)
848
13
156
Treg Down
(312 genes)
237
331
Treg Up
(510 genes)
62
23
547
Wannabe Down
(632 genes)

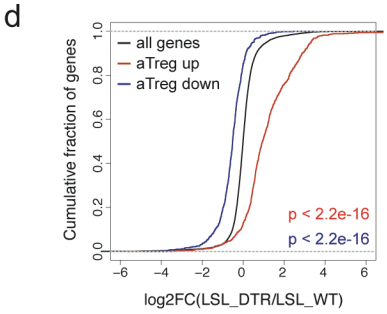
d
Cumulative fraction of genes
all genes
aTreg up
aTreg down
p < 2.2e-16
p < 2.2e-16
log2FC(LSL_DTR/LSL_WT)

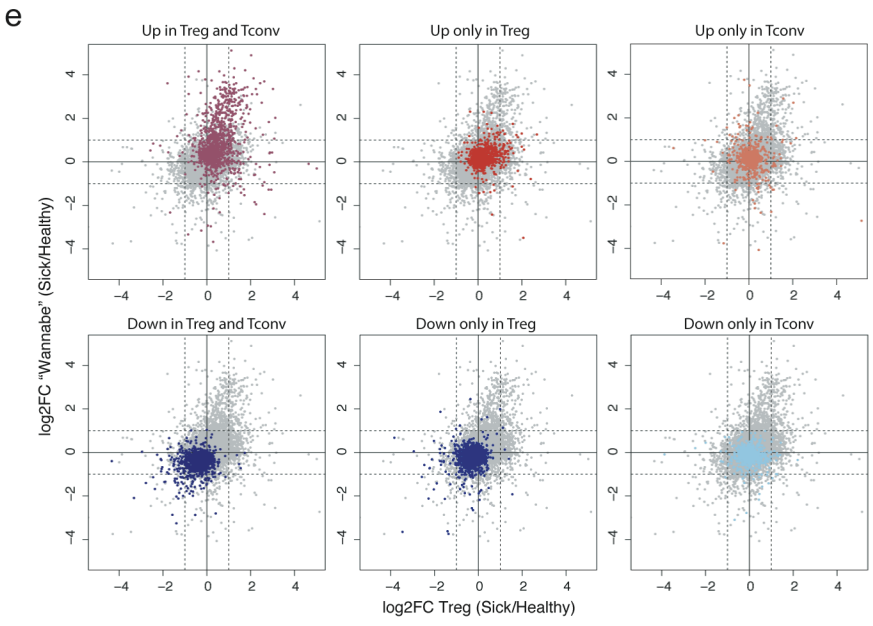
e
Up in Treg and Tconv
Up only in Treg
Up only in Tconv
Down in Treg and Tconv
Down only in Treg
Down only in Tconv
log2FC "Wannabe" (Sick/Healthy)
log2FC Treg (Sick/Healthy)

A single cohort of Treg cells provides long-term protection

To test whether the containment of autoimmunity afforded by a single cohort of Treg cells was durable, we monitored tdTomato-labeled and -unlabeled cells in 4-OHT-treated male *Foxp3*^{LSL}*Cd4*^{creERT2}*R26*^{Tom} and control *Foxp3*$^{DTR\text{-}GFP}$*Cd4*^{creERT2}*R26*^{Tom} mice for an extended period of time (Fig. 2.16a). Within a month after treatment, the *Foxp3*^{LSL}*Cd4*^{creERT2}*R26*^{Tom} mice recovered completely from otherwise lethal disease and continued to gain weight (Fig. 2.16b). At the 4-month time point, only recirculating Treg cells lacking CD73 expression were detected in the thymus, suggesting a lack of continuing thymic Treg output in agreement with our observation that *Cd4*^{creERT2}-mediated recombination ceased within 48-72 hours after 4-OHT administration (Fig. 2.16c-d) (147). The peripheral "4-month-old" Treg pool was well maintained in both lymphoid and non-lymphoid tissues and remained functionally competent (Fig. 2.16e-f). Nearly all Thy1.1^{-} GFP^{+}Foxp3^{+} Treg cells in *Foxp3*^{LSL}*Cd4*^{creERT2}*R26*^{Tom} mice expressed the tdTomato reporter, whereas Thy1.1^{+}GFP^{-} "wannabes" and Thy1.1^{-}GFP^{-}Foxp3^{-} conventional CD4 T cells in the same mice, as well as Treg and conventional CD4 T cell subsets in control *Foxp3*$^{DTR\text{-}GFP}$*Cd4*^{creERT2}*R26*^{Tom} mice, contained only a small fraction of tdTomato^{+} fate-mapped cells (Fig. 2.16g). Thus, Treg cells generated as a single cohort in diseased *Foxp3*^{LSL}*Cd4*^{creERT2} mice continued to persist while the other T cell subsets turned over. Impressively, even after 4 months, the reversal of autoimmune disease seemed complete with no tissue pathology observed and T cell activation, effector cytokine production, and myelo-proliferation, at best minimally increased (Fig. 2.17; Fig. 2.18). Thus, a single

cohort of Treg cells is capable of reversing established inflammation and affording long-term protection against autoimmunity. The rescued mice survived for at least 7 months (Fig. 2.19a). Even at this time point, the rescued mice remained largely healthy with only moderately increased T cell activation and effector cytokine production and well-maintained Treg populations in both lymphoid and non-lymphoid tissues (Fig. 2.19b-d). Despite mildly elevated serum IgG1and IgE levels in comparison to the 4-week time point, the other Ig isotype levels remained comparable to those in control *Foxp3*$^{\text{DTR-GFP/y}}$*Cd4*$^{\text{creERT2}}$ mice (Fig. 2.19e). Neither did we observe prominent immune infiltrates in the skin, liver, and small intestine (Fig. 2.19f).

Since TCR specificity and diversity are essential for Treg-mediated control of autoimmunity (72, 148), we assessed the TCR repertoires of long-lived redeemed Treg cells in *Foxp3*$^{\text{LSL/y}}$ *Cd4*$^{\text{creERT2}}$ mice by sequencing their TCRα chains at different time points after Foxp3 restoration. We observed a trend, albeit not statistically significant, toward a slight reduction in TCR diversity, as reflected in the gradually decreasing inverse Simpson indices (Fig. 2.19g). At later time points (5 and 7 months), the rescued Treg cells contained moderately reduced numbers of total unique clones compared to an earlier time point after the inflammatory disease subsided (1.5 months). The “unevenness” of the TCR repertoire measured by Gini coefficient remained unchanged throughout the entire time course (Fig. 2.19h). These results suggested that the clonal diversity of long-lived redeemed Treg cells was largely preserved even though their TCR richness might have very mildly contracted. Thus, a cohort of restored Treg cells maintained

a diverse TCR repertoire, which was likely essential for their ability to confer long-term containment of autoimmune inflammation.

Figure 2.16 Rescued Treg cells in male *Foxp3*^{LSL} mice provide long-term protection from autoimmune inflammatory disease.

a, Experimental design. Mice were treated with a single dose of 4-OHT at 2 weeks of age and analyzed 4 months later.

b, Body weight of rescued *Foxp3*^{LSL}*Cd4*^{creERT2} and control *Foxp3*$^{DTR\text{-}GFP}$*Cd4*^{creERT2} mice over a 4-month time course. Two-way ANOVA with Sidak's multiple comparison test.

c, Flow cytometric analysis of CD73 expression in Foxp3^{+} CD4 single-positive thymocytes as a discriminating marker of recirculating vs. recently generated thymic Treg cells. Two-tailed unpaired *t*-test.

d, Analysis of 4-OHT "functional" pharmacokinetics in 2-wk-old male mice. Mice were injected with 4-OHT 3-72 hours before transfer of congenically marked recombination-proficient CD4 T cells from *Cd4*^{creERT2}*R26*^{Tom} mice. 4-OHT-induced recombination was assayed 7 days later by tdTomato expression among donor CD4 T cells as a readout for 4-OHT activity. Data are pooled from two independent experiments with 2 to 4 mice per time point each. Ctrl, no 4-OHT injection.

e, Flow cytometric analysis of Treg cell percentages (upper panel) and absolute numbers (lower panel) in tissues of mice of indicated genotypes. Two-tailed unpaired *t*-tests with Holm-Sidak multiple comparison.

f, Suppression of *in vitro* proliferation of conventional CD4 T cells induced by α-CD3 antibody and antigen-presenting cells by control Treg cells from *Foxp3*$^{DTR\text{-}GFP/y}$ or rescued Treg cells from *Foxp3*$^{LSL/y}$ mice. Two-way ANOVA with Tukey's multiple comparison test.

g, Percentages of lineage-traced (tdTomato^{+}) Treg cells, Treg "wannabes", and conventional CD4 T cells. One-way ANOVA with Dunnett's multiple hypothesis test.

All error bars denote mean $\pm$ s.e.m. ns, non-significant; *, $p<0.05$; **, $p<0.01$; ***, $p<0.001$; ****, $p<0.0001$.

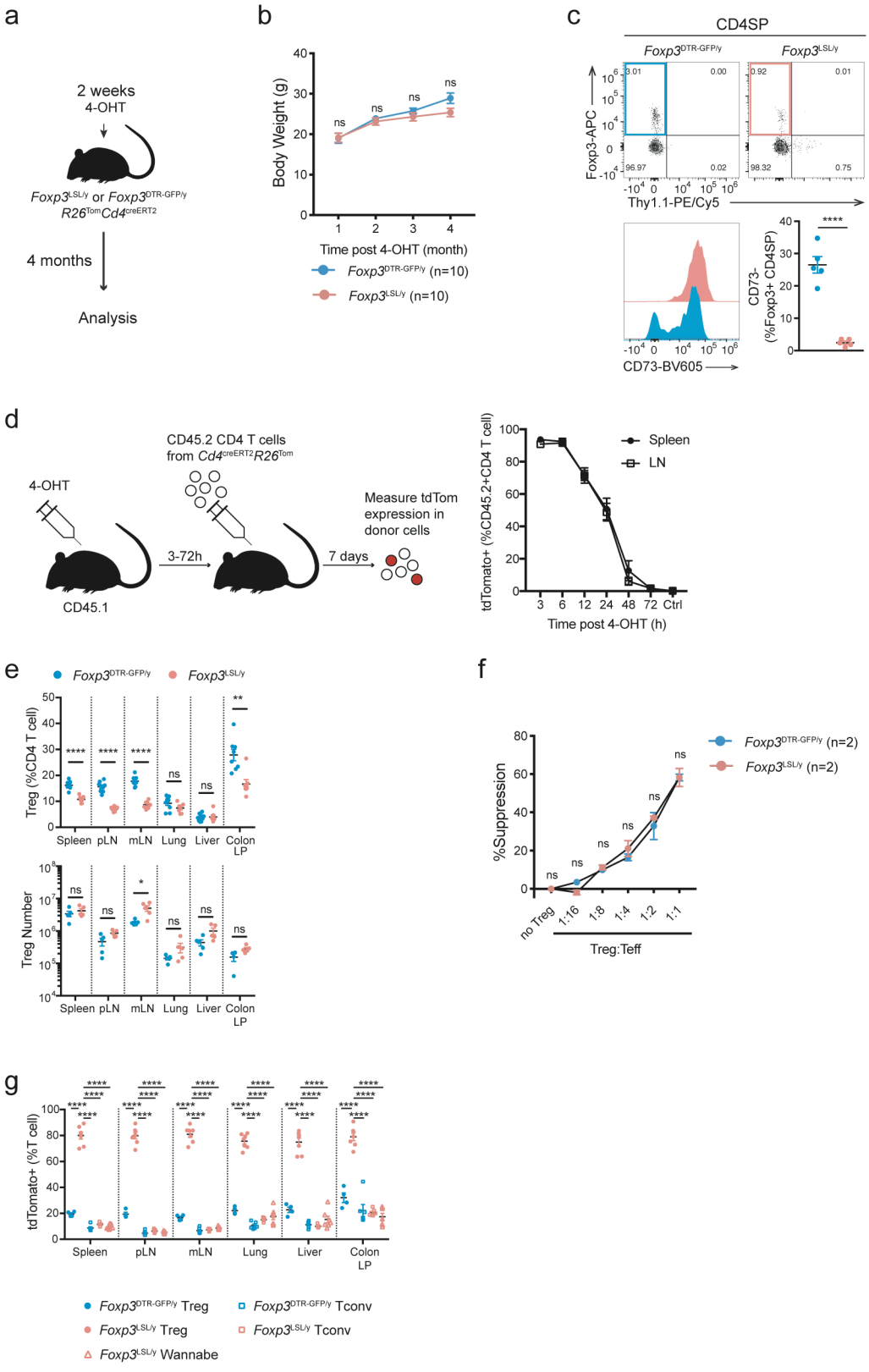
a
2 weeks
4-OHT
Foxp3LSL/y or Foxp3DTR-GFP/y
R26TomCd4creERT2
4 months
Analysis
b
Body Weight (g)
Time post 4-OHT (month)
Foxp3DTR-GFP/y (n=10)
Foxp3LSL/y (n=10)
ns
c
CD4SP
Foxp3DTR-GFP/y
Foxp3LSL/y
Foxp3-APC
Thy1.1-PE/Cy5
3.01
0.00
96.97
0.02
0.92
0.01
98.32
0.75
CD73-BV605
CD73-
(%Foxp3+ CD4SP)
****
d
CD45.2 CD4 T cells
from Cd4creERT2R26Tom
4-OHT
CD45.1
3-72h
7 days
Measure tdTom
expression in
donor cells
tdTomato+ (%CD45.2+CD4 T cell)
Spleen
LN
Time post 4-OHT (h)
3 6 12 24 48 72 Ctrl
e
Foxp3DTR-GFP/y
Foxp3LSL/y
Treg (%CD4 T cell)
Treg Number
Spleen pLN mLN Lung Liver Colon LP
f
%Suppression
Foxp3DTR-GFP/y (n=2)
Foxp3LSL/y (n=2)
no Treg
1:16
1:8
1:4
1:2
1:1
Treg:Teff
g
tdTomato+ (%T cell)
Spleen
pLN
mLN
Lung
Liver
Colon LP
Foxp3DTR-GFP/y Treg
Foxp3DTR-GFP/y Tconv
Foxp3LSL/y Treg
Foxp3LSL/y Tconv
Foxp3LSL/y Wannabe

Figure 2.17 Related to Figure 2.16.

a, Analysis of histopathology in mice of indicated genotypes. Haematoxylin and eosin staining of sections of the indicated organs. Images are representative of 9 *Foxp3*$^{DTR\text{-}GFP/y}$ and 7 *Foxp3*$^{LSL/y}$ mice.

b-d, Percentages of activated, proliferating, and cytokine-producing conventional CD4 T cells (b), CD8 T cells (c) and myeloid populations (d) from indicated organs. Data are pooled from two independent experiments. Two-tailed unpaired *t*-tests with Holm-Sidak multiple comparison. pLN, peripheral (brachial, axillary, and inguinal) lymph nodes; mLN, mesenteric lymph nodes; LP, lamina propria.

All error bars denote mean ± s.e.m. ns, non-significant; *, $p<0.05$; **, $p<0.01$; ***, $p<0.001$; ****, $p<0.0001$.

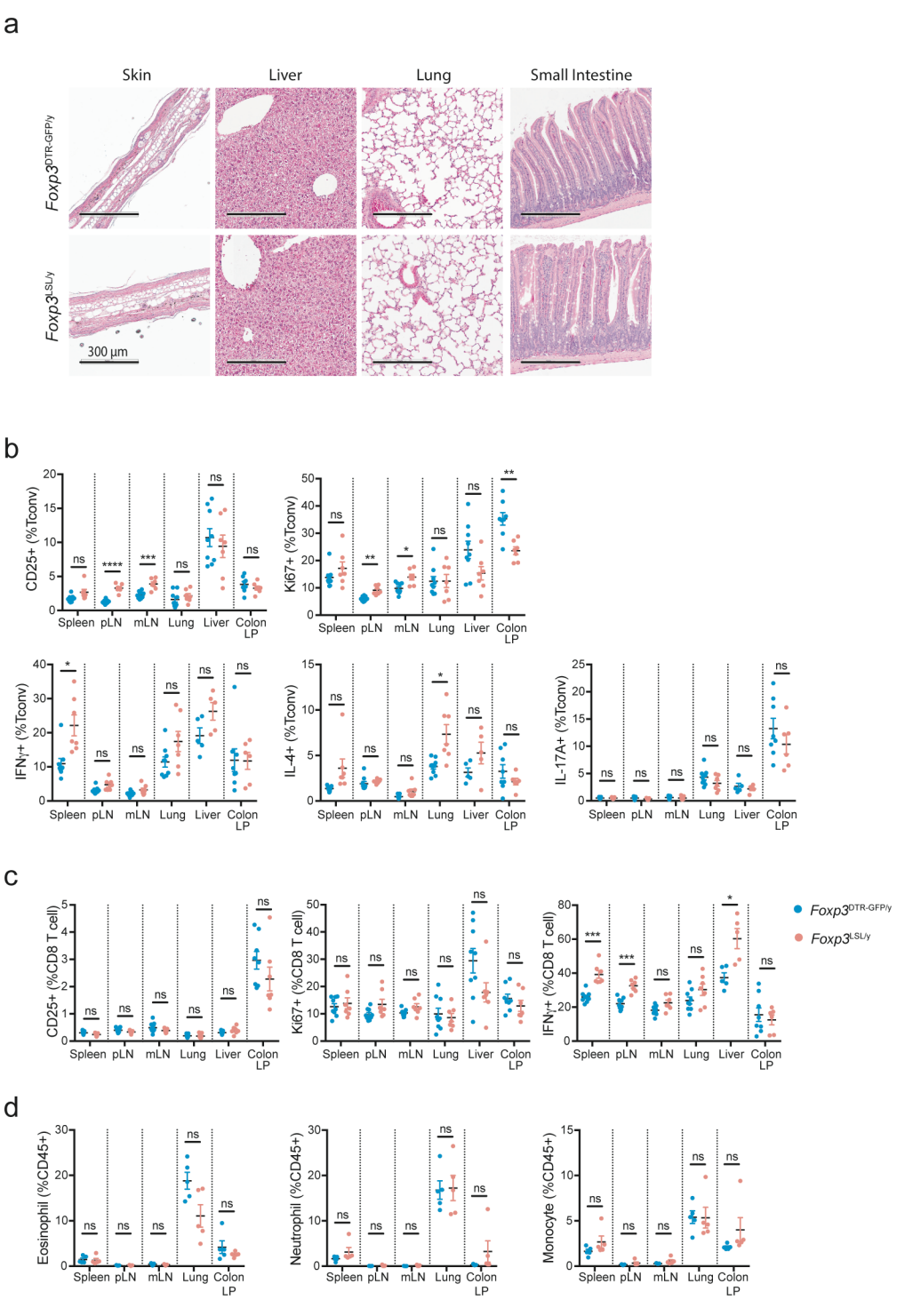
a
Skin
Liver
Lung
Small Intestine
Foxp3DTR-GFP/y
Foxp3LSL/y
300 μm
b
CD25+ (%Tconv)
Ki67+ (%Tconv)
IFNγ+ (%Tconv)
IL-4+ (%Tconv)
IL-17A+ (%Tconv)
Spleen pLN mLN Lung Liver Colon LP
c
CD25+ (%CD8 T cell)
Ki67+ (%CD8 T cell)
IFNγ+ (%CD8 T cell)
Foxp3DTR-GFP/y
Foxp3LSL/y
d
Eosinophil (%CD45+)
Neutrophil (%CD45+)
Monocyte (%CD45+)

Figure 2.18 Related to Figure 2.16.

a-c, Numbers of activated, proliferating, and cytokine-producing conventional CD4 T cells (a), CD8 T cells (b) and myeloid populations (c) in indicated tissues. pLN, peripheral (brachial, axillary, and inguinal) lymph nodes; mLN, mesenteric lymph nodes; LP, lamina propria. Data are pooled from two independent experiments. Two-tailed *t*-tests with multiple hypothesis testing correction using the Holm-Sidak method. All error bars denote mean ± s.e.m. ns, non-significant; *, $p<0.05$; **, $p<0.01$; ***, $p<0.001$; ****, $p<0.0001$.

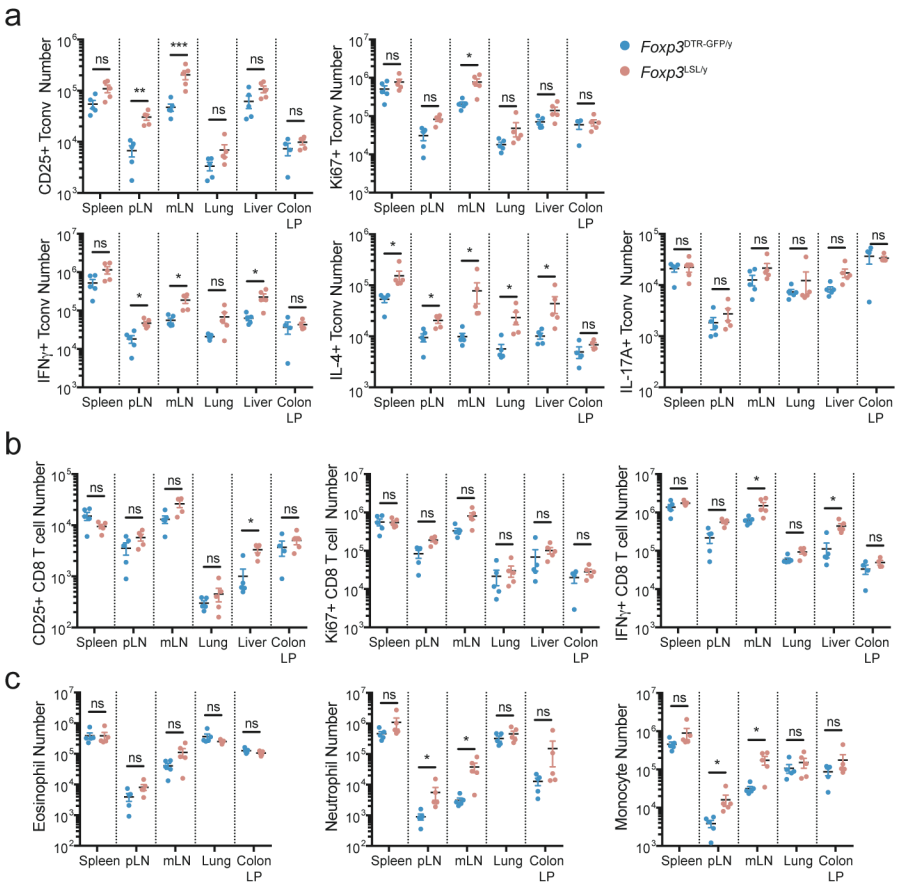
a
b
c
Foxp3DTR-GFP/y
Foxp3LSL/y
CD25+ Tconv Number
Ki67+ Tconv Number
IFNγ+ Tconv Number
IL-4+ Tconv Number
IL-17A+ Tconv Number
CD25+ CD8 T cell Number
Ki67+ CD8 T cell Number
IFNγ+ CD8 T cell Number
Eosinophil Number
Neutrophil Number
Monocyte Number
Spleen
pLN
mLN
Lung
Liver
Colon LP
ns
*
**
***

Figure 2.19 Rescued Treg cell population persisting for 7 months in male *Foxp3*^{LSL} mice prevents relapse of rampant autoimmunity.

Mice were treated with 4-OHT on postnatal day 14 and analyzed 7 months later.

a, Survival plot of 4-OHT-treated male *Foxp3*^{LSL}*Cd4*^{wt} and *Foxp3*^{LSL}*Cd4*^{creERT2} mice. Mantel-Cox test.

b-d, Frequencies of Treg cells (b) and proliferating, activated, and cytokine-producing conventional CD4 (c) and CD8 (d) T cells. Two-tailed unpaired *t*-tests with multiple hypothesis testing correction using the Holm-Sidak method.

e, Serum antibody levels. Scales were kept the same as in Figure 2.8c. Two-tailed unpaired *t*-test.

f, Representative images of haematoxylin and eosin-stained sections of the indicated organs.

g, Clonal diversity of the TCRα repertoire of the long-lived "redeemed" Treg cells from *Foxp3*$^{LSL/y}$ *Cd4*^{creERT2} mice at indicated time points after restoring Foxp3 expression upon 4-OHT treatment. The inverse Simpson Index was calculated based on the clone size distribution using clonotypes defined by full nucleotide sequence (left) or CDR3 amino acid sequence (right).

h, Total number of unique clones (left) and Gini coefficient (right) of the TCRα repertoire of the long-lived "redeemed" Treg cells. Clonotypes were defined by using the full nucleotide sequence. One-way ANOVA with Dunnett's multiple hypothesis test.

All error bars denote mean $\pm$ s.e.m. ns, non-significant; *, $p<0.05$; **, $p<0.01$; ***, $p<0.001$; ****, $p<0.0001$.

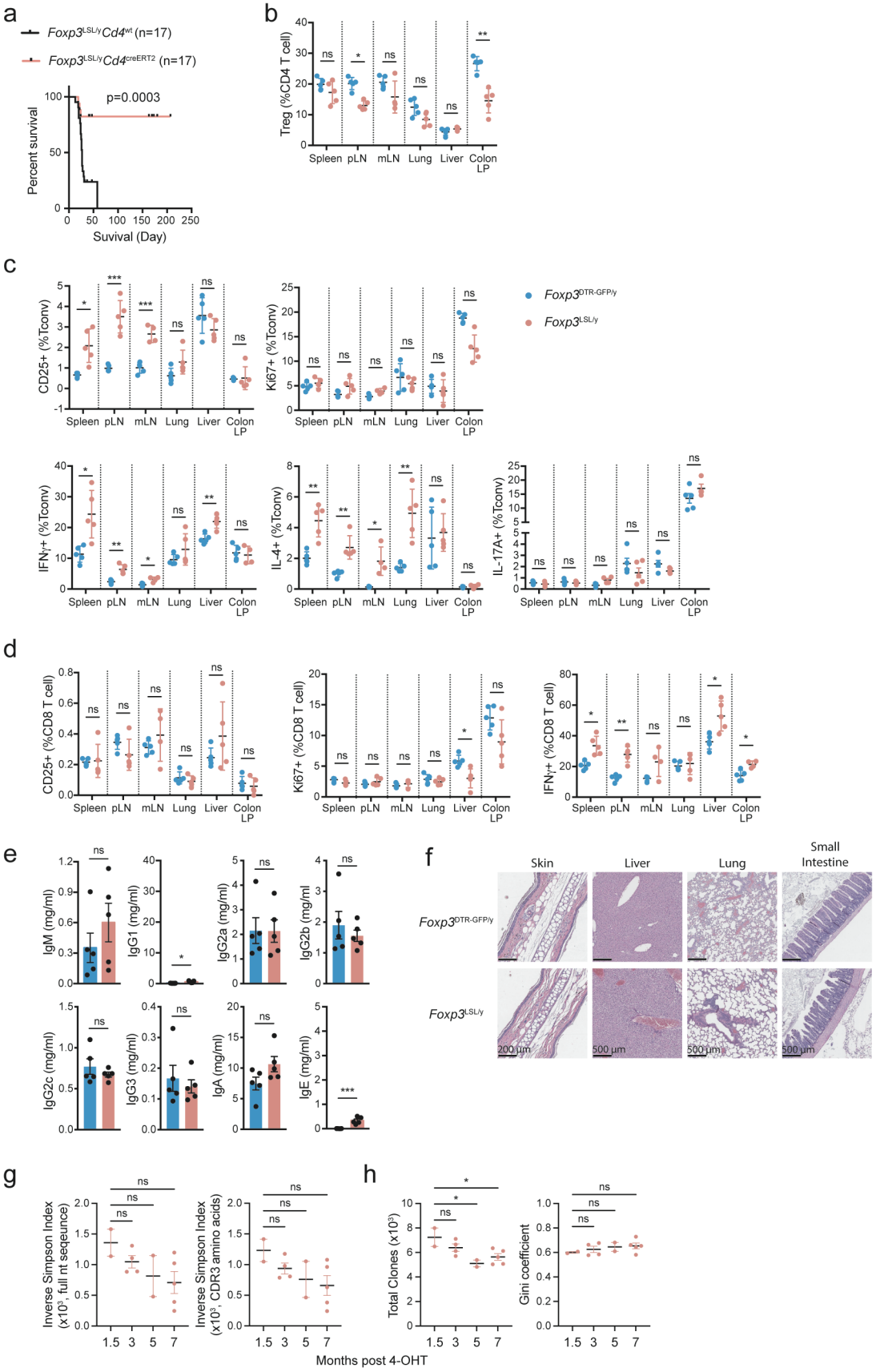
a
Foxp3LSL/yCd4wt (n=17)
Foxp3LSL/yCd4creERT2 (n=17)
p=0.0003
Percent survival
Suvival (Day)
b
Treg (%CD4 T cell)
c
CD25+ (%Tconv)
Ki67+ (%Tconv)
IFNγ+ (%Tconv)
IL-4+ (%Tconv)
IL-17A+ (%Tconv)
Foxp3DTR-GFP/y
Foxp3LSL/y
d
CD25+ (%CD8 T cell)
Ki67+ (%CD8 T cell)
IFNγ+ (%CD8 T cell)
e
IgM (mg/ml)
IgG1 (mg/ml)
IgG2a (mg/ml)
IgG2b (mg/ml)
IgG2c (mg/ml)
IgG3 (mg/ml)
IgA (mg/ml)
IgE (mg/ml)
f
Skin
Liver
Lung
Small Intestine
Foxp3DTR-GFP/y
Foxp3LSL/y
200 µm
500 µm
g
Inverse Simpson Index (x10³, full nt seqeunce)
Inverse Simpson Index (x10³, CDR3 amino acids)
Months post 4-OHT
h
Total Clones (x10³)
Gini coefficient
Spleen
pLN
mLN
Lung
Liver
Colon LP

Transcriptional features of long-lived protective Treg cells

The extraordinarily long-term protection against autoimmunity by a single cohort of self-renewing Treg cells suggests that these cells do not exhibit dysfunction typical of chronically stimulated CD4 and CD8 T cells. Thus, we sought to analyze this long-lived Treg population at single-cell resolution using single cell RNA sequencing (scRNA-seq). We compared GFP$^+$ Treg cells from *Foxp3*$^{LSL/y}$*CD4*^{creERT2}*R26*^{Tom} mice and *Foxp3*$^{DTR\text{-}GFP/y}$*CD4*^{creERT2}*R26*^{Tom} control mice 7 months after 4-OHT treatment (Fig. 2.20a). Treg cells in experimental and control mice were efficiently and comparably labeled by tdTomato shortly after 4-OHT administration (Fig. 2.20b). The percentage of tdTomato$^+$ cells among Thy1.1$^-$GFP$^+$ Treg cells in *Foxp3*$^{LSL/y}$*Cd4*^{creERT2}*R26*^{Tom} mice remained high (>80%), demonstrating their impressive persistence. However, among control *Foxp3*$^{DTR\text{-}GFP}$ Treg cells, tdTomato positivity gradually declined to ~15% at 7 months, most likely due to continuous thymic output of tdTomato$^-$ Treg cells (Fig. 2.20b).

In the scRNA-seq data analysis, we distinguished “old” and “young” control Treg cells from *Foxp3*$^{DTR\text{-}GFP/y}$*Cd4*^{creERT2}*R26*^{Tom} mice by computationally separating them into tdTomato-positive (“old”) and -negative (“young”) cells based on the expression of tdTomato transcript by the individual cells. Thy1.1$^-$GFP$^+$ Treg cells in *Foxp3*$^{LSL/y}$*Cd4*^{creERT2}*R26*^{Tom} mice, as well as tdTomato$^+$ and tdTomato$^-$ control GFP$^+$ Treg cells in *Foxp3*$^{DTR\text{-}GFP/y}$*Cd4*^{creERT2}*R26*^{Tom} mice, exhibited distinct UMAP distribution patterns (Fig. 2.20c). To better understand the most significant sources of variation among the three Treg cell populations, we performed diffusion map analysis. The first diffusion component (DC1) had a highly similar distribution

of gene expression to that of activated Treg gene signature (Fig. 2.20d). The long-lived Thy1.1^{-}GFP^{+} Treg cells had a DC1 density resembling that of tdTomato^{+} control Treg cells, both higher than that of tdTomato^{-} cells (Fig. 2.20e). This result indicates that long-lived Treg cells in *Foxp3*$^{LSL/y}$*Cd4*^{creERT2}*R26*^{Tom} and control mice tagged with tdTomato 7 month earlier and their offspring exhibited a similarly activated phenotype. Upon examining genes whose expression patterns highly correlated with DC1, we found transcripts associated with Treg activation (*Cd44*, *Sell*, *Tnfrsf18*, *Icos*, *Ctla4*), migration to non-lymphoid tissues (*Ccr4*, *Cxcr3*, *Ccr6, Itgae*), as well as tissue adaptation and suppressor function (*Maf*, *Ahr*) (Fig. 2.20f; Fig.2.21a) (98, 149). Flow cytometric analysis of CD62L (*Sell*) and CD103 (*Itgae*) expression confirmed the scRNA-seq results across multiple tissues, showing sharp reduction in CD62L^{hi} and increase in CD103^{+} cells among Treg cells in *Foxp3*$^{LSL/y}$*Cd4*^{creERT2}*R26*^{Tom} mice (Fig. 2.21b). Furthermore, the tdTomato^{+} fraction of control Treg cells were enriched for Ly6C^{-}CD103^{+} and CD44^{high}CD62L^{lo} cells, consistent with their heightened activation state (Fig. 2.21c). Despite the burden of being the sole Treg population responsible for immunosuppression, the Thy1.1^{-}GFP^{+} Treg cells did not appear less fit than their “age-matched” counterparts in control mice with continuous Treg turnover. Compared to tdTomato^{+} Treg cells in *Foxp3*$^{DTR\text{-}GFP/y}$*Cd4*^{creERT2}*R26*^{Tom} mice, Thy1.1^{-}GFP^{+} Treg cells in *Foxp3*$^{LSL/y}$*Cd4*^{creERT2}*R26*^{Tom} mice exhibited comparable expression of genes associated with T cell exhaustion and apoptosis, and similar levels of *Mcl1*, an anti-apoptotic gene critical for Treg survival (Fig. 2.20e) (150, 151). Genes involved in cell cycle progression and various metabolic pathways were also comparably

expressed by tdTomato^{+} Treg cells in *Foxp3*$^{DTR\text{-}GFP/y}$*Cd4*^{creERT2}*R26*^{Tom} mice and Thy1.1^{-}GFP^{+} Treg cells in *Foxp3*$^{LSL/y}$*Cd4*^{creERT2}*R26*^{Tom} mice (Fig. 2.21d). These shared transcriptional features highlighted the similarities in metabolic status and proliferative potential between the long-lived Treg cells in *Foxp3*$^{LSL/y}$*Cd4*^{creERT2}*R26*^{Tom} mice and "age-matched" tdTomato^{+} control *Foxp3*$^{DTR\text{-}GFP/y}$ Treg cells.

To further compare Thy1.1^{-}GFP^{+} Treg cells in *Foxp3*$^{LSL/y}$*Cd4*^{creERT2}*R26*^{Tom} mice and long-lived control cells present within the peripheral Treg pool under physiologic conditions, we performed trajectory analysis using the Palantir algorithm, which generates a high-resolution pseudotime ordering of cells at different developmental stages (152). The pseudotime gradient started from resting Treg cells, proceeded towards activated Treg cells, and ended with cells reminiscent of Treg cells residing in non-lymphoid organs in agreement with a previous report (Fig. 2.20g) (153). The analysis successfully recapitulated known gene expression dynamics during Treg activation including downregulation of *Tcf7*, *Sell*, and *Klf2,* and upregulation of *Foxp3*, *Ctla4*, and *Ikzf2* (Fig. 2.20h). Next, we compared the pseudotemporal ordering of Thy1.1^{-}GFP^{+} Treg cells from *Foxp3*$^{LSL/y}$*Cd4*^{creERT2}*R26*^{Tom} mice derived from cells whose Foxp3 expression was "restored" 7 months ago, with that of similarly "old" tdTomato^{+} and of "young" tdTomato^{-} Treg cells from control *Foxp3*$^{DTR\text{-}GFP/y}$*Cd4*^{creERT2}*R26*^{Tom} mice. Both "old" Treg populations were positioned late in the inferred differentiation trajectory in comparison to tdTomato^{-} Treg cells—consistent with their activated phenotype—and were characterized by comparably high pseudotime values (Fig. 2.20i). Thus,

Thy1.1^{-}GFP^{+} Treg cells in *Foxp3*$^{LSL/y}$*Cd4*^{creERT2}*R26*^{Tom} mice closely resembled a subset of long-lived cells present in the normal Treg cell pool under physiologic conditions.

To gain further insights into the long-term persistence of Thy1.1^{-}GFP^{+} Treg cells in *Foxp3*^{LSL}*Cd4*^{creERT2}*R26*^{Tom} mice, we performed a refined clustering analysis of the scRNA-seq dataset. Among the 13 clusters identified, clusters 0 and 3 were primarily composed of tdTomato^{-} *Foxp3*$^{DTR\text{-}GFP}$ control Treg cells, whereas clusters 1, 6, 7 and 8 were enriched for Thy1.1^{-}GFP^{+} Treg cells (Fig. 2.22a). Importantly, cells from cluster 1 had higher expression of IL-2–Stat5 and Wnt–β-catenin pathway gene signatures (Fig. 2.22b), which have been implicated in Treg cell maintenance and self-renewal (79, 154, 155). Moreover, these cells were lower in pseudotime values compared to most Thy1.1^{-}GFP^{+} Treg cells, suggesting that they were less differentiated and had the potential to give rise to the rest of the cells and sustain the Treg pool (Fig. 2.22c). Gene expression analysis revealed transcripts enriched (*Ifngr1*, *Epcam*, *Lrrc32*, *Il4ra, etc.*) and depleted (*Sell*, etc.) in cluster 1 cells (Fig. 2.22d). Using flow cytometry, we corroborated these results by demonstrating a marked enrichment of an IL-4Rα^{hi}IFNγR1^{hi}Epcam^{+}GARP^{hi}CD25^{hi} (γREG^{+}) cell subset within activated CD62L^{lo} rescued Treg population in *Foxp3*^{LSL}*Cd4*^{creERT2}*R26*^{Tom} mice (Fig. 2.23a-b, 2.24Fig. 10a-e). In normal mice, these cells were also present, albeit at lower frequencies, within Treg population in secondary lymphoid organs and at even lower frequencies in non-lymphoid tissues, such as the liver and lung, but were virtually undetectable among newly differentiated CD73^{-} thymic Treg cells (Fig. 2.23c). γREG^{+} Treg cells were enriched

in the parenchyma of highly vascularized organs such as spleen and lung, as evidenced by their higher frequencies among cells not labeled by intravenously administered CD45 antibody. This suggested that these cells were largely non-circulatory and likely contributed to local maintenance of the Treg pools (Fig. 2.24f). To compare the capacity of perinatal and adult Treg populations to give rise to γREG$^+$ Treg cells, we labeled Treg cells in healthy 2-week-old and 8-week-old *Foxp3*$^{DTR\text{-}GFP}$*Cd4*^{creERT2}*R26*^{Tom} mice by 4-OHT treatment and assessed the frequencies of γREG$^+$ Treg cells within tdTomato$^+$ and tdTomato$^-$ Treg subsets 4 months later. In mice treated as perinates, tdTomato$^+$ Treg cells harbored higher frequencies of γREG$^+$ Treg cells than their tdTomato$^-$ counterparts (Fig. 2.23d). In contrast, tdTomato$^+$ Treg cells time-stamped during adulthood were not enriched for γREG$^+$ Treg cells over their tdTomato$^-$ counterpart, and similar percentages of γREG$^+$ cells were found among tdTomato$^-$ Treg cells in perinatally labeled mice (Fig. 2.23d). These observations were independently confirmed by similar time-stamping of Treg cells in young vs. adult *Foxp3*^{creERT2}*R26*^{Tom} mice (Fig. 2.23d). These results were consistent with the enrichment of γREG$^+$ Treg cells among Treg populations in secondary lymphoid organs and non-lymphoid tissues in unmanipulated 2-week-old vs. 8-week-old mice (Fig. 2.24g). Our results suggest γREG$^+$ Treg cells, capable of persisting in peripheral lymphoid and non-lymphoid organs, are selectively overrepresented within the Treg population generated early in life.

Figure 2.20 Single-cell transcriptomic analysis of control and long-lived rescued Treg cells.

a, Experimental design. Mice were treated with 4-OHT at 2 weeks of age and Foxp3^{+} Treg cells, FACS-purified based on GFP expression, were subjected to scRNA-seq analysis using 10X Genomics platform 7 months later.

b, Percentages of fate-mapped splenic Treg cells and conventional CD4 T cells in control and rescued mice at indicated time points post 4-OHT treatment. Scatter plot shows mean ± s.e.m. Two-way ANOVA with Tukey's multiple comparison correction.

c, UMAP visualization of the single-cell transcriptomes of experimental *Foxp3*^{LSL} and control tdTomato^{-} or tdTomato^{+} *Foxp3*$^{DTR\text{-}GFP}$ Treg cells.

d, UMAP visualization colored by diffusion component 1 (DC1, left) and the expression level of activated Treg cell gene signature (right).

e, Histograms depicting the density of *Foxp3*^{LSL} and tdTomato^{+} or tdTomato^{-} *Foxp3*$^{DTR\text{-}GFP}$ Treg cells along DC1, *Mcl1* expression, and the average expression levels of indicated gene sets.

f, Correlation of curated genes with DC1.

g, UMAP visualization colored by pseudotime generated with Palantir. Arrow indicates the direction of differentiation across the map.

h, Expression of representative genes along the pseudotime trajectory.

i, Violin plots showing the pseudotime values of *Foxp3*^{LSL} and tdTomato^{+} or tdTomato^{-} *Foxp3*$^{DTR\text{-}GFP}$ Treg cells. White dots denote medians. Thick vertical bars delimit the interquartile ranges. Thin vertical lines represent upper and lower adjacent values. Histograms show distributions of the data, maxima and minima. Two-tailed *t*-test.

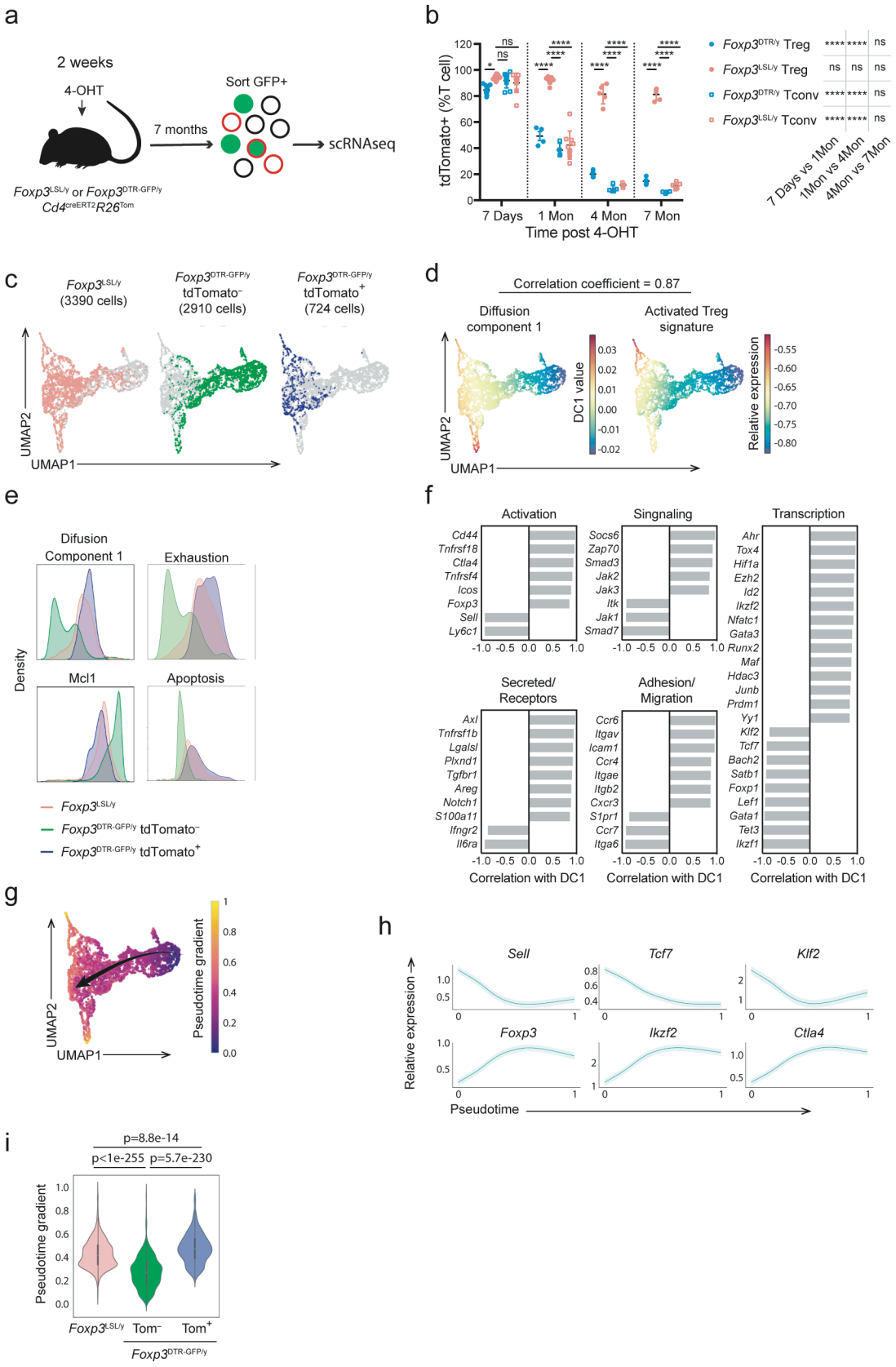
a
2 weeks
4-OHT
7 months
Sort GFP+
scRNAseq
Foxp3LSL/y or Foxp3DTR-GFP/y
Cd4creERT2R26Tom
b
tdTomato+ (%T cell)
7 Days
1 Mon
4 Mon
7 Mon
Time post 4-OHT
Foxp3DTR/y Treg
Foxp3LSL/y Treg
Foxp3DTR/y Tconv
Foxp3LSL/y Tconv
7 Days vs 1Mon
1Mon vs 4Mon
4Mon vs 7Mon
c
Foxp3LSL/y (3390 cells)
Foxp3DTR-GFP/y tdTomato- (2910 cells)
Foxp3DTR-GFP/y tdTomato+ (724 cells)
UMAP2
UMAP1
d
Correlation coefficient = 0.87
Diffusion component 1
Activated Treg signature
DC1 value
Relative expression
e
Difusion Component 1
Exhaustion
Density
Mcl1
Apoptosis
Foxp3LSL/y
Foxp3DTR-GFP/y tdTomato-
Foxp3DTR-GFP/y tdTomato+
f
Activation
Singnaling
Transcription
Secreted/ Receptors
Adhesion/ Migration
Correlation with DC1
g
Pseudotime gradient
h
Sell
Tcf7
Klf2
Foxp3
Ikzf2
Ctla4
Relative expression
Pseudotime
i
p=8.8e-14
p<1e-255
p=5.7e-230
Pseudotime gradient
Foxp3LSL/y
Tom-
Tom+
Foxp3DTR-GFP/y

Figure 2.21 Analysis of long-lived Treg cells in *Foxp3*^{LSL} and control *Foxp3*$^{DTR\text{-}GFP}$ mice.

Mice were treated with 4-OHT on postnatal day 14 and analyzed 7 months later.

a, UMAP visualization of the single-cell transcriptomes colored by imputed expression levels of representative genes.

b, Frequencies of CD62L^{hi} and CD103^{+} cells among Treg cells in rescued *Foxp3*^{LSL}*Cd4*^{creERT2} and control *Foxp3*$^{DTR\text{-}GFP}$*Cd4*^{creERT2} mice. Two-tailed multiple *t*-tests.

c, *Foxp3*^{WT}*Cd4*^{creERT2}*R26*^{Tom} mice were treated with 4-OHT on postnatal day 14 and analyzed 4 months later. Representative contour plots show expression of activation markers by tdTomato^{+} and tdTomato^{-} Foxp3^{+} CD4 T cells.

d, Histogram depicting the density of *Foxp3*^{LSL} and tdTomato^{+} or tdTomato^{-} *Foxp3*$^{DTR\text{-}GFP}$ Treg cells along the average expression values for the indicated gene sets.

All error bars denote mean ± s.e.m. ns, non-significant; *, p<0.05; **, p<0.01; ***, p<0.001; ****, p<0.0001.

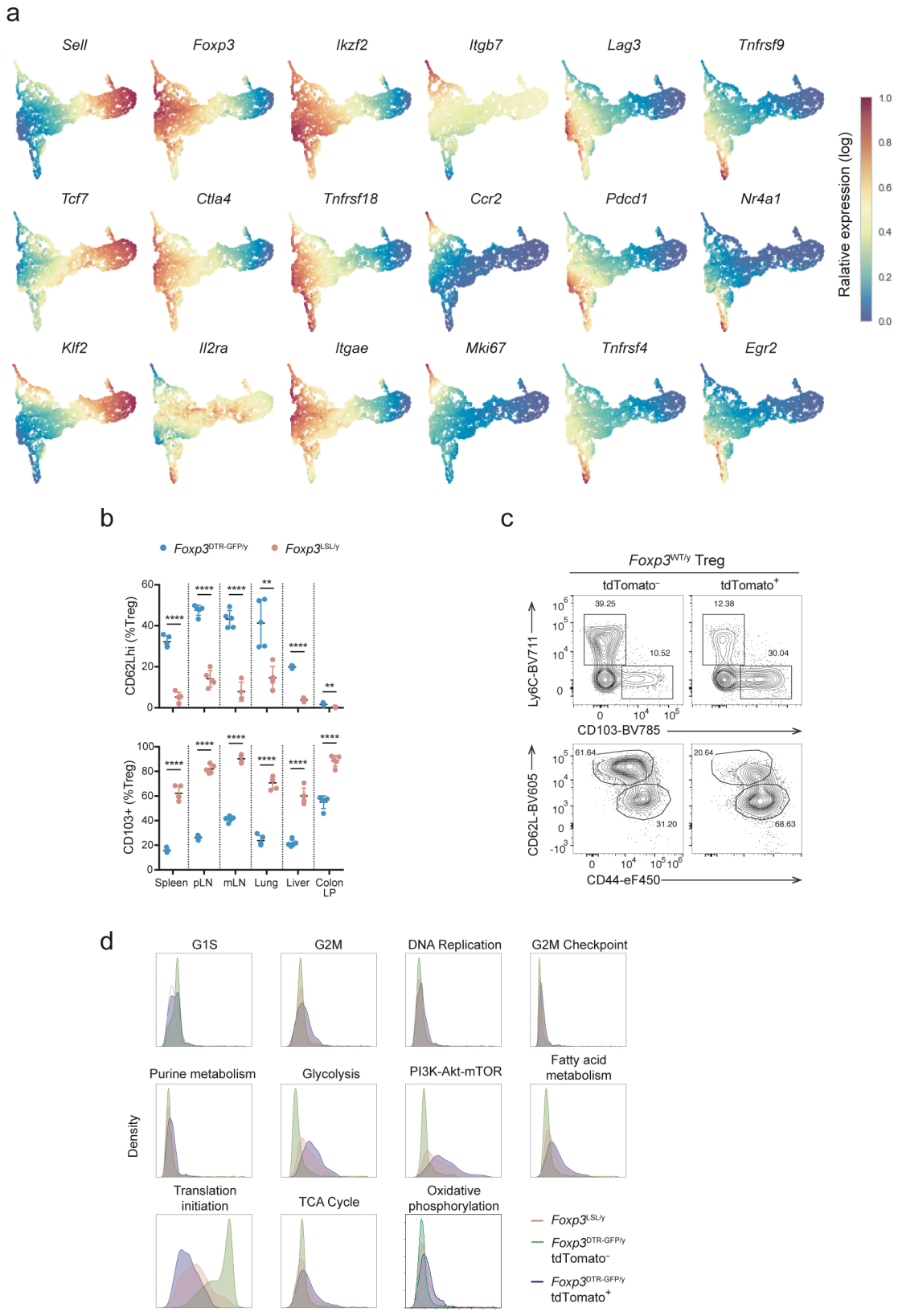
a
Sell
Foxp3
Ikzf2
Itgb7
Lag3
Tnfrsf9
Tcf7
Ctla4
Tnfrsf18
Ccr2
Pdcd1
Nr4a1
Klf2
Il2ra
Itgae
Mki67
Tnfrsf4
Egr2
Ralative expression (log)
1.0
0.8
0.6
0.4
0.2
0.0
b
Foxp3DTR-GFP/y
Foxp3LSL/y
CD62LhI (%Treg)
CD103+ (%Treg)
Spleen
pLN
mLN
Lung
Liver
Colon LP
c
Foxp3WT/y Treg
tdTomato−
tdTomato+
Ly6C-BV711
CD103-BV785
CD62L-BV605
CD44-eF450
39.25
10.52
12.38
30.04
61.64
31.20
20.64
68.63
d
G1S
G2M
DNA Replication
G2M Checkpoint
Purine metabolism
Glycolysis
PI3K-Akt-mTOR
Fatty acid metabolism
Translation initiation
TCA Cycle
Oxidative phosphorylation
Density
Foxp3LSL/y
Foxp3DTR-GFP/y tdTomato−
Foxp3DTR-GFP/y tdTomato+

Figure 2.22 Identification and analysis of γREG$^+$ Treg cells from the single-cell RNA-seq data.

a, UMAP visualization colored by the clusters. Bar graph shows the numbers of cells from each sample that contributed to the individual clusters.

b, UMAP visualization of *Foxp3*^{LSL} Treg cells colored by the Seurat module scores for the indicated gene sets.

c, Violin plots showing the pseudotime values of *Foxp3*^{LSL} Treg cells from the top 10 clusters. White dots denote medians. Thick vertical bars delimit the interquartile ranges. Thin vertical lines represent upper and lower adjacent values. Histograms show distributions of the data, maxima and minima. Horizontal bars indicate the numbers of *Foxp3*^{LSL} Treg cells contributing to each cluster.

d, Dot plot showing the expression of top enriched genes and underrepresented genes ($p<0.05$) from cluster 1 expressed by more than 20% of the cells in at least one cluster. P-values for enriched genes were calculated with two-tailed *t*-test, as used by the default parameters of Scanpy.

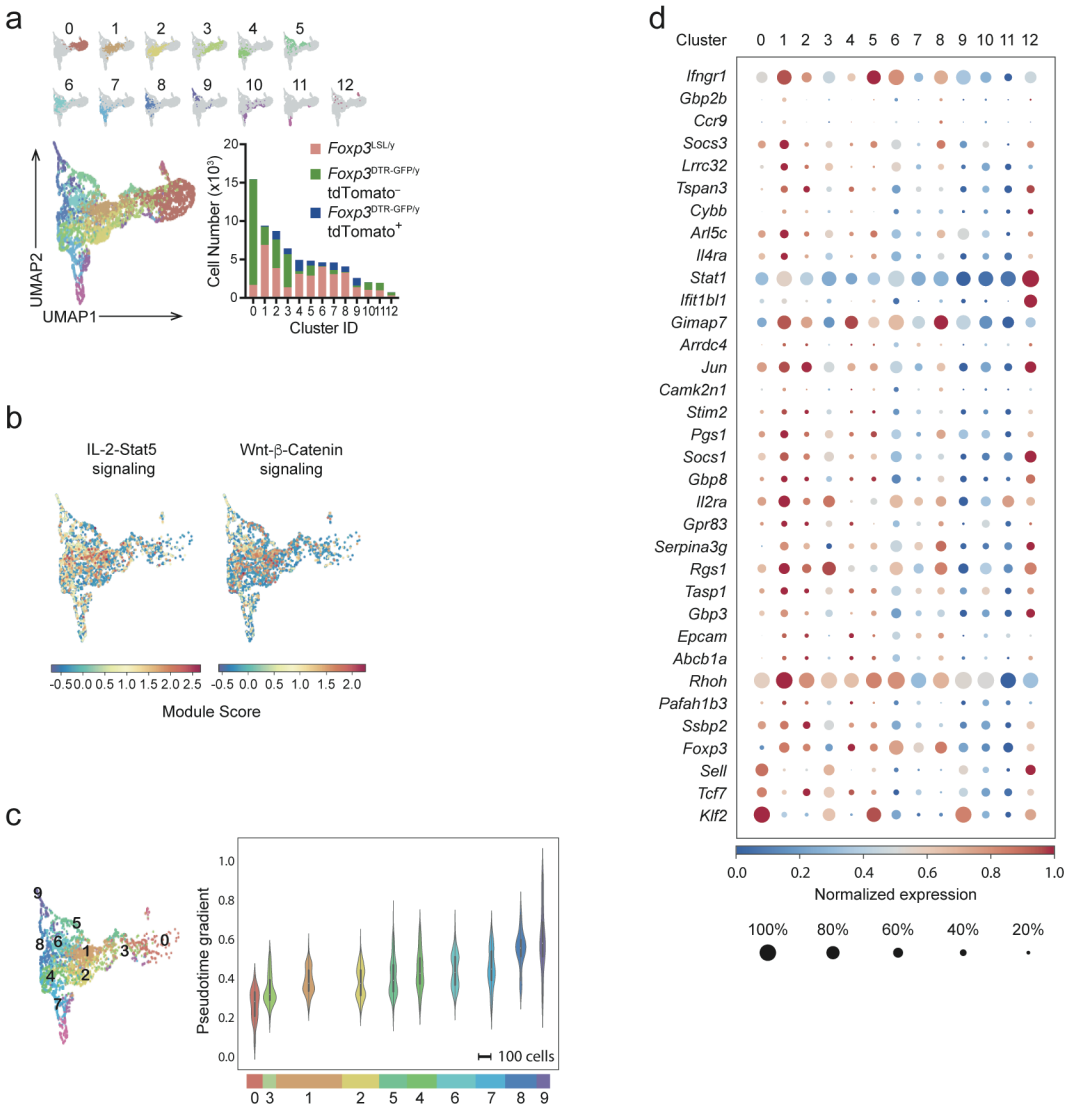
a
0 1 2 3 4 5
6 7 8 9 10 11 12
UMAP2
UMAP1
Cell Number (x10³)
Cluster ID
Foxp3LSL/y
Foxp3DTR-GFP/y tdTomato⁻
Foxp3DTR-GFP/y tdTomato⁺
b
IL-2-Stat5 signaling
Wnt-β-Catenin signaling
Module Score
c
Pseudotime gradient
100 cells
d
Cluster
Ifngr1
Gbp2b
Ccr9
Socs3
Lrrc32
Tspan3
Cybb
Arl5c
Il4ra
Stat1
Ifit1bl1
Gimap7
Arrdc4
Jun
Camk2n1
Stim2
Pgs1
Socs1
Gbp8
Il2ra
Gpr83
Serpina3g
Rgs1
Tasp1
Gbp3
Epcam
Abcb1a
Rhoh
Pafah1b3
Ssbp2
Foxp3
Sell
Tcf7
Klf2
Normalized expression
100% 80% 60% 40% 20%

Figure 2.23 Related to Figure 2.22.

a-b, Representative plots (a) and combined data (b) showing the frequencies of γREG$^+$ Treg cells among splenic CD62L^{lo} Treg cells in rescued and control mice treated with 4-OHT on postnatal day 14 and analyzed 4 months later. Two-tailed unpaired *t*-tests with Holm-Sidak multiple comparison.

c, Frequencies (left) and absolute numbers (right) of γREG$^+$ Treg cells in various tissues of unmanipulated 8-week-old *Foxp3^{GFP}* mice.

d, Percentages of γREG$^+$ Treg cells among tdTomato$^+$ or tdTomato$^-$ Treg cells "time-stamped" in adult (8-week-old) or perinatal (2-week-old) mice and analyzed after 4 months. Two-way ANOVA with Tukey's multiple comparison test.

All error bars denote mean ± s.e.m. ns, non-significant; *, $p<0.05$; **, $p<0.01$; ***, $p<0.001$; ****, $p<0.0001$. pLN, peripheral (brachial, axillary, and inguinal) lymph nodes; mLN, mesenteric lymph nodes; PB, peripheral blood; cLP, colonic lamina propria.

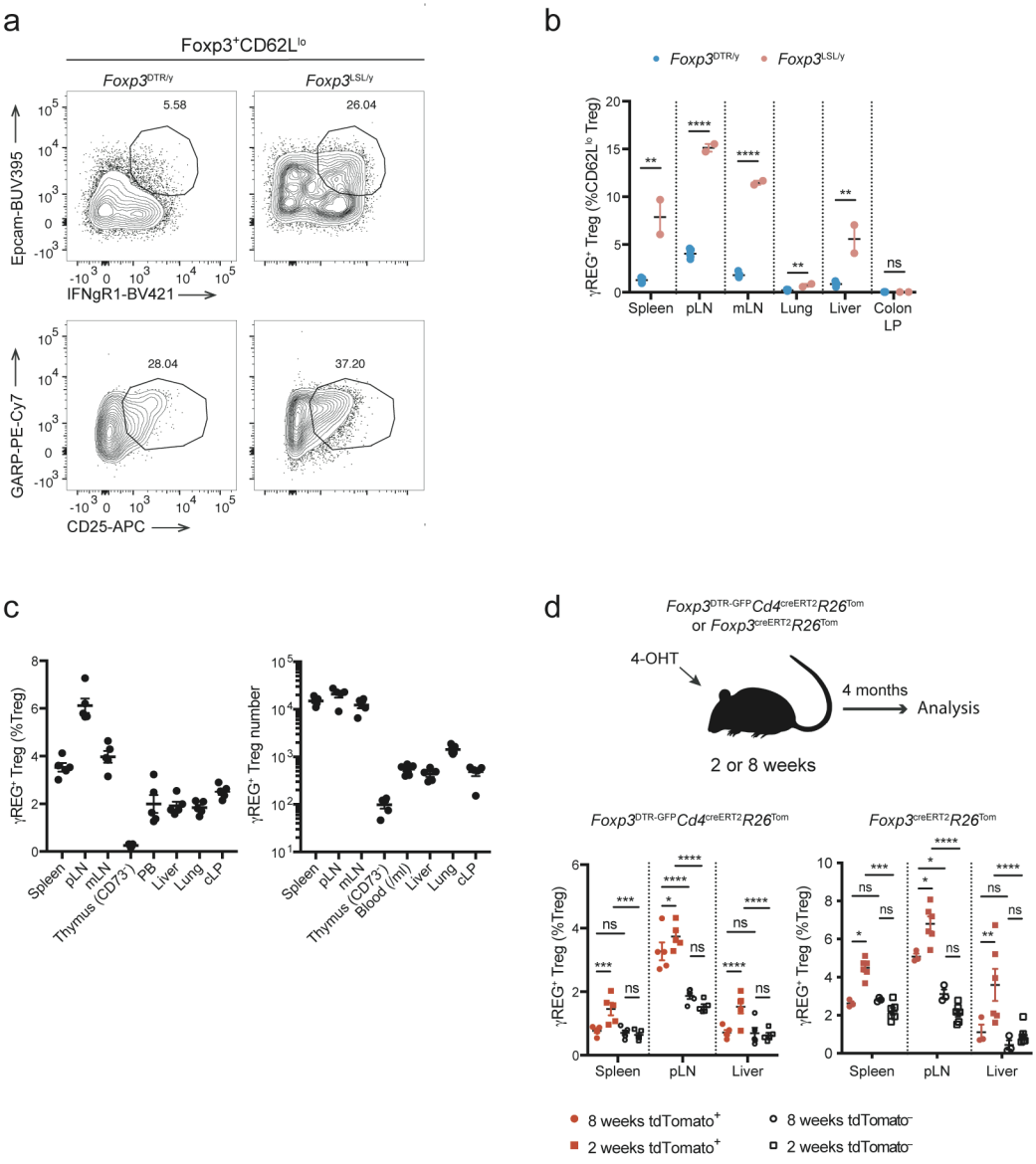
a
Foxp3+CD62Llo
Foxp3DTR/y
Foxp3LSL/y
5.58
26.04
28.04
37.20
Epcam-BUV395
IFNgR1-BV421
GARP-PE-Cy7
CD25-APC
b
Foxp3DTR/y
Foxp3LSL/y
γREG+ Treg (%CD62Llo Treg)
Spleen
pLN
mLN
Lung
Liver
Colon LP
c
γREG+ Treg (%Treg)
γREG+ Treg number
Spleen
pLN
mLN
Thymus (CD73-)
PB
Liver
Lung
cLP
Blood (/ml)
d
Foxp3DTR-GFPCd4creERT2R26Tom
or Foxp3creERT2R26Tom
4-OHT
4 months
Analysis
2 or 8 weeks
Foxp3DTR-GFPCd4creERT2R26Tom
Foxp3creERT2R26Tom
γREG+ Treg (%Treg)
Spleen
pLN
Liver
8 weeks tdTomato+
2 weeks tdTomato+
8 weeks tdTomato-
2 weeks tdTomato-

Figure 2.24 Flow cytometric analysis of γREG$^+$ Treg cells.

a, Gating strategy for γREG$^+$ Treg cells in adult mice.

b, c, Representative histogram (b) and quantification (c) of IL-4Rα expression in γREG$^+$ and other Treg cell populations identified in a. Two-way ANOVA with Tukey's multiple comparison correction.

d, e, Representative histogram (d) and quantification (e) of CD25 expression in γREG$^+$ and other Treg cell populations identified in a. Two-way ANOVA with Tukey's multiple comparison correction.

f, Percentages of γREG$^+$ Treg cells in lymphoid organs and non-lymphoid tissues of CD45 i.v.-labeled 8-10-wk-old *Foxp3*^{GFP} mice. One-way ANOVA with Sidak's multiple comparison test.

g, Percentages (left) and numbers (right) of γREG$^+$ Treg cells in different organs of 2- or 8-wk-old *Foxp3*$^{GFP\text{-}BirA\text{-}AVI\text{-}TEV}$ mice. Two-sided unpaired *t*-tests with correction for multiple hypothesis testing using the Holm-Sidak method.

All error bars denote mean ± s.e.m. ns, non-significant; *, $p<0.05$; **, $p<0.01$; ***, $p<0.001$; ****, $p<0.0001$.

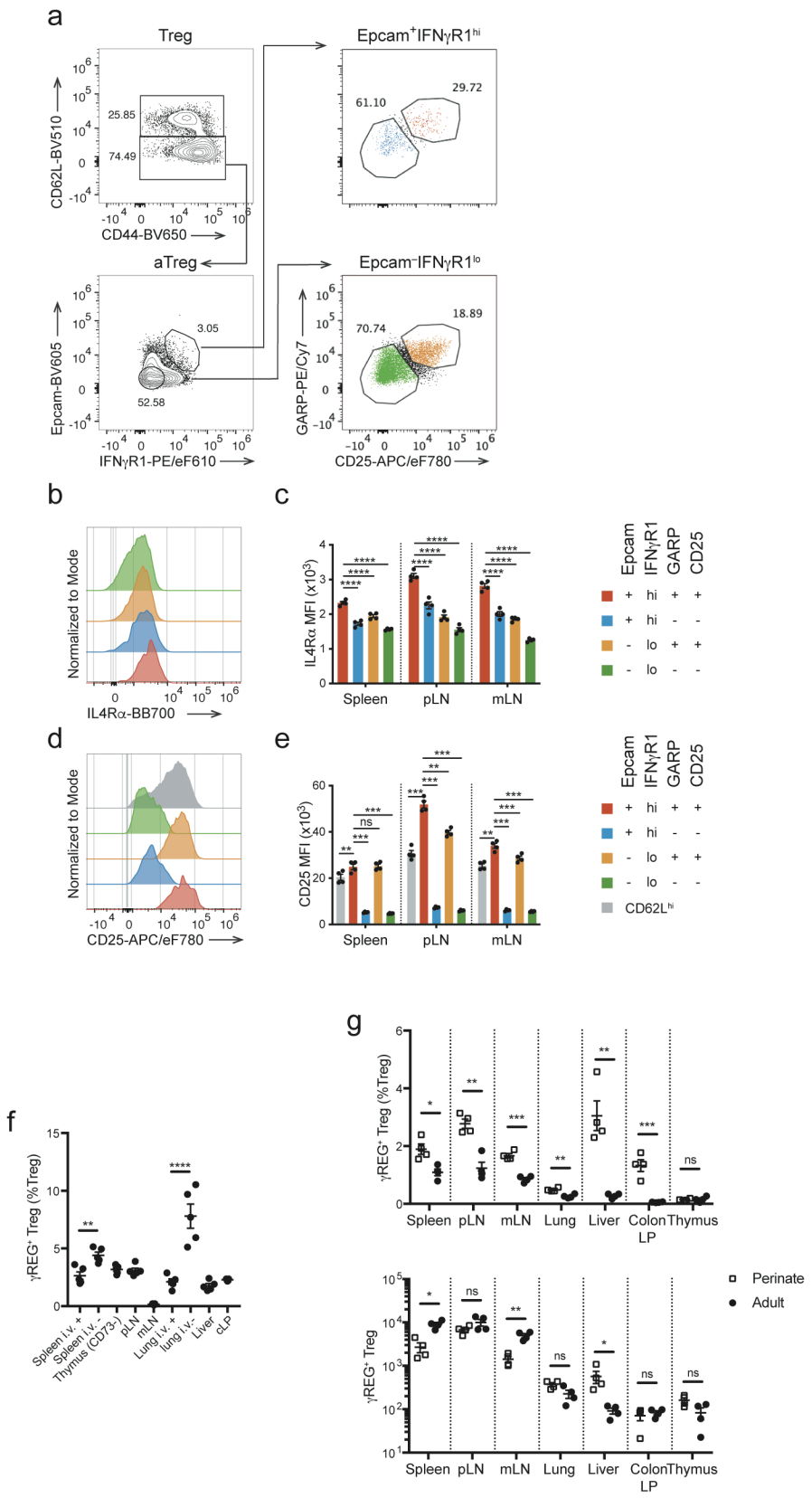
a
Treg
Epcam+IFNγR1hi
CD62L-BV510
CD44-BV650
25.85
74.49
61.10
29.72
aTreg
Epcam-IFNγR1lo
Epcam-BV605
IFNγR1-PE/eF610
3.05
52.58
GARP-PE/Cy7
CD25-APC/eF780
70.74
18.89
b
Normalized to Mode
IL4Rα-BB700
c
IL4Rα MFI (x10³)
Spleen
pLN
mLN
Epcam
IFNγR1
GARP
CD25
d
Normalized to Mode
CD25-APC/eF780
e
CD25 MFI (x10³)
CD62Lhi
f
γREG+ Treg (%Treg)
Spleen i.v. +
Spleen i.v. -
Thymus (CD73-)
pLN
mLN
Lung i.v. +
lung i.v.-
Liver
cLP
g
γREG+ Treg (%Treg)
γREG+ Treg
Spleen
pLN
mLN
Lung
Liver
Colon LP
Thymus
Perinate
Adult

Discussion

The adaptive immune system is characterized by unlimited antigen recognition specificity, amplification of innate immune responses, novel effector functions, and memory formation, affording vertebrates with a versatile anticipatory defense against rapidly evolving infectious agents. This superior protection is confounded by a major fitness constraint due to the threat of autoimmune inflammation posed by the inherent self-reactivity of T cells. The importance of Treg cells in forestalling autoimmunity has been most vividly demonstrated by wide-ranging clinical manifestations of human monogenic disorders resulting from Treg deficiency or dysfunction due to *FOXP3*, *STAT5B, IL2RA,* and *LRBA* mutations or *CTLA4* haplo-insufficiency (126, 127). In IPEX patients, these manifestations include endocrinopathies (diabetes, thyroiditis, pancreatitis, adrenal dysfunction), hepatitis, enteropathies (autoimmune gastritis, IBD, celiac disease), skin disorders (exudative dermatitis, alopecia), food allergy, hyper-IgE syndrome, autoimmune hematologic disorders (autoimmune thrombocytopenia, hemolytic anemia), myelo- and lymphoproliferation (splenomegaly, lymphadenopathy), polyneuropathy, as well as pulmonary and nephrotic syndromes (128). In mice, Treg deficiency or depletion causes equally widespread and fatal autoimmune inflammatory disease (22).

However, the potent immunosuppressive function of Treg cells indispensable for preventing autoimmune inflammation can in turn compromise protective immunity against infections. This provided rationale for the concept that Treg cells are ineffectual in the inflammatory settings of infections. Indeed,

numerous studies showed that infection-associated inflammatory milieu can cause downregulation of Foxp3 expression by Treg cells, impede their suppressor and proliferative capacity, or even confer pro-inflammatory properties, i.e. effector cytokine production; furthermore, pro-inflammatory cytokines, IL-6 and IL-1 in particular, can make effector cells refractory to Treg-mediated suppression. On the other hand, some studies suggested that Treg cells are capable of modulating virus-specific immune responses and limiting associated pathologies (24, 26, 28, 29, 31, 32). In all these studies, however, Treg cells were present from the onset of infection, making it impossible to discriminate their activity prior to, or after the onset of infection-induced inflammation (40-45). Thus, the ability of Treg cells to function in infection-induced inflammation remains an open question.

Since inflammation elicited by various infectious, metabolic, and genetic causes, including Treg deficiency, shares principal cellular and soluble mediators, a corollary to the above concept is the notion that in established autoimmune inflammation, Treg activity is also expected to be severely attenuated or even lacking. In this regard, autoimmune and inflammatory pathologies were reported to exert varying effects on Treg numbers. In contrast to the aforementioned monogenic Treg deficiency-linked disorders, many studies of polygenic autoimmune diseases have found unchanged or even increased frequencies of Treg cells at inflammatory sites and in circulation (156). Meanwhile, analyses of Treg cells isolated from autoimmune patients suggested that their function is impaired in the inflammatory environment (33-35, 156-158). However, considering numerous genetic polymorphisms linked to the pathophysiological manifestations

of polygenic autoimmune diseases, the reported inferior Treg functionality can be one of these sequelae. Indeed, an enrichment for such autoimmunity-associated single nucleotide polymorphisms has been observed within Treg-specific cis-regulatory elements (138, 159, 160). As a potential counterargument to the above findings, adoptive transfer of Treg cells after the initiation of T cell-induced colitis was shown to cause its amelioration over time in an IL-10-dependent manner, highlighting their potential to control local inflammation elicited upon homeostatic expansion of a relatively small number of naïve CD4 T cells in lymphopenic mice (38, 39). Thus, it remained possible that the reparative activity of Treg cells observed in this setting may be specific to the colon aided by its continuous epithelial cell turnover, or particular to the adoptive transfer model.

By genetically introducing a limited Treg pool in *Foxp3*^{LSL} mice, we demonstrated that Treg cells are able to function in settings of systemic autoimmune inflammation, reverse the fatal disease and tissue pathology, and offer long-term protection. The reversal of inflammation was not a simple diversion of a large number of pro-inflammatory effector T cells into Treg cells because indistinguishable fatal autoimmunity observed in Foxp3-deficient mice harboring Treg “wannabes” and *Foxp3*^{DTR} neonates subjected to chronic ablation of Treg cells suggests that Treg “wannabes” do not provide notable non-redundant contribution to the disease progression (17, 22, 136). It is noteworthy that upon generation of functional Treg cells in *Foxp3*^{LSL} mice, the reduction in myeloid cells was observed with a markedly slower kinetics than the decrease in activated T cell numbers and responses, suggesting that the reversal of myelo-proliferation was

largely an indirect effect of suppression of T cell activation. Nevertheless, a parallel direct suppression of myeloid cell activation and survival by Treg cells may also contribute to the recovery of *Foxp3*^{LSL} mice from autoimmunity. The ability of Treg cells to suppress established inflammation was not limited to young mice but was also observed in adult animals. Notably, Treg cells introduced into the inflammatory environment suppressed Th2 autoimmunity and associated increased serum IgG1 and IgE levels, as efficiently as Th1 and Th17 responses, even though Th2 responses are known to be the most sensitive to diminished Treg numbers or functionality (20, 140).

The observed normalization of lympho- and myeloproliferation, acute phase response, and reversal of tissue inflammation highlighted the ability of Treg cells to function in a cytokine storm. Rather than impeding functionality, we found that exposure to this highly inflammatory milieu endowed the newly generated Treg cells with heightened suppressor activity in comparison to Treg cells from healthy control mice, while the latter and Treg cells generated upon a similar conversion of Treg “wannabes” in healthy heterozygous female mice had indistinguishable suppressor activity. Treg cells employ multiple and partially redundant modes of suppression, including secreted immunomodulatory factors, IL-2 consumption, and ATP-to-adenosine conversion, and may directly partake in tissue regeneration and repair via the production of amphiregulin (47, 161). Accordingly, redeemed Treg cells in *Foxp3*^{LSL} mice exhibited increased expression of IL-2R, IL-10, galectin-1 and -3, Fgl2, CTLA4, CD39, ST2, and amphiregulin. While we cannot unambiguously pinpoint the inflammation-sensing pathways responsible for the

potentiation of their function, prominent STAT5 activation gene signature in these cells implicates common γ chain receptor signaling cytokines including IL-2. Accordingly, administration of therapeutic IL-2 formulations and expression of an active form of STAT5b in Treg cells promote their expansion and superior suppressor function (87, 162, 163). Notably, the observed suppressor activity of Treg cells in inflammatory settings was not limited to recent thymic emigrants as efficient suppression of autoimmunity in systemically inflamed mice was observed upon pharmacological thymic export blockade. The reversal of inflammatory disease and long-term maintenance of health by a single pool of Treg cells was enabled by its stability, which may be aided by a subset of preferentially tissue-residing cells with increased expression of IFNγR, IL-4Rα, EpCAM, CD25, and GARP. Based on gene set enrichment and pseudo-time analyses, these cells may contribute to long-term Treg maintenance by giving rise to terminally differentiated progenies locally. Interestingly, time-stamped “old” peripheral Treg population in lymph nodes of adult mice was enriched for γREG$^+$ Treg cells in comparison to other sites such as the spleen or liver, raising the possibility of specific niches that favor their generation or maintenance.

Collectively, we show that Treg cells can function in established severe inflammation and reverse all known types of inflammation, and that a single cohort of Treg cells can afford long-lasting protection against autoimmunity. Our findings provide general rationale and support for the emerging efforts to develop adoptive Treg therapy not only for intrauterine and neonatal IPEX syndrome and other

monogenic Treg deficiencies, but also for a broad spectrum of autoimmune and inflammatory disorders.

Methods

Mice

Experiments in this study were approved by the Sloan Kettering Institute (SKI) Institutional Animal Care and Use Committee under protocol 08-10-023 and conducted in compliance with institutional ethics guidelines. Mice were housed at the SKI animal facility under SPF conditions on a 12-hour light/dark cycle with free access to water and regular chow diet. The average ambient temperature is 21.5°C and the average humidity is 48%. All control and experimental animals were age-matched, and littermates were used as controls unless otherwise indicated. Age, sex, and numbers of animals used in each experiment are indicated in the respective Figure Legends.

Foxp3$^{\text{DTR-GFP}}$ (22), Foxp3$^{\text{GFP}}$ (19), *Foxp3*$^{\text{creERT2}}$ (164), *Foxp3*$^{\textit{GFP-BirA-AVI-TEV}\text{ly}}$ (in preparation), *Cd4*$^{\text{creERT2}}$ (165), *Tcrb*$^{-/-}$*Tcrd*$^{-/-}$ (166) and *Rosa26*$^{\text{LSL-}\textit{td}\text{Tom}\textit{ato}}$ (167) mice were maintained in the Sloan Kettering Institute animal facility. The *Rosa26*$^{\text{LSL-}\textit{td}\text{Tom}\textit{ato}}$ allele was bred to homozygosity for fate mapping studies.

Generation of *Foxp3*$^{\text{LSL}}$ mice

The targeting construct was made by first subcloning an 8.5 kb *SphI* fragment harboring the *Foxp3* genomic sequence from exon -1a to exon 7 obtained from the RP23-143D8 cosmid into a cloning vector carrying a Pgk-DTA-polyA cassette allowing for negative selection of random genomic integration. The FRT-PGK-neo-polyA-FRT positive selection cassette was then cloned into the *DraIII*

site within the intron between exons -1b and 1, and the loxP-Thy1.1 coding sequence-triple-tandem SV40 polyA-eGFP coding sequence cassette was cloned into the *AvrII* site within exon 1. The Thy1.1 and eGFP sequences are preceded by a start codon (ATG). The targeting construct was then electroporated into albino C57BL/6 ES cells. After neomycin selection, Southern blotting and karyotyping, correctly targeted clones were injected into WT C57BL/6 blastocysts. The resulting chimeric mice were bred to albino C57BL/6 mice. Founders identified based on the coat color and genotyping were mated to a Flp deleter strain of mice to remove the neo cassette.

4-hydroxytamoxifen, diphtheria toxin, tamoxifen, and FTY720 treatment

4-hydroxytamoxifen (4-OHT, Sigma-Aldrich, H7904) stock solution was made by reconstituting in ethyl alcohol 200 proof (Sigma-Aldrich, E-7023) at a concentration of 20 mg/mL, then diluting 1:1 (v/v) with Cremophor EL (Sigma-Aldrich, 238470). 20 μg/g body weight of 4-OHT diluted in PBS was administered intraperitoneally.

Diphtheria toxin (DT, List Biological Laboratories, 150) was dissolved in PBS. 1μg (first dose) or 250 ng (subsequent doses) was injected intraperitoneally for each mouse. For tamoxifen administration, 20 mg of tamoxifen (Sigma-Aldrich, T5648) was resuspended in 1 mL corn oil (Sigma-Aldrich, C8267) by rotating and tilting at 37°C until fully dissolved. Each mouse was orally gavaged with 4 mg of tamoxifen per treatment.

4-OHT was used whenever possible because it bypasses the conversion of tamoxifen to 4-hydroxytamoxifen in the liver. Compared to tamoxifen, 4-OHT offers

a much sharper pharmacokinetics and enables a highly synchronized labeling of cells. In addition, 4-OHT has a much shorter half-life than tamoxifen, particularly in adults. Therefore, tamoxifen instead of 4-OHT was used for *in vivo* suppression assays (Extended Data Fig. 1g) and in studies of adult female mice (Fig. 2, Fig. 3 h-j, and Extended Data Fig. 5) to achieve sufficient recombination of the *Foxp3*^{LSL} allele.

FTY720 (Sigma-Aldrich, SML0700-5MG) stock solution was made by reconstituting in dimethyl sulfoxide (Sigma-Aldrich, D8418-250ML) at a concentration of 20 mg/ml. 0.8 μg/g body weight of FTY720 diluted to 0.1 mg/ml in 2% β-hydroxypropanylcyclodextrin (Sigma-Aldrich, H5784-10ML) was administered intraperitoneally.

Reagents and antibodies

The following antibodies and streptavidin were used in this study for flow cytometry, with clones, venders, catalog numbers, and dilutions indicated in the parentheses: anti-Siglec-F (E50-2440, BD, 562681, 400), anti-I-A/I-E (M5/114.15.2, BioLegend, 107641, 1000), anti-NK1.1 (PK136, ThermoFisher, 47-5941-82, 200), anti-CD45 (30-F11, BioLegend, 103136, 600), anti-CD11b (M1/70, BioLegend, 101257, 800), anti-CD3ε (17A2, BioLegend, 100237, 500), anti-Ly-6C (HK1.4, BioLegend, 128037, 1000), anti-CD90.2 (30-H12, BioLegend, 105331, 1000), anti-Foxp3 (FJK-16s, ThermoFisher, 17-5773-82, 400), anti-CD19 (6D5, BD, 563557, 400), anti-Ly-6G (1A8, BioLegend, 127618, 500), anti-TCRβ (H57-597, ThermoFisher, 61-5961-82, 400), anti-F4|80 (BM8, ThermoFisher, 61-4801-82, 200), anti-CD90.1 (HIS51, ThermoFisher, 17-0900-82, 200), anti-CD4 (RM4-5,

BioLegend, 100553, 400), anti-CD8α (53-6.7, BioLegend, 100759, 400), anti-GITR (DTA-1, ThermoFisher, 48-5874-82, 400), anti-CD73 (TY/11.8, BioLegend, 127215, 400), anti-CD44 (IM7, BD, 563971, 400; ThermoFisher, 48-0441-82, 400; BioLegend, 103049, 400), anti-CD103 (M290, BD, 564322, 200), anti-CD62L (MEL-14, BioLegend, 104438, 1600; BioLegend, 104441, 400), anti-CTLA4 (UC10-4B9, BioLegend, 106314, 600), anti-Helios (22F6, BioLegend, 137218, 400), anti-Ki-67 (16A8, BioLegend, 652420, 400), anti-CD25 (PC61.5, ThermoFisher, 47-0251-82, 400; ThermoFisher, 17-0251-82, 400), anti-PD-1 (29F.1A12, BioLegend, 135225, 400), anti-ICOS (7E.17G9, ThermoFisher, 12-9942-82, 400), anti-CD45.1 (A20, BioLegend, 110738, 100), anti-CD45.2 (104, BD, 612778, 200), anti-IL-2 (JES6-5H4, BioLegend, 503818, 400), anti-IL-17A (17B7, ThermoFisher, 48-7177-82), anti-IFNγ (XMG1.2, ThermoFisher, 17-7311-82, 500), anti-IL-4 (BVD6-24G2, ThermoFisher, 25-7042-82, 400), anti-GARP (YGIC86, ThermoFisher, 25-9891-82, 200), anti-CD119 (2E2, BD, 550482, 100; GR20, BD, 740032, 100), anti-EpCAM (G8.8, BioLegend, 118227, 100; BD, 740281, 100), anti-CD124 (mIL4R-M1, BD, 742172, 100), anti-TCR Vβ5.1, 5.2 (MR9-4, BioLegend, 139508, 400), anti-TCR Vβ6 (RR4-7, ThermoFisher, 46-5795-82, 300), anti-TCR Vβ8 (F23.1, BD, 553860, 400), streptavidin (BioLegend, 405225, 4000; ThermoFisher, 61-4317-82, 4000), anti-CD45R/B220 (RA3-6B2, ThermoFisher, 47-0452-82, 400).

The following antibodies were used to capture antigens for ELISA in this study: purified anti-mouse IgE (R35-72, BD Pharmingen, 553413), Goat Anti-Mouse IgG1 (RRID: AB_2794408, SouthernBiotech, 1070-01), Goat Anti-Mouse

IgG3 (RRID: AB_2794567, SouthernBiotech, 1100-01), Goat Anti-Mouse IgG2a (RRID: AB_2794475, SouthernBiotech, 1080-01), Goat Anti-Mouse IgG2b (RRID: AB_2794517, SouthernBiotech, 1090-01), Goat Anti-Mouse IgG2c (RRID: AB_2794464, SouthernBiotech, 1079-01), Goat Anti-Mouse IgA (RRID: AB_2314669, SouthernBiotech, 1040-01), Goat Anti-Mouse IgM (RRID: AB_2794197, SouthernBiotech, 1020-01), Mouse Pentraxin 2/SAP Antibody (R & D Systems, MAB2558).

The following antibodies were used to detect antigens for ELISA in this study: Goat Anti-Mouse Ig-HRP (RRID: AB_2728714, SouthernBiotech, 1010-05), Biotin Rat Anti-Mouse IgE (R35-118, BD Pharmingen, 553419), Biotinylated Pentraxin 2/SAP Antibody (R & D Systems, BAF2558).

The following reagents were used to construct standard curves for ELISA in this study: Purified Mouse IgE, kappa, Isotype Control (C38-2, BD Pharmingen, 557079), Purified Mouse IgA, kappa, Isotype Control (M18-254, BD Pharmingen, 553476), Purified Mouse IgG3, kappa, Isotype Control (A112-3, BD Pharmingen, 553486), Purified Mouse IgG1, kappa, Isotype Control (15H6, SouthernBiotech, 0102-01), Purified Mouse IgG2a, kappa, Isotype Control (UPC-10, Sigma, M5409), IgM Isotype Control from murine myeloma (MOPC 104E, Sigma, M5909), IgG2b Isotype Control from murine myeloma (MOPC-141, Sigma, M5534), Mouse IgG2c (6.3, RRID: AB_2794064, SouthernBiotech, 0122-01), Recombinant Mouse Pentraxin 2 (R & D Systems, 2558-SA-050).

Enzyme-linked immunosorbent assay (ELISA)

ELISA experiments were conducted as previously described (71). Briefly, mouse peripheral blood was collected via cardiac puncture immediately after euthanasia into BD SST microcontainer tubes (02-675-185) and sera were harvested after centrifugation. Flat-bottom 96-well plates were coated with capturing antibodies in 50 μL 0.1 M $NaHCO_3$ solution at pH 9.5 O/N at 4°C. The plates were then emptied, blocked with 200 μL 1% bovine serum albumin (VWR, 97061-422) in PBS, and washed 3 times with PBS containing 0.05% Tween-20 (Sigma-Aldrich, P1379). 50 μL of sera at appropriate dilutions was added and incubated O/N at 4°C. The plate was then incubated in sequential orders with 50 μL of biotinylated detection antibodies for 2-3 hours, 50 μL of avidin-HRP (ThermoFisher, 18-4100-51) for 30 minutes, and 100 μL of TMB solution (ThermoFisher, 00-4201-56) at 25°C, with 3-4 washes with PBS-Tween in between each incubation steps. The colorimetric reaction was stopped with 100 μL of 1M H_3PO_4 (Sigma-Aldrich, P5811) after 5-10 minutes of adding TMB and absorbance at 450 nm was measured with a Synergy HTX plate reader (BioTek). Concentrations of antigens were determined using standard curves constructed with purified recombinant proteins and calculated with Gen5 3.02.2 (BioTek).

Isolation of cells from lymphoid organs, livers, lungs, and colonic lamina propria

For flow cytometric analyses, animals were perfused with a total of 20 mL PBS into both left and right ventricles immediately after euthanasia. Cells were retrieved from spleens, peripheral (brachial, axillary, and inguinal) lymph nodes, mesenteric lymph nodes, thymuses, and livers by meshing the organs through a 100 μm strainer (Corning, 07-201-432) with a syringe plunger. Cells in the colonic

lamina propria were isolated as previously described (119). Briefly, colons were cleaned by flushing the luminal content out with PBS using a syringe, defatted, opened up longitudinally and diced into 1-2 cm pieces. Tissues were then incubated in 25 mL IEL solution [1x PBS w/ 2% FBS (ThermoFisher, 35010CV), 10 mM HEPES buffer (ThermoFisher, MT 25–060-CI), 1% penicillin/streptomycin (ThermoFisher, MT 30–002-CI), 1% L-glutamine (ThermoFisher, MT 25–005-CI), plus 1 mM EDTA (Sigma-Aldrich, E4884) and 1 mM DTT (Sigma-Aldrich, D9779) added immediately before use] for 15 minutes at 37°C with vigorous shaking (250 rpm) to remove the epithelial fraction. Tissues were then retrieved, washed extensively, and digested in 25 mL LPL solution [1x RPMI 1640 w/2% FBS, 10 mM HEPES buffer, 1% penicillin/streptomycin, 1% L-glutamine, 0.2 U/mL collagenase A (Sigma, 11088793001) and 1 U/mL DNase I (Sigma-Aldrich, 10104159001)] for 30 minutes at 37°C with vigorous shaking (250 rpm). ¼inch ceramic beads (MP Biomedicals, 116540034) were added during this step (3–4 per sample) to facilitate tissue dissociation. The digested samples were passed through a 100 μm strainer, pelleted at 450 g for 5 minutes and washed extensively. Lungs were digested in the same fashion as the lamina propria fraction of the colons but for 45 minutes. Cells from non-lymphoid organs were centrifugated in 40% PBS-adjusted Percoll (v/v, ThermoFisher, 45–001-747) in PBS to enrich for lymphocytes. Erythrocytes in the spleen, lung, and liver samples were lysed with ACK lysis buffer [150 mM NH_4Cl (Sigma-Aldrich, A9434), 10 mM $KHCO_3$ (Sigma-Aldrich, P7682), 0.1 mM Na_2EDTA, pH 7.4].

For fluorescence-activated cell sorting, cell suspension was made from pooled secondary lymphoid organs (spleen; peripheral and mesenteric lymph nodes) as above and CD4 T cells were enriched with the Dynabeads Flowcomp Mouse CD4 Kit (ThermoFisher, 11461D) according to manufacturer's instructions, stained with antibodies, washed extensively, resuspended in isolation buffer (PBS w/ 2% FBS, 10 mM HEPES buffer, 1% L-glutamine, and 2 mM EDTA) containing 0.01% SYTOX Blue dead cell stain (ThermoFisher, S34857) to facilitate dead cell exclusion, and sorted on a FACSAria (BD) instrument. Treg cells ($TCR\beta^+CD4^+CD8^-NK1.1^-Foxp3^+Thy1.1^-$), Treg "wannabes" ($TCR\beta^+CD4^+CD8^-NK1.1^-Thy1.1^+Foxp3^-$) and naïve conventional CD4 T cells ($TCR\beta^+CD4^+CD8^-NK1.1^-Foxp3^-Thy1.1^-CD44^{lo}CD62L^{hi}$) were sorted by gating on the respective populations.

Histology and TUNEL assay

Sample embedding, sectioning, haematoxylin and eosin staining, pathology grading, and TUNEL (terminal deoxynucleotidyl transferase dUTP nick end labeling) assay were conducted at HistoWiz (Brooklyn, NY). Tissues were fixed in 10% neutral buffered formalin and embedded in paraffin before sectioned into 5-micron slices. Lymphocytic and acute (neutrophils) or chronic (monocytes) myeloid inflammation was blindly scored with the following criteria: 0-normal, 1-mild increase, 2-moderate increase, 3-medium increase, 4-sever increase.

For TUNEL assay, liver sample sections were processed under standardized conditions using the DeadEnd Fluorometric Detection System (Promega, G3250), and subsequent immunohistochemistry was carried out using

BOND Polymer Refine Detection Kit (Leica, DS9800) according to manufacturers' instructions. $TUNEL^+$ cells were quantified with ImageJ v2.0.0-rc-69/1.52p.

Measurement of serum albumin

Serum albumin level was measured by Laboratory of Comparative Pathology, SKI, using the Albumin kit (Beckman Coulter, OSR6102), according to manufacturer's instruction.

Flow cytometric analysis of cytokine production

To measure cytokine production after *ex vivo* restimulation, single cell suspensions were incubated at 37°C for 3-4 hours with 5% CO_2 in 96-well flat-bottom plates in the presence of 50 ng/mL phorbol-12-myristate-13-acetate (PMA, Sigma-Aldrich, P8139) and 500 ng/mL ionomycin (Sigma-Aldrich, I0634) with 1 μg/mL brefeldin A (Sigma-Aldrich, B6542) and 2 μM monensin (Sigma-Aldrich, M5273) to inhibit ER and Golgi transport. Cells were then stained with Ghost Dye Violet 510 (Tonbo, 13-0870), Ghost Dye Red 780 (Tonbo, 13-0865), or Zombie NIR Flexible Viability Kit (Biolegend, 423106) in PBS for 10 minutes at 4°C to help identify dead cells and then with purified anti-Mouse CD16/CD32 (2.4G2, Tonbo, 70-0161) in staining buffer [0.5% (w/v) BSA, 2 mM EDTA, 10 mM HEPES, 0.02% NaN_3 (Sigma-Aldrich, S2002) in 1x PBS] for 10 minutes at 4°C to block the Fc receptors. Samples were then incubated with fluorescently conjugated antibodies against cell surface antigens in staining buffer for 25 minutes at 4°C and then washed extensively. For accessing intracellular antigens, cells were fixed and permeabilized with the BD Cytofix/Cytoperm Kit for measuring cytokine production, or with the ThermoFisher Transcription Factor Fix/Perm Kit for staining cytosolic

and nuclear antigens, according to manufacturers' instructions. Samples were recorded on an LSR II cytometer (BD) using the BD FACS DIVA software v8.0 or an Aurora cytometer (Cytek) using the SpectroFlo software v2.2.0.3 and analyzed with FlowJo v10.6.1 (BD).

In vitro suppression assay

A 2-fold titration series of FACS-sorted Treg cells starting from 40,000 cells/well was set up in U-bottom 96-well plates. 40,000 FACS-sorted, CellTrace Violet (ThermoFisher, C34571)-labeled naïve CD4 T cells and 100,000 erythrocyte-lysed splenocytes from *Tcrb*$^{-/-}$*Tcrd*$^{-/-}$ mice as antigen-presenting cells were then added to each well. α-mouse CD3 (145-2C11, BioXCell, BE0001-1) was then added to a final concentration of 1 μg/mL. Cells were incubated in a final volume of 200 μL complete RPMI w/ 10% FBS and with 5% CO_2 at 37°C for 72 hours before analysis. Cells that have had more than 4 rounds of CTV dilution were considered divided for calculating Treg cell-mediated suppression using the following formula:

$$\%Suppression\ (Sample\ X) = \frac{\%divided\ (no\ Treg) - \%divided\ (Sample\ X)}{\%divided\ (no\ Treg)}$$

Bulk RNA sequencing and data analysis

Doubly sorted cells were directly placed into TRIzol reagent (ThermoFisher, 15596-018) for subsequent RNA extraction. RNA was precipitated with isopropanol and linear acrylamide, washed with 75% ethanol, and resuspended in RNase-free water. After RiboGreen quantification and quality control by Agilent BioAnalyzer, 2ng of total RNA underwent amplification using the SMART-Seq v4 Ultra Low Input RNA Kit (Clontech, 63488), with 12 cycles of amplification. 3.8 – 4

ng of amplified cDNA was then used to prepare libraries with the KAPA Hyper Prep Kit (Kapa Biosystems, KK8504) using 8 cycles of PCR. Barcoded samples were run on a HiSeq 4000 instrument in a 50bp/50bp paired-end run, using the HiSeq 3000/4000 SBS Kit (Illumina). An average of 41 million paired reads were generated per sample with % mRNA bases per sample ranging from 67% to 77%. In experiments shown in Fig. 3, Treg cells (TCRβ^+CD4$^+$Foxp3$^+$) from *Foxp3*$^{DTR\text{-}GFP/y}$ and *Foxp3*$^{LSL/y}$*Cd4*$^{creERT2/+}$ mice and Treg "wannabe" (TCRβ^+CD4$^+$Foxp3$^-$ Thy1.1$^+$) cells from *Foxp3*$^{LSL/y}$*Cd4*$^{+/+}$ mice were analyzed (2-3 biological replicates). In experiments shown in Extended Data Fig. 6, Treg "wannabes" from 3 *Foxp3*$^{LSL/+}$ mice and 2 *Foxp3*$^{LSL/DTR\text{-}GFP}$ mice were analyzed. RNA-seq reads from fastq files were aligned to the reference mouse genome GRCm38 (https://www.ncbi.nlm.nih.gov/assembly/GCF_000001635.20/) using the STAR aligner v2.7.3a (168), and local realignment was performed using the Genome Analysis Toolkit v4.1.4.1 (169). For each sample, raw count of reads per gene was measured using R v4.0.2, and the DESeq2 R package v1.28.1 was used to perform differential gene expression analysis across different conditions (170). A cutoff of 0.05 was set on the obtained FDR-adjusted p-values to get the significant genes of each comparison. All detectable genes were rlog-normalized and then used for the principal component analysis.

Single cell RNA sequencing and data analysis

Library Preparation and sequencing

Library preparation and sequencing for the scRNA-Seq of doubly-FACS-sorted Treg cells isolated from the secondary lymphoid organs of 7 months post-

4-OHT treatment *Foxp3*$^{DTR\text{-}GFP}$ (cells pooled from 5 mice) and *Foxp3*^{LSL}*Cd4*$^{creERT2/+}$ mice (cells pooled from 4 mice) were performed by the Single Cell Research Initiative, SKI, using 10X genomics Chromium Single Cell 3' Library & Gel bead Kit V3 according to manufacturer's protocol. Cells, with a mean viability of 75%, were encapsulated in microfluidic droplets at a dilution of ~60 cells/μL with the multiplet fraction being 3.5%. After the RT step, the barcoded-cDNA was purified with DynaBeads, followed by 12-cycles of PCR-amplification (98°C for 180 s; [98°C for 15 s, 67°C for 20 s, 72°C for 60 s] x 12-cycles; 72°C for 60 s). Next, 50 ng of PCR-amplified barcoded cDNA was fragmented with the reagents provided in the kit and purified with SPRI beads to obtain an average fragment size of 600 bp. The fragmented DNA was ligated to sequencing adapters which was then indexed with PCR (98°C for 45 s; [98°C for 20 s, 54°C for 30 s, 72°C for 20 s] x 10 cycles; 72°C for 60 s). The resulting DNA library was double-size purified (0.6-0.8X) with SPRI beads and sequenced on an Illumina NovaSeq 6000 System (R1 – 26 cycles, i7 – 8 cycles, R2 – 96 cycles) at a depth of 210 million reads per sample (average reads per single cell being 31,000 and average reads per transcript 3.96 – 4.10), with a median sequencing saturation of 74%.

Data Pre-processing

Fastq files were processed using Cell Ranger v3.0 (10x Genomics) and reads were aligned to the mouse genome mm10 from ENSEMBL GRCm38 that was modified to include sequences corresponding to the coding region and the 3'UTR of the *R26*^{Tom} allele. Cells containing over 5% mitochondria-derived transcripts were filtered out, resulting in 3,634 *Foxp3*$^{DTR\text{-}GFP}$ cells and 3,390

Foxp3^{LSL} cells that passed QC metrics, with a median of 3,580 molecules/cell. Cells with total molecule counts below 1000, as determined by the lower mode of the distribution of total molecules per cell, were additionally filtered out to remove putative empty droplets. Genes that were expressed in more than 10 cells were retained for further analysis. The resulting count matrices from both samples were then combined, resulting in a final set of 7,024 cells x 12,432 genes, and normalized to median library size, where library size is defined as total molecule counts per cell. The normalized data are then log transformed as log (counts + 1) for downstream analysis.

Principal component analysis

For dimensionality reduction and visualization of data, we further excluded genes with very low or very high expression of transcripts (log average expression <0.02 or >3 and dispersion >0.15), and principal component analysis was then performed on the log-transformed normalized data. Using 40 principal components, where the number of principal components was determined by the knee-point in eigenvalues, yielded a good representation of the variability in the data.

MAGIC imputation

To account for missing values in scRNA-seq due to a high dropout rate, we employed MAGIC v0.1.1, a method of "de-noising" and imputing missing expression values through data diffusion between cells with similar covariate gene relationships (171). We constructed the diffusion map matrix using k = 30, ka = 10, and t = 6 as input parameters, where t specifies the number of times the affinity matrix is powered for diffusion.

Diffusion components and pseudotime calculation

Instead of constructing a tSNE map using 40 PCs, we followed the strategy outlined by Setty et al (152). In order to characterize potential pseudotime non-linear trajectories and to visualize single-cell gene expression in a UMAP embedding of diffusion components. Based on the eigen gap, we chose to use 15 diffusion components for downstream analysis in Palantir v1.0.0 and for calculating diffusion distances. We scaled each included diffusion component by the factor $\lambda/(1-\lambda)$ where λ is the associated eigenvalue, to reflect 'multi-scale' diffusion distances. Then, we calculate each cell position in pseudotime based on modeling cell fate in a continuous probabilistic model.

Clustering and gene ranking

Clustering of cells was performed using PhenoGraph v1.5.7 setting k = 15 nearest neighbors (172). A cluster was removed because of its disparity with the rest of the data (t-SNE projected this cluster as a separate component that comprised cells from both populations), and those cells also had a relatively lower number of total molecules compared with other populations. Significant differentially expressed genes in each cluster were identified using *t*-test (where the variance of small groups is overestimated), which was implemented in Single-Cell Analysis in Python (Scanpy) v1.7.2 with default parameters (173).

*td*Tom*ato expression and gene set module score calculation*

Because of a high dropout rate of single cell sequencing, we performed MAGIC imputation of tdTomato expression (as described above) only for *Foxp3*$^{DTR\text{-}GFP}$ cells since the overwhelming majority of the *Foxp3*^{LSL} cells were

tdTomato^{+} which could potentially cause over-imputation. A cutoff of 1.04 was set for the imputed tdTomato expression where any cells with higher expression were categorized as tdTomato^{+}(~15% of cells) and those with lower expression as tdTomato^{-} (~85% of cells) in agreement with flow cytometric measurements. Gene set module scores for Il2-Stat5 (GSEA HALLMARK_IL2_STAT5_SIGNALING) and Wnt/β-catenin (GSEA HALLMARK_WNT_BETA_CATENIN_SIGNALING) were calculated with the AddModuleScore function in Seurat v 3.1.5 using the default parameters (174).

TCR sequencing and data analysis

Bulk sequencing of the TCRα chain was performed using a 5' RACE-based method as previously described (72). Briefly, 70,000 rescued Treg cells (TCRβ^{+}CD4^{+}GFP^{+}Thy1.1^{-}) from *Foxp3*$^{LSL/y}$*Cd4*^{creERT2} mice were FACS-sorted from pooled spleen and lymph nodes at different time points post 4-OHT administration. Total RNA was extracted using the RNAeasy Plus Micro Kit (Qiagen 74034) according to the manufacturer's instructions. cDNA was synthesized using the SMARTScribe Reverse Transcriptase (Clontech 639537) with a mixture of oligo(dT)$_{24}$ and primers targeting the mouse TCRα constant regions. A template switching DNA-RNA hybrid oligo containing 12 random nucleotides was used to hybridize onto the 3' end of the first stand cDNA and to barcode the individual cDNA molecules. After removal of the hybrid oligo with Uracil-DNA glycosylase (New England Biolabs M0280), the cDNA was further PCR amplified to introduce sample barcodes, sequencing primer binding sites, as well as the Illumina P5 and P7 sequencing adaptors. The final PCR products were

separated on a 1% agarose gel and a single band around 700 bp was cut and purified using the NucleoSpin Gel and PCR Clean-up Kit (Clontech 740609). After PicoGreen quantification and quality control by Agilent TapeStation, libraries were pooled in equimolar ratios and run on a MiSeq in a PE200 run, using the MiSeq Reagent Kit v3 (600 Cycles) (Illumina). The loading concentration was 7-18 pM and a 10-20% spike-in of PhiX was added to the run to increase diversity and for quality control purposes (libraries were sequenced 3 times; loading concentration and PhiX spike-in amounts were adjusted based on initial performance). The runs yielded an average of 815K reads per sample.

The fastq files containing the TCR sequencing reads were aligned using the MiXCR software v3.0.13 to reference the V, D and J genes of mouse T cell receptors (175). MiXCR was also used to assemble clonotypes using alignments obtained from the previous step in order to extract the highly variable CDR3 region. The resulting clonotypes were pre-processed using VDJtools 1.2.1 in two steps (176). The first is a frequency-based correction to eliminate erroneous clonotypes. The algorithm searched the sample for clonotype pairs that differ by up to 2 mismatches. In case the ratio of the smallest to the largest clonotype sizes was lower than a specified threshold of 0.05^(number of mismatches), correction was performed by discarding the smaller clonotypes. The second step was to filter non-functional clonotypes. Specifically, the ones that contained a stop codon or frameshift in their receptor sequences were discarded. The resulting clonotypes and clone sizes were used to calculate the Simpson index and Gini coefficient.

Two different clonotype matching strategies were used: 1) V, J and CDR3 nucleotide sequences and 2) the CDR3 amino-acid sequence.

Statistics

Statistical significance was determined using tests indicated in the respective figure legends. P-values for *t*-test and Mantel-Cox test on flow cytometric and survival data were calculated with GraphPad Prism 7 and had been corrected for multiple hypothesis testing using the Holm-Sidak method, when applicable. P-values for ANOVA were computed with R for Fig. 2b and GraphPad Prism 7 elsewhere and had been corrected for multiple hypothesis testing using the Tukey method (when using R and Prism), the Dunnett's method or the Sidak method (when using Prism, according to its recommendations). P-values for Kolmogorov-Smirnov test were calculated with R. Throughout the entire study, error bars represent mean ± s.e.m., and the following notation was used to report statistical significance: ns, non-significant; *, $p < 0.05$; **, $p < 0.01$; ***, $p < 0.001$; ****, $p < 0.0001$.

Data availability

All sequencing data generated in this study can be accessed at GEO under accession number GSE179710. The custom mouse genome used for scRNA-seq analysis, which was generated by adding the tdTomato sequence to GRCm38 (https://www.ncbi.nlm.nih.gov/assembly/GCF_000001635.20/), is also available at GEO.

CHAPTER THREE:

Combinatorial regulation of peripheral regulatory T cell generation by *Foxp3* enhancers prevents intestinal type 2 inflammation

Introduction

Apart from restraining autoreactive Tconv cells, Treg cells are also crucial for preventing undue immune response to innocuous 'non-self' antigens, including dietary constituents and commensal microbes, and allergens (92). As a pivotal component of immune tolerance, these Treg cells specific for foreign moieties ensure proper barrier tissue function under homeostatic conditions, such as nutrient absorption at the intestinal epithelium as well as gas exchange in the lung, which can be drastically disrupted by immunopathology. The small intestine pathology in GF *Foxp3*^{KO} mice is less severe than SPF counterparts, indicating that a large proportion of the small intestine inflammation in the absence of Treg cells is directed against the microbiota (23). In addition, numerical deficiency or functional impairment of Treg cells has been implicated in multiple barrier tissue inflammatory disorders in humans, including inflammatory bowel disease, celiac disease, psoriasis, atopy, and asthma (126-128, 177).

Because foreign antigens are not encoded in the host germline or expressed by mTECs, non-self-specific Treg cells are thought to be generated in the periphery from naïve T cells. This process is best illustrated by using T cells expressing transgene-encoded TCRs specific for a model dietary antigen or commensal species; when transferred into mice that are also given OVA or the cognate microbes intragastrically, naïve T cells bearing receptors for OVA or the gut microbiota develop into Treg cells, which reside in the small and large intestine, respectively, as well as in the associated lymphoid tissues (93, 97-99). Accordingly, the frequency and number of Treg cells in the small and large intestine are

diminished in mice fed with an antigen-free diet and housed under gnotobiotic conditions, respectively (178-180). pTreg cell differentiation is intricately regulated by the balance between tolerogenic and pro-inflammatory signals, disruption of which can also give rise to protective or pathogenic conventional effector T cells, such as Th17 cells (181). Therefore, foreign antigens of dietary and microbial origins greatly shape the Treg cell compartment at the intestinal mucosa, which in turn confers immune tolerance and homeostasis to the host tissue.

Despite their vastly different TCR specificities and developmental trajectories, questions remain whether thymically and peripherally generated Treg cells possess distinct biological functions, utilize unique suppressive mechanisms, and play non-overlapping roles at the intestinal mucosal surfaces. Answering these questions would require ways to accurately distinguish and specifically manipulate Treg cells of different ontogeny under various conditions, which is particularly challenging for an environment as complex, diverse, and variable as the gut. From experiments utilizing gnotobiosis, elemental diet, or adoptive transfers, several markers, including high expression of Neuropilin-1 (Nrp-1, CD304) as well as Helios for tTreg cells and RORγt for pTreg cells, have been proposed to be marking these Treg cell subsets (101-103, 179, 180). RORγt expression, which is often mutually exclusive with Helios expression in Treg cells, is dependent on the presence of microbiota and is highly enriched in Treg cells in the large intestine lamina propria compared to lymphoid organs, while in the small intestine the frequency of Nrp-1^{-} Treg cells increases in mice in the absence of dietary antigens (178-180).

However, the use of these markers to distinguish pTreg vs thymically generated ones (tTreg) is contentious for several reasons. First, expression of markers can be regulated by signals other than those promoting tTreg or pTreg differentiation, thus uncoupling marker expression from cell ontogeny. For example, tTreg cells could upregulate RORγt upon exposure to IL-6 after migrating to the intestinal lamina propria, which activates transcription factors that bind to *Rorc* enhancers required for its expression in Th17 and Treg cells (182). Second, markers identified under homeostatic or adoptive transfer settings may not fully recapitulate pTreg cell induction and transcriptional program during perturbations such an infection or organ-specific autoimmune inflammation, where cell-extrinsic factors could further confound the interpretation of marker expression. Third, it is possible that mucosal Treg cell populations are stratified, with cells expressing a particular marker being in a distinct state of activation. In fact, colonic Treg cells expressing IL-10, which almost completely overlaps with RORγt expression, are more activated than their IL-10^{-} counterparts (S.D. & A.Y.R., unpublished observations), whereas lymphoid tissue Treg cells upregulate Helios upon activation (101, 183, 184). Therefore, any phenotypical differences between tTreg and pTreg cells identified using a particular marker could result from discordant activation status rather than intrinsic properties imparted by distinct developmental trajectories. Lastly, experimental treatments used to track or perturb the ontogeny of Treg cells (e.g. elemental diet) will almost inevitably affect other components of the gut ecosystem, such as Tconv cells, APCs, epithelial cells, and microbial species, which in turn could have an impact on Treg cell populations. Thus, better

approaches for identifying and manipulating tTreg and pTreg cells are required to further our understanding of their biology.

One strategy to specifically target and ablate pTreg cells is to interfere with the transmission of pTreg cell-inducing signals to the *Foxp3* locus. Upon TCR ligation, naïve Tconv cells readily turn on Foxp3 in 24-72 h *in vitro* when cultured in the presence of TGF-β and IL-2 (104, 110). Furthermore, the requirement for TGF-β signaling in the differentiation of transgenic TCR-expressing T cells into Treg cells *in vivo* have been clearly elucidated (97, 185). Mechanistically, TGF-β activates Smad3, which binds to the CNS1 intronic enhancer of *Foxp3* (69, 116). Retinoic acid enhances TGF-β-dependent Foxp3 upregulation by inducing the binding of its nuclear receptor to the corresponding response element within CNS1 (116). However, CNS1 ablation considerably diminishes, but not completely abrogates, Foxp3 induction upon activation of naïve T cells under permissive conditions (70, 119). In addition, generation of a pool of pTreg cells from T cells expressing microbiota-specific TCR *in vivo* in the absence of CNS1 is diminished in a time dependent manner rather than eliminated, with the defect gradually mitigated over time, presumably through proliferation of few generated pTreg cells or prolonged exposure of precursors to other Treg cell-inducing signals (186). Therefore, additional CNS1-independent mechanisms of pTreg cell induction may exist that compensate for its absence.

In contrast, the role of IL-2 during *in vivo* pTreg cell induction is less studied, although its function for tTreg cell generation has been evidently demonstrated (187, 188). STAT5, the transcription factor activated by IL-2 signaling, induces

Foxp3 expression by binding to the CNS0 enhancer located in the intron of the gene upstream of *Foxp3* (73, 74). CNS0-deficient $CD25^{+}Foxp3^{-}$ thymic Treg cell precursors show impaired Foxp3 expression when exposed to IL-2, and CNS0KO mice have a diminished Treg cell compartment in lymphoid organs that becomes less severe as the mice age (73). However, no conspicuous Treg cell dysfunction or immune activation is detected in the large intestine of these mice (73). The seeming discrepancy between this observation with the boosting effect IL-2 has on *in vitro* Treg cell induction suggests that either IL-2 is dispensable for pTreg cell generation *in vivo*, or other mechanisms can compensate for the absence of CNS0.

Considering the complex, heterogenous microenvironment of the intestinal mucosa and associated lymphoid tissues, and the copious numbers of cells other than Treg cells or their precursors residing therein that consume or scavenge TGF-β and IL-2, it is likely that the conditions enabling pTreg cell induction *in vivo* are far more complicated than what can be reliably modeled *in vitro.* Nevertheless, Treg cells are very abundant in the gut, accounting for 20-40% of all CD4 T cells (178-180). Therefore, we hypothesize that compensatory mechanisms of pTreg cell generation must be present to ensure robust immune tolerance at the intestinal mucosa while withstanding fluctuations in the availability of pTreg cell-promoting cues, with one such mechanism being synergistic regulation of *Foxp3* gene induction by CNS1 and CNS0 enhancers. By generating mice with germline CNS1 deficiency coupled to inducible CNS0 ablation immediately prior to weaning, we demonstrated that CNS1/0 double knockout (DKO) CD4 T cells were irresponsive to TGF-β or IL-2 *in vitro* and had drastically impaired induction of Foxp3 that was

more severe than either single knockout. Although systemic autoimmunity was absent in DKO mice, pronounced type 2 immune activation, one that was markedly more exacerbated than CNS1KO and featured overt Th2 response as well as expansion of B cells and increased switching to IgG1, was observed in the large intestine and associated lymphoid tissues. While the immune dysregulation in CNS1 or CNS0 single deficient mice was mild and mostly transient, the immunopathology in DKO mice was much more severe and persistent with no signs of normalization over time. Our results indicate that CNS1 and CNS0 cooperatively facilitate pTreg cell generation in the large intestine, which suppresses unwanted type 2 response against dietary and microbial antigens.

Generation of Foxp3$^{GFP\text{-}\Delta CNS0\text{-}\Delta CNS1}$ mice

A very short distance between CNS1 and CNS0 enhancers on the X chromosome precludes their combinatorial targeting by intercrossing the two single knockout or conditional alleles. Therefore, we performed CRISPR/Cas9-mediated deletion of CNS1 in zygotes harvested from mice carrying the previously described *Foxp3$^{GFP\text{-}CNS0fl}$* allele, which harbors an N-terminal GFP-Foxp3 fusion protein and loxP sites flanking CNS0 (73). Conditional CNS0 allele could then be deleted by combining the resulting *Foxp3$^{GFP\text{-}CNS0fl\text{-}\Delta CNS1}$* allele with a ubiquitously expressed tamoxifen-inducible CreER^{T2} recombinase (*Ndor1$^{Ubc\text{-}creER}$*) to generate a CNS1/CNS0 double knockout (DKO) allele upon tamoxifen treatment (Fig. 3.1) (189). Deletion of CNS1 was confirmed with PCR, and Sanger sequencing of the *Foxp3$^{GFP\text{-}CNS0fl\text{-}\Delta CNS1}$* allele revealed a simple deletion similar to the previously reported *Foxp3$^{GFP\text{-}\Delta CNS1}$* allele (Fig. 3.2) (70, 119).

Figure 3.1 Generation of *Foxp3*$^{GFP\text{-}\Delta CNS0\text{-}\Delta CNS1}$ mice.
Schematics of the *Foxp3*$^{GFP\text{-}\Delta CNS0\text{-}\Delta CNS1}$ allele before and after CRISPR/Cas9 editing and Ubc-creER-mediated recombination. Blue arrows denote CRISPR cut sites. Horizontal arrows represent genotyping primer binding sites. Dashed black lines delimit homologous regions. Dark blue boxes represent exons.

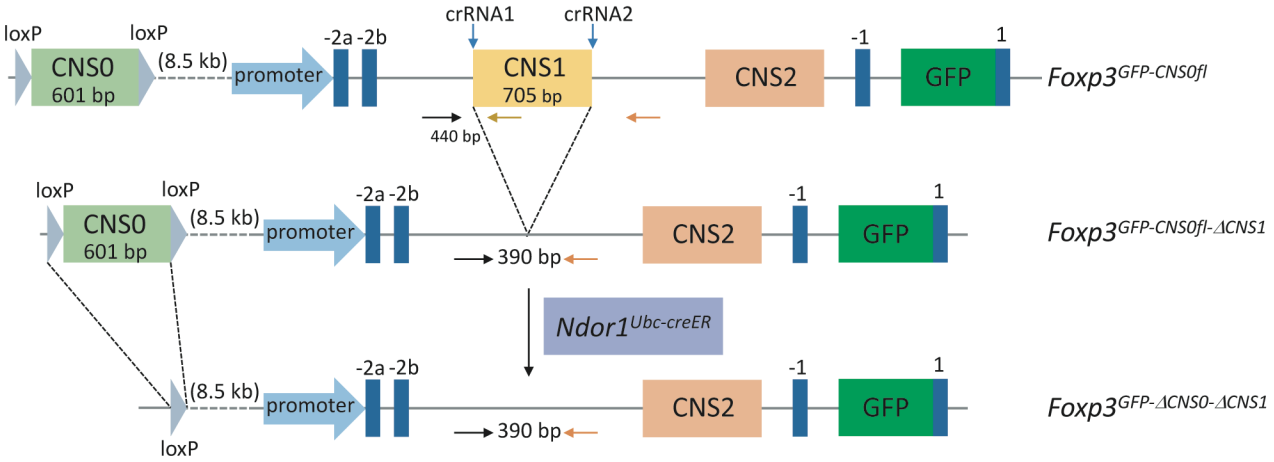
loxP
loxP
CNS0
601 bp
(8.5 kb)
promoter
-2a -2b
crRNA1
crRNA2
CNS1
705 bp
CNS2
-1
1
GFP
Foxp3GFP-CNS0fl
440 bp
loxP
loxP
CNS0
601 bp
(8.5 kb)
promoter
-2a -2b
CNS2
-1
1
GFP
Foxp3GFP-CNS0fl-ΔCNS1
390 bp
Ndor1Ubc-creER
(8.5 kb)
promoter
-2a -2b
CNS2
-1
1
GFP
Foxp3GFP-ΔCNS0-ΔCNS1
390 bp
loxP

Figure 3.2 Related to Figure 3.1.

a, Representative genotyping results using primers in Figure 3.1.

b, Representative Sanger sequencing track of the *Foxp3*$^{GFP\text{-}\Delta CNS0\text{-}\Delta CNS1}$ allele.

a

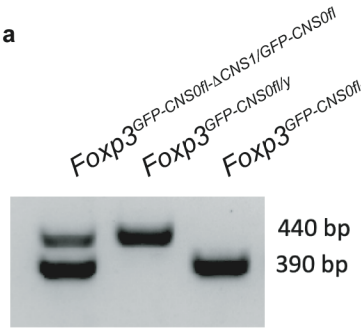

b

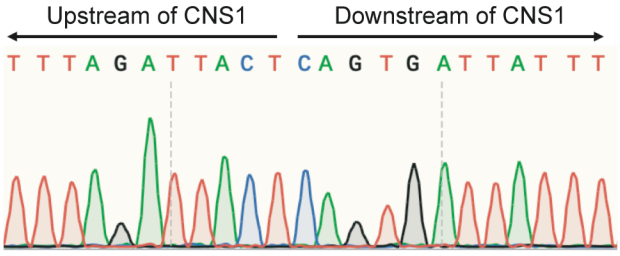

Foxp3$^{GFP\text{-}CNS0fl\text{-}\Delta CNS1/y}$

CNS1/CNS0 DKO resulted in a severe impairment in Foxp3 induction in Tconv cells compared to single KO's

It is possible that CNS1 and CNS0 may independently promote *Foxp3* gene induction. Alternatively, either enhancer could require the activity of the other for optimal induction of the *Foxp3* gene. To study the potential genetic interaction between CNS1 and CNS0 during *Foxp3* induction, we set up a breeding scheme to generate WT, CNS1KO, CNS0KO, and DKO male mice. In all F1 males, CNS0 was flanked by loxP sites and its deletion or lack thereof was due to the presence or absence of the Ubc-creER deleter. Using these mice as bone marrow (BM) hematopoietic stem cell donors, we then transferred T cell-depleted BM cells into lethally irradiated congenically marked recipients, which were treated with tamoxifen 8 weeks after BM transfer to allow for donor-derived T cell reconstitution. Donor-derived (CD45.2) naïve conventional T (nTconv) cells were isolated 1 week after the third dose of tamoxifen to set up *in vitro* Foxp3 induction assays, which were analyzed 24 hrs later (Fig. 3.3a).

While Foxp3 induction in WT and CNS0KO CD4 T cells was equally responsive to TGF-β or RA titration, albeit with different starting efficiencies, in CNS1KO CD4 T cells its sensitivity to TGF-β was attenuated while response to RA lacking. On the other hand, decreasing IL-2 concentration led to a reduced Foxp3 induction in WT and CNS1KO, but not CNS0KO CD4 T cells (Fig. 3.3b-d). While these results were consistent with previously observed effects single deficiencies in CNS1 and CNS0 on Foxp3 induction in CD4 T cells isolated from *Foxp3*$^{GFP\text{-}\Delta CNS1}$ and *Foxp3*$^{GFP\text{-}\Delta CNS0}$ mice (70, 73), we observed a highly pronounced further

impairment in Foxp3 induction in DKO cells, which were barely responsive to any of the three major Foxp3 inducing factors with < 3% of cells expressing Foxp3 under optimal culture conditions (Fig. 3.3b-d). These results indicate that the blockade of *in vitro* induction of Foxp3 in DKO CD4 T cells was close to complete contrary to a partial deficiency in CNS1KO T cells (70). The observed induction defects in CNS0KO and DKO cells were not due to the Ubc-creER used to induce CNS0 deletion or the associated heterozygosity at the *Ndor1* locus, the integration site of the lentiviral vector encoded Ubc-creER transgene (190), as the Foxp3 induction efficiencies in Ubc-creER^{+} or Ubc-creER^{-} *Foxp3*^{GFP} mice were comparable (Fig. 3.3e-g). These data indicate that CNS1 and CNS0 do not require the activity of the other enhancer to promote *Foxp3* expression, with the induction defect in DKO cells much more severe than either single KO.

Figure 3.3 Foxp3 induction was severely impaired in DKO nTconv cells.
a, Breeding and experimental scheme. Tam, tamoxifen.
b-g, *In vitro* Foxp3 induction assay with donor-derived nTconv cells of indicated genotypes. See Methods for details. Dot and error bar represent mean ± S.E.M. n = 3. Results representative of 3 (b-d) or 1 (e-g) experiment. RA, retinoic acid. rhIL-2, recombinant human interleukin 2.

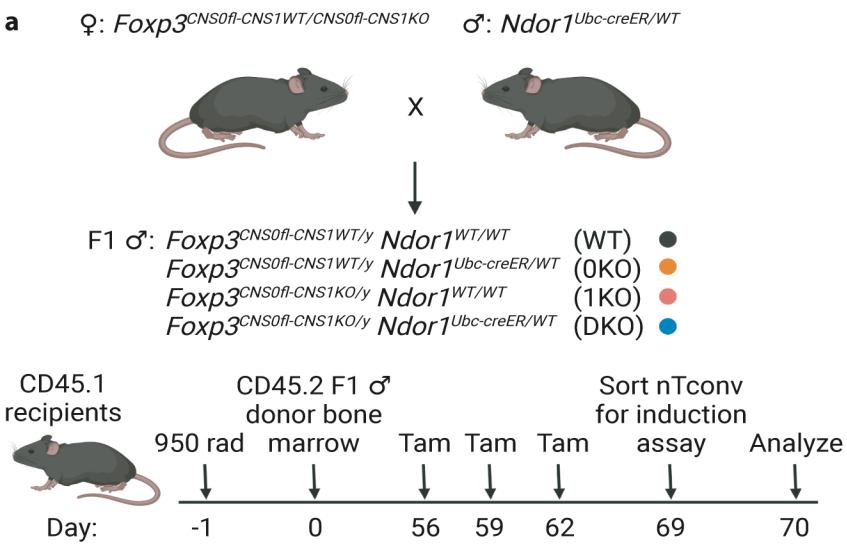
a
♀: Foxp3CNS0fl-CNS1WT/CNS0fl-CNS1KO
♂: Ndor1Ubc-creER/WT
X
F1 ♂: Foxp3CNS0fl-CNS1WT/y Ndor1WT/WT (WT)
Foxp3CNS0fl-CNS1WT/y Ndor1Ubc-creER/WT (0KO)
Foxp3CNS0fl-CNS1KO/y Ndor1WT/WT (1KO)
Foxp3CNS0fl-CNS1KO/y Ndor1Ubc-creER/WT (DKO)
CD45.1 recipients
CD45.2 F1 ♂ donor bone marrow
Sort nTconv for induction assay
950 rad
Tam
Tam
Tam
Analyze
Day:
-1
0
56
59
62
69
70

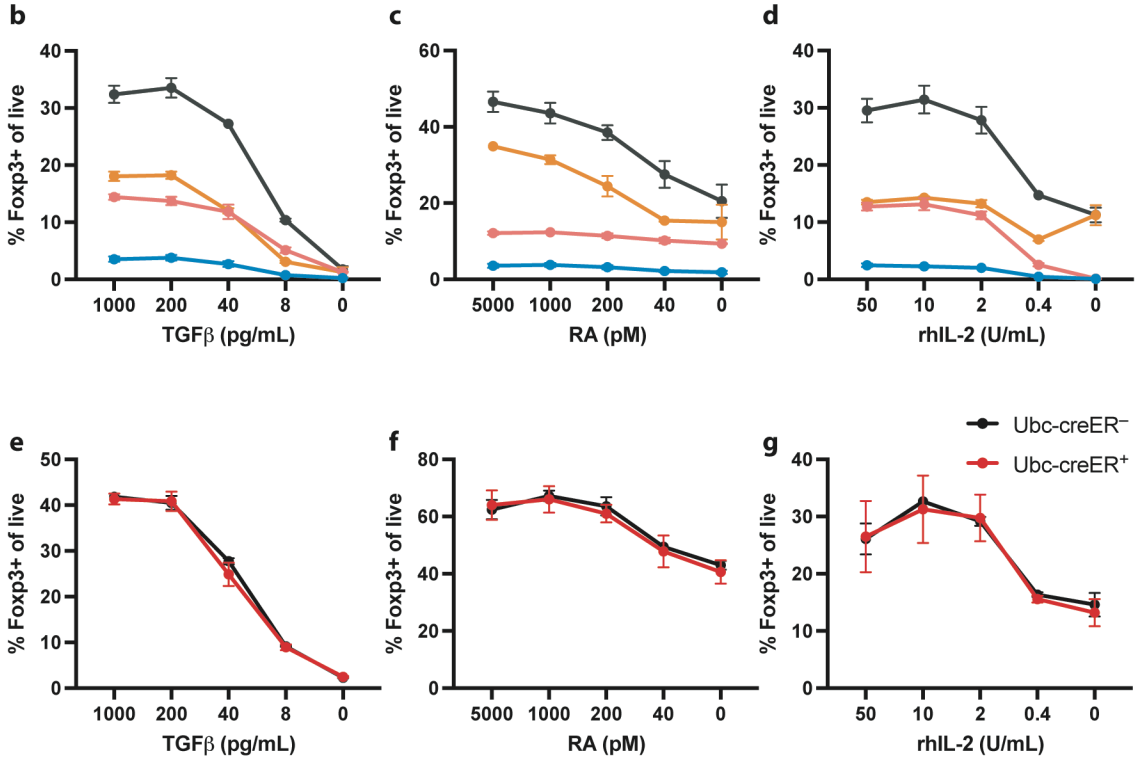
b
% Foxp3+ of live
TGFβ (pg/mL)
1000 200 40 8 0
c
RA (pM)
5000 1000 200 40 0
d
rhIL-2 (U/mL)
50 10 2 0.4 0
e
f
g
Ubc-creER⁻
Ubc-creER⁺

DKO mice did not have systemic autoimmunity

With DKO nTconv cells seemingly incapable of generating pTreg cells, we then asked what the biological consequences of this deficiency were. To this end, we analyzed 12-16-week-old WT, CNS1KO, and DKO littermates treated on P14-P16 with 4-hydroxytamoxifen (4-OHT), the pharmacologically active form of tamoxifen (Fig. 3.4). While CNS1 is dispensable for tTreg cell development, CNS0 is required for optimal tTreg cell generation, in particular, during the first two weeks life by sensitizing the *Foxp3* locus to IL-2 signaling (70, 73, 74). Therefore, we chose to delete CNS0 on P14 in T cells as well as progenitor cells using Ubc-creER to avoid impeding tTreg cell generation within the first 14 days, which were shown to possess non-redundant tolerogenic function (191). Furthermore, this regimen would also ablate CNS0 right before intestinal pTreg cells started to engender during the postnatal period as a result of the transition from breast milk feeding to solid food and the consequent colonization with a complex intestinal microbiota (119, 178). Importantly, lineage fidelity of the Treg cells present by P14 would not be affected, because CNS0 is not required for stable *Foxp3* expression while CNS2 is intact (73, 130).

Mice lacking functional *Foxp3* gene or subjected to Treg cell ablation develop fulminant systemic autoimmunity featuring rampant lympho- and myelo-proliferation and cytokine production in lymphoid organs and non-lymphoid tissues (17, 22, 136). To assess whether pTreg cell-deficient DKO mice developed signs of systemic immune activation and autoimmunity, we analyzed the Treg and Tconv cell compartments in the spleen and skin-draining peripheral lymph nodes (pLNs).

Compared to WT or CNS1KO mice, DKO mice had fewer Treg cells that were also more activated, as illustrated by an increase in the $CD44^{hi}$ or $CTLA4^{+}$ fractions of Treg cells (Fig. 3.5a-c). These results resembled mice with germline CNS0 deficiency (73, 74), suggesting that induced CNS0 ablation might have compromised the tTreg cells generated after P14. However, the numerical reduction in Treg cells did not result in considerable activation of Tconv cells, with CD69 expression in DKO Tconv and CD8 T cells in the pLN remaining unchanged (Fig. 3.5e,h). The proportions of $CD44^{hi}$ and $IFN\gamma^{+}$ splenic Tconv and CD8 T cells were mildly elevated at best (Fig. 3.5d,f,g,i). In addition, type 2 and type 3 cytokines, which were greatly increased in *Foxp3*^{KO} mice, were barely detectable in all three groups (Fig. 3.5j-m) (46). Accordingly, severe splenomegaly and lymphadenopathy characteristic of Foxp3 deficiency were not observed in DKO mice (data not shown). Body weight of DKO mice at 12-16 weeks was comparable to that of CNS1KO, suggesting lack of wasting disease (Fig. 3.5n). Taken together, the Treg cell compartment in the secondary lymphoid organs of pTreg cell-deficient DKO mice, although numerically diminished, was functional and fully capable of suppressing autoimmunity, consistent with the notion that most Treg cells in lymphoid organs were thymically derived.

Figure 3.4 Experimental scheme for analyzing *in vivo* phenotypes in WT, CNS1KO, and DKO littermates.
4-OHT, 4-hydroxytamoxifen.

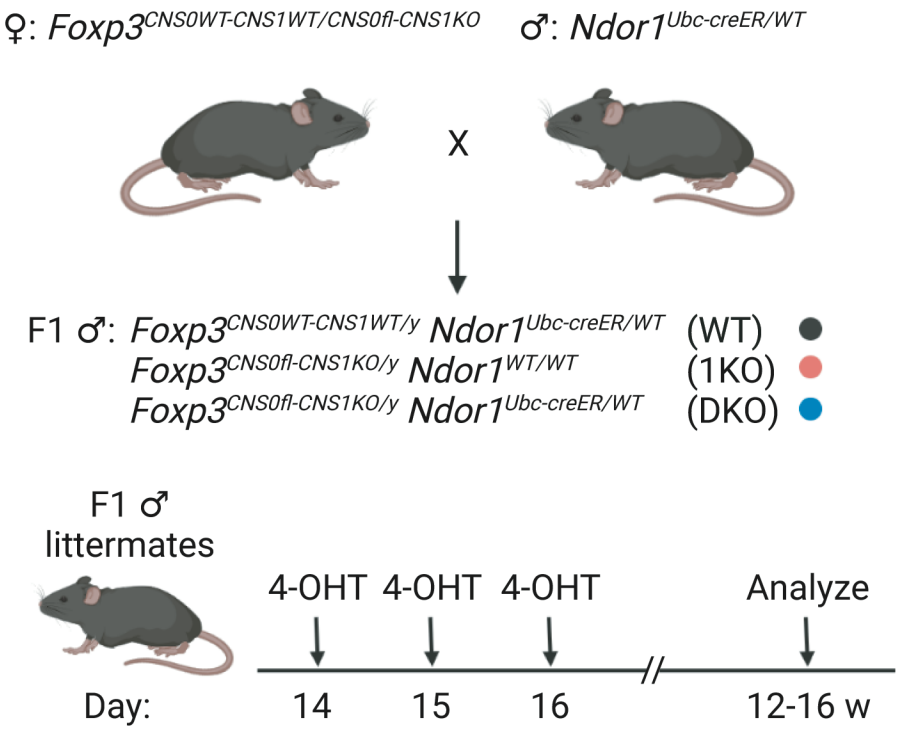
♀: Foxp3CNS0WT-CNS1WT/CNS0fl-CNS1KO
♂: Ndor1Ubc-creER/WT
X
F1 ♂: Foxp3CNS0WT-CNS1WT/y Ndor1Ubc-creER/WT (WT)
Foxp3CNS0fl-CNS1KO/y Ndor1WT/WT (1KO)
Foxp3CNS0fl-CNS1KO/y Ndor1Ubc-creER/WT (DKO)
F1 ♂
littermates
4-OHT 4-OHT 4-OHT
Analyze
Day:
14 15 16
12-16 w

Figure 3.5 Lack of systemic autoimmunity in DKO mice.
All mice were treated and analyzed as in Fig. 3.4.
a, Frequencies of Treg cells among CD4 T cells in indicated organs.
b-c, Frequencies of activated Treg cells.
d-m, Frequencies of activated or cytokine producing Tconv or CD8 T cells.
n, Body weight of mice. Spl, spleen. pLN, peripheral (brachial, axillary, inguinal) lymph nodes.
Bars represent mean. a-m, Two-way ANOVA with Dunnett's multiple hypothesis test. n, One-way ANOVA with Dunnett's multiple hypothesis test. ns, not significant; *, $p < 0.05$; **, $p < 0.01$; ***, $p < 0.001$; ****, $p < 0.0001$.

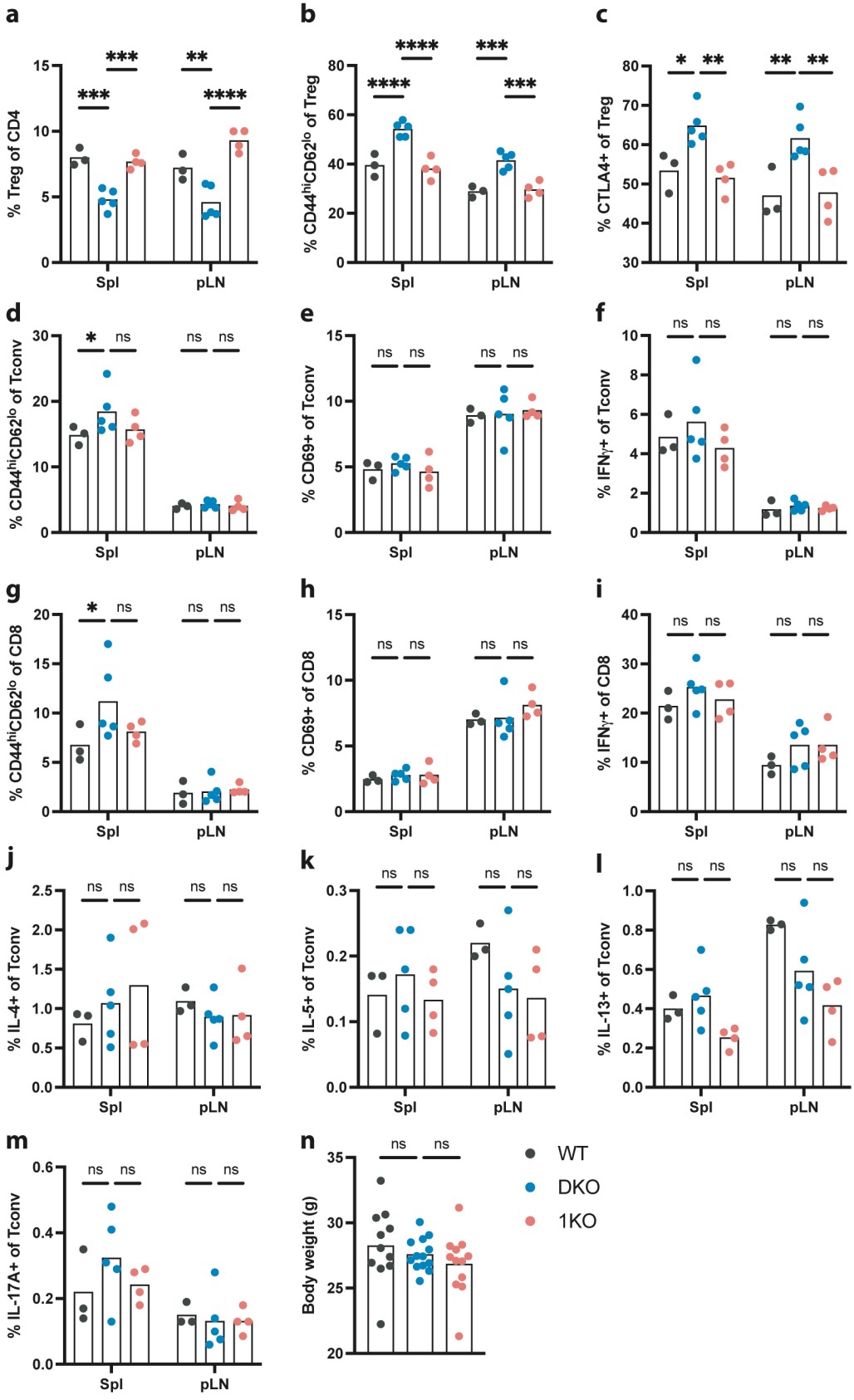
a
% Treg of CD4
b
% CD44hiCD62lo of Treg
c
% CTLA4+ of Treg
d
% CD44hiCD62lo of Tconv
e
% CD69+ of Tconv
f
% IFNγ+ of Tconv
g
% CD44hiCD62lo of CD8
h
% CD69+ of CD8
i
% IFNγ+ of CD8
j
% IL-4+ of Tconv
k
% IL-5+ of Tconv
l
% IL-13+ of Tconv
m
% IL-17A+ of Tconv
n
Body weight (g)
Spl
pLN
ns
WT
DKO
1KO

pTreg cell ablation caused prominent Th2 response in the intestine

The small and large intestine is thought to be a major site of generation of pTreg cells in response to dietary and microbial antigens and of their residence (178-180). *Foxp3*$^{GFP\text{-}\Delta CNS1}$ mice, which exhibit delayed pTreg cell development, present with a transient increase in type 2 cytokine production by colonic effector CD4 T cells (Th2) upon microbial colonization (119). Therefore, we next examined the intestine and mesenteric lymph nodes of 3-4-month-old DKO mice with a near-complete pTreg cell generation block for potentially exacerbated manifestations. Similar to the spleen and pLN, the percentage of Treg cells was decreased in the mesenteric lymph nodes draining the small intestine (sMLN) and proximal colon (cMLN) of DKO mice, compared to WT or CNS1KO (Fig. 3.6a). This did not necessarily indicate a defect in pTreg cell generation, though, because the majority of Treg cells in the MLNs were likely recirculating tTreg cells. In contrast, the Treg cell frequency in the large intestine lamina propria (LILP) of DKO mice at 3-4 months of age was comparable to WT and CNS1KO mice, indicating that the LILP Treg cell compartment in DKO mice was not numerically defective, presumably as a result of compensatory expansion or cell-extrinsic mechanisms (Fig. 3.6a). As noted above, RORγt and Helios expression are commonly associated with pTreg and tTreg cells, respectively (98, 101). Accordingly, Treg cell population in the sMLN and LILP of DKO mice were mildly enriched for Helios$^+$ cells and depleted of RORγt$^+$ cells (Fig. 3.6b,c). Nonetheless, the proportion of RORγt-expressing Treg cells was elevated in DKO cMLN, suggesting potential upregulation of RORγt

in tTreg cells due to unique environment of the proximal colon or its draining lymph node or additional mechanisms which remain to be explored (Fig. 3.6b).

Despite normal proportion of LILP Treg cells in DKO mice, we observed prominent expansion of Th2 cells, as identified by high Gata3 expression, in the LILP and to a lesser extent small intestine-draining and colon-draining MLNs (Fig. 3.6a,d). While *Foxp3*$^{GFP\text{-}\Delta CNS1}$ mice have been reported to present with heightened Th2 response and accumulation of mast cells in the large intestine (119), these manifestations were notably further intensified in DKO mice (Fig. 3.6d,e). Consistently, IL-13 producing CD4 T cells were increased in the MLNs and LILP of DKO mice, and a similar trend was observed for IL-5 expressing CD4 T cells in the LILP (Fig. 3.6f,g). The immune activation in DKO intestine was strictly limited to Th2 responses, because IFNγ producing Th1 and IL-17 producing Th17 cells did not increase (Fig. 3.7a-d). In addition, the elevated type 2 cytokine production was restricted to CD4 T cells, as the proportion of ILC2 and their cytokine production were not different between DKO and CNS1KO mice (Fig. 3.6h, Fig. 3.7 e-h).

It was possible that the heightened Th2 response in DKO mice compared to CNS1KO was due to CNS0 deletion independent of CNS1. Therefore, we analyzed similarly treated WT, CNS0KO, and DKO littermates (Fig. 3.8a). Importantly, CNS0KO mice did not show elevated Gata3^{+} Th2 cells in either the LILP or MLNs, unlike their DKO littermates (Fig. 3.8b,c). Nor did we observe increases in IL-5 or IL-13 producing T cells in CNS0KO mice, compared to WT controls (Fig. 3.8d,e). The differences between DKO and CNS1KO mice were also

not due of the Ubc-creER because Ubc-creER^{+} or Ubc-creER^{-} *Foxp3*^{GFP} mice were comparable in terms of frequencies of Th2 cells and type 2 cytokine production in the LILP and MLNs (Fig. 3.9). Collectively, these results demonstrated that CNS0 deficiency alone did not cause gut pathology but in combination with CNS1 deletion markedly escalated the Th2 response in the large intestine as compared to CNS1 single deficiency. Therefore, a lack of Th2 phenotype in CNS0KO mice despite *in vitro* induction defect was due to compensation by CNS1; only when CNS1 was also deleted could CNS0KO not be compensated for, hence further impairing pTreg cell generation and exacerbating Th2 pathology.

Although we observed similarly aggravated Th2 response in the DKO sMLN, we were unfortunately not able to isolate immune cells from DKO small intestine for flow cytometric analysis despite our best efforts (data not shown). This was likely because of highly pronounced type 2 inflammation, which had been known to pose great challenges to retrieving live cells from small intestine due to excessive mucus production. The extent of immunopathology in DKO small intestine is currently being assessed using histology, immunofluorescence, and ELISA.

Figure 3.6 Further intensified Th2 response in the intestine and mesenteric lymph nodes of DKO mice compared to CNS1KO.

All mice were treated and analyzed as in Fig. 3.4.

a, Frequencies of Treg cells among CD4 T cells in indicated organs.

b-c, Frequencies of Treg cells expressing RORγT or Helios.

d, Frequencies of $Gata3^{+}$ cells among Tconv cells.

e, Frequencies of mast cells as percentage of total live hematopoietic cell in the intraepithelial fraction of large intestine (LI IEL).

f-h, Frequencies of IL-5 and IL-13 producing Tconv cells and innate lymphoid cells.

sMLN, small intestine (mostly jejunum and ileum) draining mesenteric lymph nodes. cMLN, proximal colon-draining mesenteric lymph node. LILP, large intestine lamina propria. ILC, innate lymphoid cells.

Bars represent mean. a-d, f-h, Two-way ANOVA with Tukey's multiple hypothesis test. Cage effect was considered as a factor in addition to genotype when constructing the linear model. e, One-way ANOVA with Dunnett's multiple hypothesis test. ns, not significant; *, $p < 0.05$; **, $p < 0.01$; ***, $p < 0.001$; ****, $p < 0.0001$.

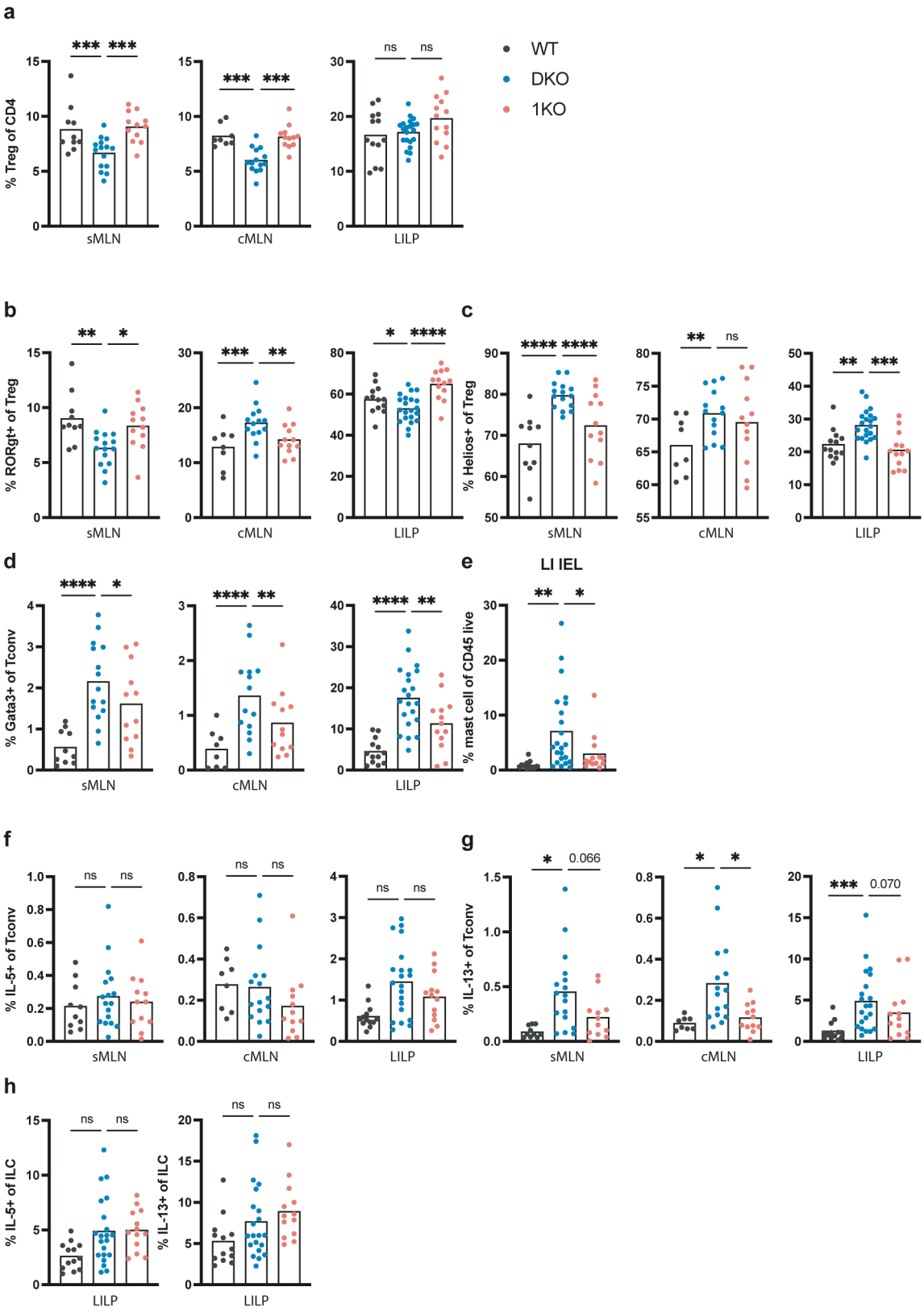
a
% Treg of CD4
sMLN
cMLN
LILP
WT
DKO
1KO
b
% RORgt+ of Treg
c
% Helios+ of Treg
d
% Gata3+ of Tconv
e
LI IEL
% mast cell of CD45 live
f
% IL-5+ of Tconv
g
% IL-13+ of Tconv
h
% IL-5+ of ILC
% IL-13+ of ILC

Figure 3.7 Lack of amplified Th1 or Th17 response in DKO intestine and mesenteric lymph nodes.

All mice were treated and analyzed as in Fig. 3.4.

a-h, Cytokine-producing Tconv, CD8 T, and innate lymphoid cells in indicated organs. sMLN, small intestine (mostly jejunum and ileum) draining mesenteric lymph nodes. cMLN, proximal colon-draining mesenteric lymph node. LILP, large intestine lamina propria. ILC, innate lymphoid cells. Bars represent mean. One-way ANOVA with Dunnett's multiple hypothesis test. ns, not significant; *, $p < 0.05$; **, $p < 0.01$; ***, $p < 0.001$.

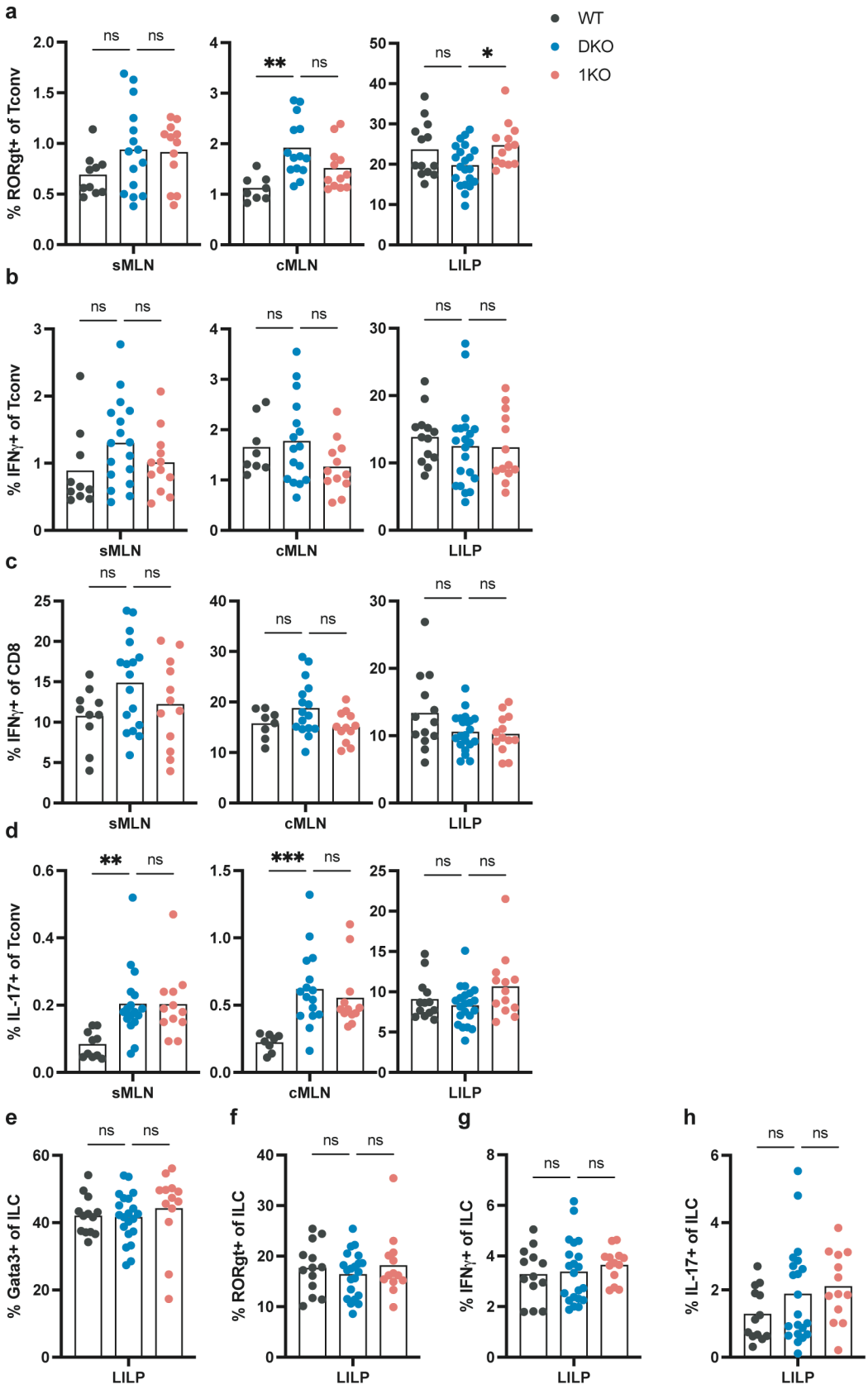
a
b
c
d
e
f
g
h
WT
DKO
1KO
% RORgt+ of Tconv
% IFNγ+ of Tconv
% IFNγ+ of CD8
% IL-17+ of Tconv
% Gata3+ of ILC
% RORgt+ of ILC
% IFNγ+ of ILC
% IL-17+ of ILC
sMLN
cMLN
LILP
ns
*
**
***

Figure 3.8 Elevated Th2 response in DKO mice was not due to CNS0KO alone.
a, Experimental scheme for analyzing *in vivo* phenotypes in WT, CNS0KO, and DKO littermates. 4-OHT, 4-hydroxytamoxifen.
b-e, Frequencies of Treg, Th2, and cytokine-producing Tconv cells in indicated organs of WT, CNS0KO, and DKO mice. sMLN, small intestine (mostly jejunum and ileum) draining mesenteric lymph nodes. cMLN, proximal colon-draining mesenteric lymph node. LILP, large intestine lamina propria. Bars represent mean. One-way ANOVA with Dunnett's multiple hypothesis test. ns, not significant; *, $p < 0.05$; **, $p < 0.01$.

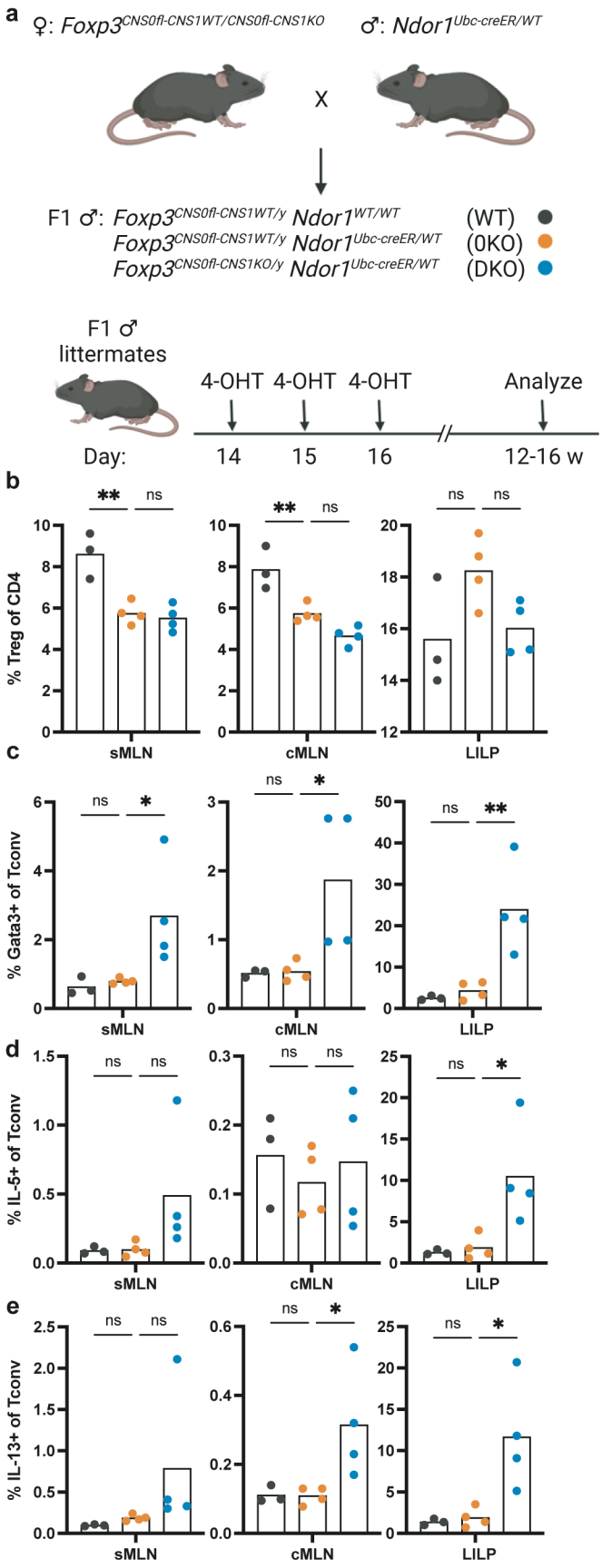
a
♀: Foxp3CNS0fl-CNS1WT/CNS0fl-CNS1KO
♂: Ndor1Ubc-creER/WT
X
F1 ♂: Foxp3CNS0fl-CNS1WT/y Ndor1WT/WT (WT)
Foxp3CNS0fl-CNS1WT/y Ndor1Ubc-creER/WT (0KO)
Foxp3CNS0fl-CNS1KO/y Ndor1Ubc-creER/WT (DKO)
F1 ♂ littermates
4-OHT 4-OHT 4-OHT
Analyze
Day:
14
15
16
12-16 w
b
% Treg of CD4
c
% Gata3+ of Tconv
d
% IL-5+ of Tconv
e
% IL-13+ of Tconv
sMLN
cMLN
LILP
ns
*
**

Figure 3.9 Elevated Th2 response in DKO mice was not due to Ubc-creER.
a-d, Frequencies of Treg, Th2, and cytokine-producing Tconv cells in indicated organs of similarly treated Ubc-creER^{+} or Ubc-creER^{-} *Foxp3*^{GFP} mice. sMLN, small intestine (mostly jejunum and ileum) draining mesenteric lymph nodes. cMLN, proximal colon-draining mesenteric lymph node. LILP, large intestine lamina propria. Bars represent mean. Two-tailed unpaired *t*-tests with Holm-Sidak multiple hypothesis testing correction. ns, not significant.

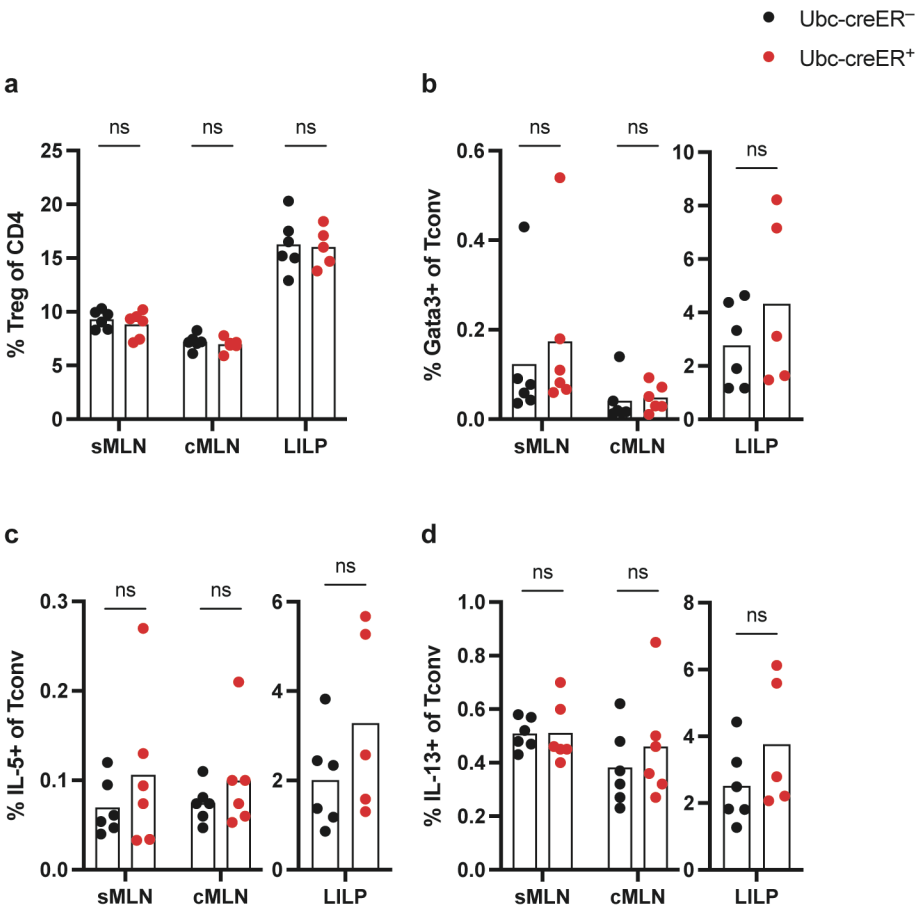
Ubc-creER⁻
Ubc-creER⁺
a
b
c
d
% Treg of CD4
% Gata3+ of Tconv
% IL-5+ of Tconv
% IL-13+ of Tconv
ns
sMLN
cMLN
LILP

B cell proliferation and switching to IgG1 in DKO mice

We noticed that small intestine, but not colon draining MLNs were drastically enlarged in DKO mice in comparison to WT or 1KO mice (data not shown). The lymphadenopathy was chiefly driven by B cell proliferation, as B cells accounted for a larger proportion of total cellularity in DKO small intestine draining MLNs (Fig. 3.10a). The sMLN B cell expansion was in part caused by heightened B cell activation and more prominent germinal center (GC) reaction (Fig. 3.10b). Type 2 cytokines, in particular IL-4, causes B cell proliferation and class switching to IgG1 and IgE (192, 193). Indeed, we observed a more than two-fold increase in the frequency of GC B cells switching to IgG1 in DKO sMLN, at the cost of other isotypes including IgA and IgG2b (Fig. 3.10c-f). Although B cell expansion relative to total cellularity was not evident in the colon draining MLN and Peyer's Patches (PP), a similar trend of preferential switching to IgG1 was also observed in these two compartments (Fig. 3.10a-f). These results were consistent with the elevated intestinal Th2 responses in DKO mice. Similar to local changes in T cell responses, the observed alterations in B cell activation states were not systemic but strictly limited to gut-associated lymphoid tissues, and were not due to the Ubc-creER (Fig. 3.11). Compared to WT littermates, CNS0KO small intestine draining MLN had a larger fraction of GC B cells switching to IgG1, but to a markedly lesser extent than in DKO mice (Fig. 3.12c). In addition, increased B cell proliferation was not found in CNS0KO small intestinal MLN, and the percentages of $IgG1^+$ GC B cells in CNS0KO colonic MLN and PP were not higher than WT (Fig. 3.12a-c). Therefore, elevated IgG1 class-switching and B cell proliferation observed in small

intestine draining MLNs were unique to DKO mice, suggesting that these local B cell responses are controlled by pTreg cells whose generation is dependent on cooperative activity of CNS1 and CNS0.

While it is possible that the increased $IgG1^+$ GC B cells in DKO mice could eventually migrate to the LILP and produce IgG1 locally, we did not observe an increase in the percentage of plasma cells in DKO LILP, and the vast majority of LILP plasma cells still produced IgA (Fig. 3.10g,h). Serum IgG1 titer was also comparable between DKO and 1KO mice, but we did detect a trend towards an increasing level of serum IgE (Fig. 3.10i,j). This is consistent with the notion that IgG1 memory B cells can undergo secondary switching and further differentiate into IgE-secreting cells (194). It was possible that these circulatory IgE were raised against dietary antigens and could mediate food allergy, which needed to be verified.

In conclusion, CNS1 and CNS0 enhancers regulate pTreg cell differentiation in a cooperative manner, with DKO Tconv cells having severely compromised Foxp3 induction *in vitro.* Although CNS0 deficiency alone does not cause overt disease in mice, it further exacerbates the heightened Th2 inflammation in the intestine and associated lymphoid tissues observed in CNS1KO mice. Moreover, DKO mice develop pronounced B cell expansion and IgG1 switching in the small intestine draining mesenteric lymph nodes, which may explain the elevated serum IgE level. Further study of CNS1- and CNS0-dependent pTreg cell induction could pave the way to understanding the etiology

of and developing novel therapeutics for common human gastrointestinal disorders, including food allergy, celiac disease, and inflammatory bowel disease.

Figure 3.10 Prominent B cell proliferation and switching to IgG1 in DKO sMLN.
All mice were treated and analyzed as in Fig. 3.4.
a, Frequencies of B cells as percentage of total live hematopoietic cells in indicated organs.
b, Frequencies of B cells undergoing germinal center (GC) reaction (Fas^+CD38^-).
c-f, Frequencies of B cells undergoing GC reaction that were switching to various isotypes or unswitched (IgM^+).
g, Frequencies of plasma cells ($Lineage^-Blimp\text{-}1^+Fas^+$) as percentage of total live hematopoietic cells.
h, Percentages of IgA-secreting plasma cells.
i, j, Titers of IgG1 and IgE in the serum measured with ELISA.
sMLN, small intestine (mostly jejunum and ileum) draining mesenteric lymph nodes. cMLN, proximal colon-draining mesenteric lymph node. PP, Peyer's patch. LILP, large intestine lamina propria. Bars represent mean. a-j, One-way ANOVA with Dunnett's multiple hypothesis test. ns, not significant; *, $p < 0.05$; **, $p < 0.01$; ***, $p < 0.001$; ****, $p < 0.0001$.

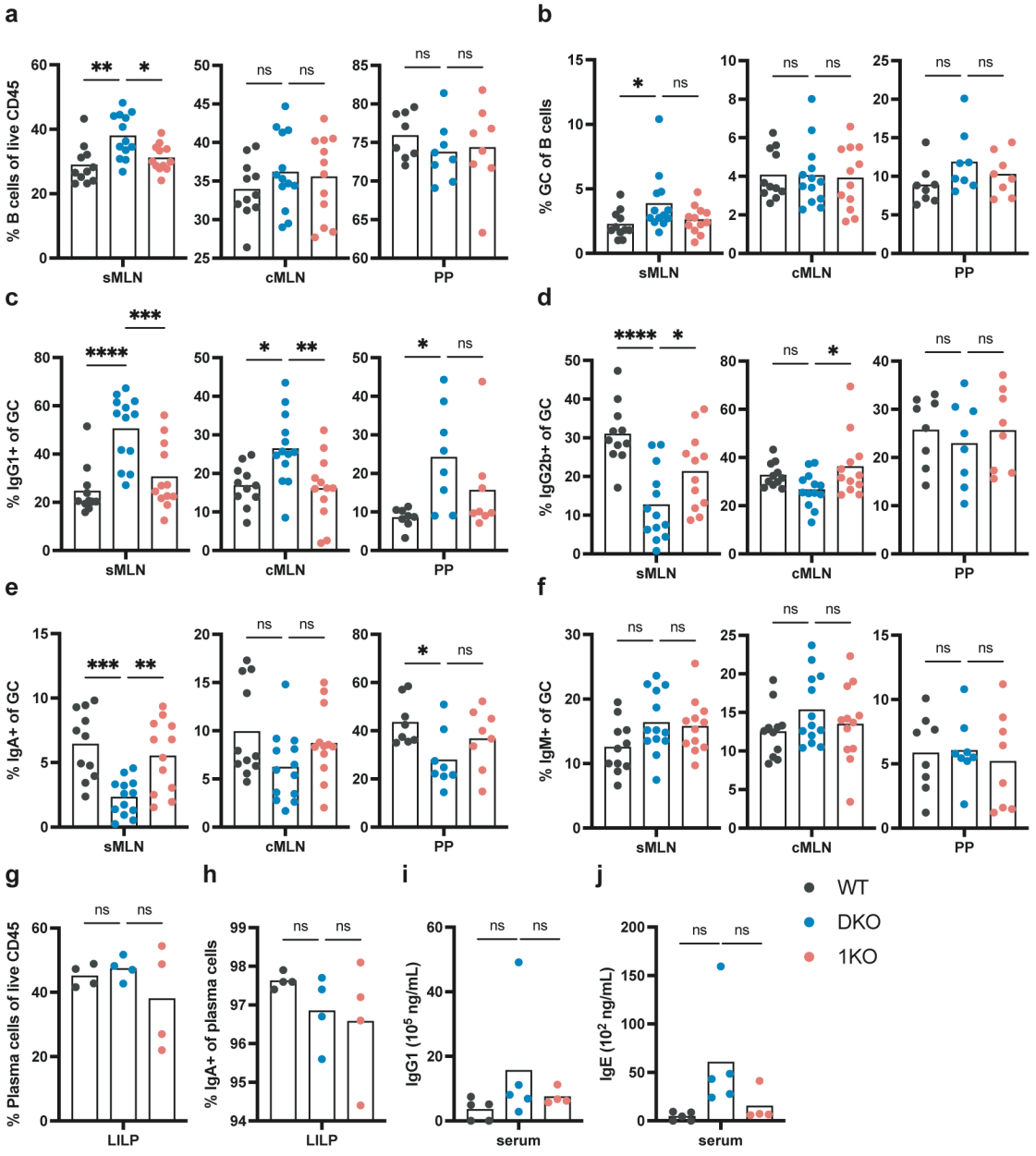
a
% B cells of live CD45
sMLN
cMLN
PP
b
% GC of B cells
c
% IgG1+ of GC
d
% IgG2b+ of GC
e
% IgA+ of GC
f
% IgM+ of GC
g
% Plasma cells of live CD45
LILP
h
% IgA+ of plasma cells
i
IgG1 (10^5 ng/mL)
serum
j
IgE (10^2 ng/mL)
WT
DKO
1KO
ns

Figure 3.11 B cell proliferation and switching to IgG1 in DKO sMLN was not due to CNS0KO alone or Ubc-creER.

a-f, Frequencies of B cells among total live CD45^{+} cells (a, d), germinal center (GC) B cells among all B cells (b, e), and IgG1+ cells among GC B cells (c, f) in the indicated organs of WT, CNS1KO, and DKO littermates treated as in Fig. 3.4 (a-c), and similarly treated Ubc-creER^{+} or Ubc-creER^{-} *Foxp3*^{GFP} mice (d-f). sMLN, small intestine (mostly jejunum and ileum) draining mesenteric lymph nodes. cMLN, proximal colon-draining mesenteric lymph node. PP, Peyer's patch. Spl, spleen. pLN, peripheral (brachial, axillary, inguinal) lymph nodes. Bars represent mean. a-c, Two-way ANOVA with Dunnett's multiple hypothesis test. d-f, Two-tailed unpaired *t*-tests with Holm-Sidak multiple hypothesis testing correction. ns, not significant; *, $p < 0.05$.

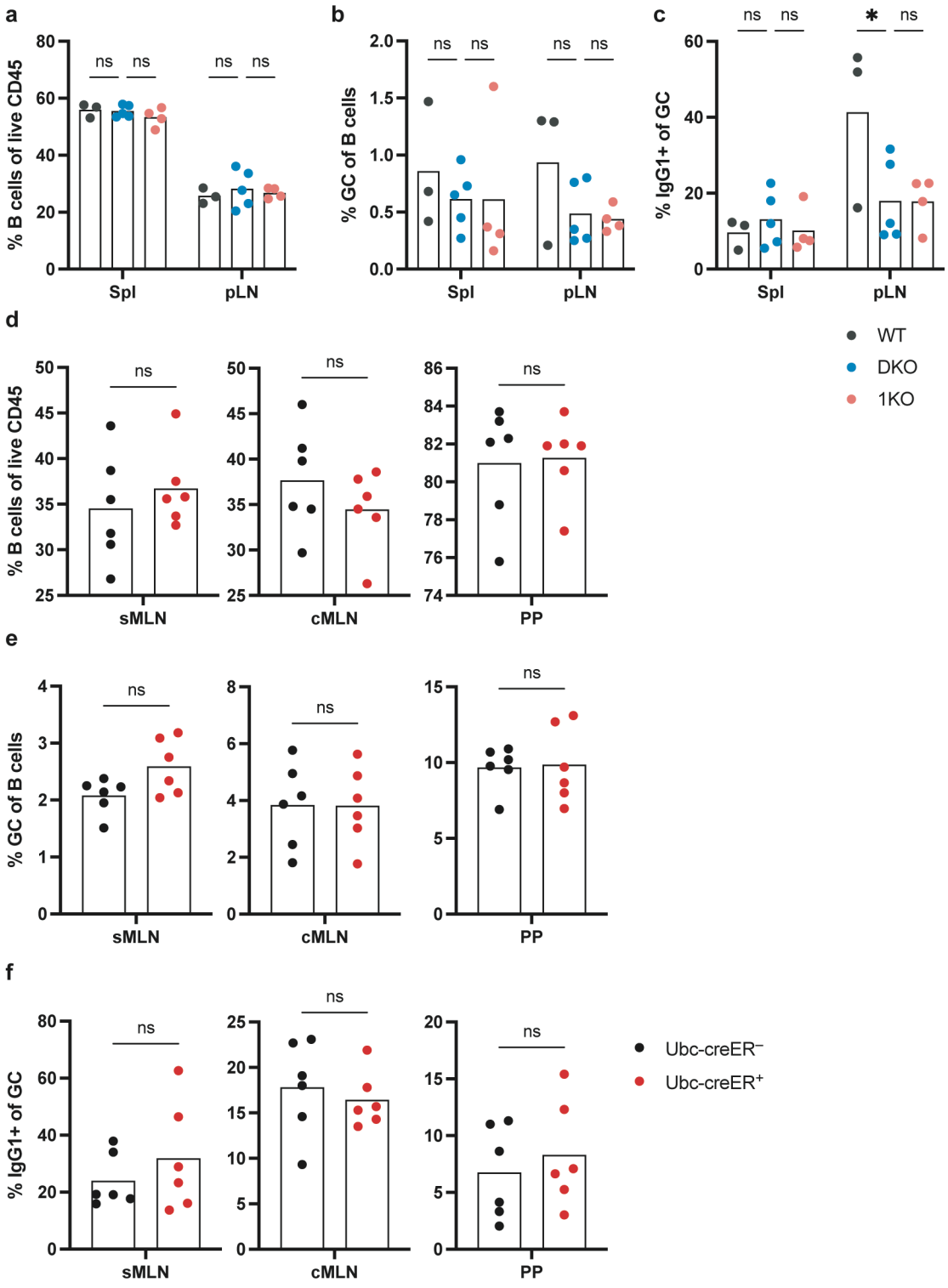
a
% B cells of live CD45
80
60
40
20
0
ns
ns
ns
ns
Spl
pLN
b
% GC of B cells
2.0
1.5
1.0
0.5
0.0
ns
ns
ns
ns
Spl
pLN
c
% IgG1+ of GC
60
40
20
0
ns
ns
*
ns
Spl
pLN
WT
DKO
1KO
d
% B cells of live CD45
50
45
40
35
30
25
86
84
82
80
78
76
74
ns
sMLN
cMLN
PP
e
% GC of B cells
4
3
2
1
0
8
6
4
2
15
10
5
ns
sMLN
cMLN
PP
f
% IgG1+ of GC
80
60
40
20
25
20
15
10
5
Ubc-creER⁻
Ubc-creER⁺
sMLN
cMLN
PP

Figure 3.12 B cell proliferation and switching to IgG1 in DKO sMLN was not due to CNS0KO alone.

a-c, Frequencies of B cells among total live $CD45^+$ cells (a), germinal center (GC) B cells among all B cells (b), and IgG1+ cells among GC B cells (c) in the indicated organs of WT, CNS0KO, and DKO littermates treated as in Fig. 3.8a (a-c). sMLN, small intestine (mostly jejunum and ileum) draining mesenteric lymph nodes. cMLN, proximal colon-draining mesenteric lymph node. PP, Peyer's patch. Bars represent mean. One-way ANOVA with Dunnett's multiple hypothesis test. ns, not significant; *, $p < 0.05$; **, $p < 0.01$.

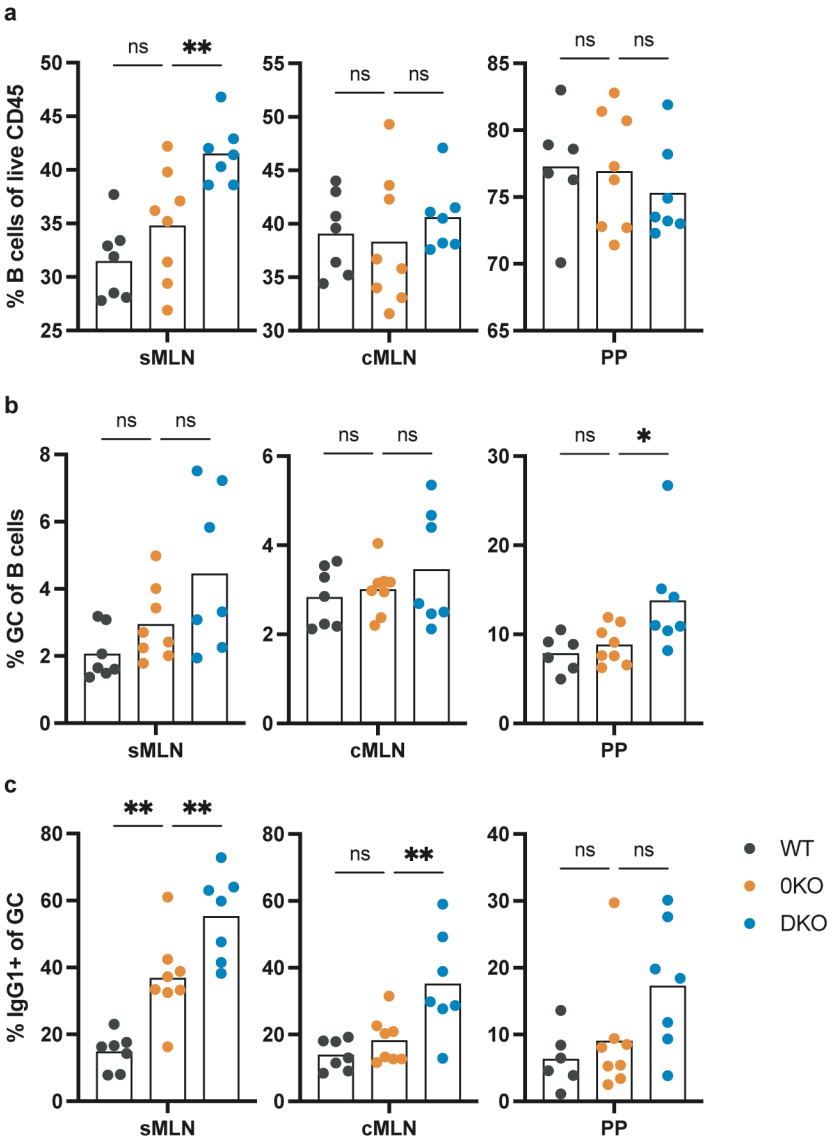
a
% B cells of live CD45
ns
**
ns
ns
ns
ns
sMLN
cMLN
PP
b
% GC of B cells
ns
ns
ns
ns
ns
*
sMLN
cMLN
PP
c
% IgG1+ of GC
**
**
ns
**
ns
ns
sMLN
cMLN
PP
WT
0KO
DKO

Discussion

By generating mice deficient in both CNS1 and CNS0 enhancers, we have demonstrated that CD4 T cells from the resulting DKO mice were almost incapable of expressing Foxp3 when cultured in pTreg cell-inducing cytokines. Lack of pTreg cells *in vivo* caused intestinal but not systemic Th2 immune activation as well as B cell proliferation and switching to IgG1. While Th2 inflammation had been observed in *Foxp3*$^{GFP\text{-}\Delta CNS1}$ mice (70, 119), the T cell changes in DKO mice were more pronounced and lasted longer, and the B cell alterations were only observed in DKO mice. These were consistent with the *in vitro* induction assay results, where CNS1/CNS0 double deficiency led to a more complete developmental block in pTreg cells than CNS1KO alone.

Synergistic behavior is a common feature of transcriptional regulation, where different transcription factors or enhancers control the activity of a shared target *cis*-element or promoter, respectively, in a combinatorial manner (195). Regulation of *Foxp3* gene expression by multiple enhancers confers at least three benefits. First, by responding to distinct environmental cues, the activity of different enhancers or lack thereof can generate various combinations of potential regulatory states that by far outnumber the enhancer themselves, thus drastically increasing the number of potential regulatory nodes and allowing for context-specific fine-tuning of Treg cell generation. Second, the overlapping biochemical features and functions that some *Foxp3* enhancers share impart more robust *Foxp3* gene induction, where they can compensate for the loss of one another as in the case of CNS1 buffering the effect of CNS0 deficiency on intestinal pTreg cell

development (74, 130). Third, collective regulation of transcription by more than one *cis*-elements makes emergent properties feasible, where genetic and biochemical interactions among enhancers may more efficiently initiate transcription than their combined independent effect. Modeling synergy between CNS1 and CNS0 can be difficult, especially because their exact molecular regulatory mechanisms of *Foxp3* expression (e.g. looping) are largely elusive. Exploring the potential synergy between CNS1 and CNS0 not only requires choosing the proper mathematical methods, but also depends on a better understanding of the effects they have on one another in terms of biochemical (e.g. chromatinization, histone modifications) and functional properties.

In addition to host factors modeled in *in vitro* induction assays, including TGF-β, RA, and IL-2, copious microbiota-derived compounds (e.g., short-chain fatty acids, bile acids) (120, 121) and other signaling molecules (IL-6, IL-23) (115, 196, 197) could promote or antagonize pTreg cell differentiation *in vivo*, respectively. Therefore, we are also currently investigating the effect of CNS1 and CNS0 on pTreg cell generation *in vivo* using T cells expressing transgenic TCR specific for *Helicobacter hepaticus*, which efficiently supports conversion of WT CD4 T cells to Treg cells in an IL-10-dependent manner (98, 99). This would allow us to elucidate the involvement of IL-2 in pTreg cell development *in vivo* as well as unique genetic interactions between the two enhancers different from that *in vitro.* Given that *H. hepaticus*-specific Treg cells only engender in the proximal colon, it is possible that other regions of the intestinal mucosa and their associated lymphoid tissues are preferentially enriched for distinct pTreg cell-inducing factor,

thus having differential dependence on *Foxp3* enhancers. Therefore, it would be potentially informative to eventually expand the use of transgenic TCRs to other model antigens, such as OVA which facilitates small intestine pTreg cell induction.

The preferential B cells expansion in MLNs draining small but not large intestine in DKO mice is particularly intriguing. Provided MLNs receiving antigens from both jejunum and ileum were enlarged (data not shown) while most commensal microbes reside in the terminal ileum and large intestine, it is likely that the B cell changes were triggered by food-derived antigens. The intestinal immune activation did not seem to interfere with nutrient absorption, as DKO mice did not weigh less than CNS1KO mice. However, the elevated serum IgE of putative specificity for dietary antigens could precipitate food allergy in the event of a barrier breach caused by injury or infection, which can be studied using mouse models of peanut allergy. In addition, the antigenic specificity of the serum IgE can be elucidated by feeding the mice with elemental diet, or by incubating the serum with proteins purified from the chow.

Lastly, although we observed a clear genotypic effect on pTreg cell generation and the associated biological sequela in our experiments, it is possible that the predisposition for type 2 immunopathology imparted by CNS1/CNS0 double deficiency only manifested because of the unique composition of the microbiota in our colony. One particular intestinal protozoan pathobiont present in our facility, *Tritrichomonas muris*, has been shown to cause hyperplasia of and elevated IL-25 production by tuft cells as well as ILC2 expansion in the small intestine, features consistent with a Th2 response (198). Therefore, uncovering the

microbial contribution to the type 2 pathology associated with defective pTreg cell generation would greatly further our understanding of the etiology of common human gastrointestinal disorders such as inflammatory bowel disease and irritable bowel syndrome, which like many other common diseases are believed to be triggered by exposure to specific environmental factors combined with multigenic predisposition (199, 200).

Methods

Mice

Experiments in this study were approved by the Sloan Kettering Institute (SKI) Institutional Animal Care and Use Committee under protocol 08-10-023 and conducted in compliance with institutional ethics guidelines. Mice were housed at the SKI animal facility under SPF conditions on a 12-hour light/dark cycle with free access to water and regular chow diet. The average ambient temperature is 21.5°C and the average humidity is 48%. All control and experimental animals were age-matched, and littermates were used as controls unless otherwise indicated. *Foxp3*^{GFP} (78), *Foxp3*$^{GFP\text{-}CNS0fl}$ (73), and *Ndor1*$^{Ubc\text{-}creER}$ (189) mice were maintained in the Sloan Kettering Institute animal facility. B6.SJL-*Ptprc*^{a} *Pepc*^{b}/BoyJ (CD45.1) mice were purchased from The Jackson Laboratory.

Generation of *Foxp3*$^{GFP\text{-}CNS0fl\text{-}\Delta CNS1}$ mice

Foxp3$^{GFP\text{-}CNS0fl\text{-}\Delta CNS1}$ mice were generated at the MSKCC Mouse Genetics Core Facility. CNS1 was targeted with one crRNA on each side (5': TAGATTACTCTTTTCTTGTG; 3': GCTGGAGGACTGATGCTGCT). *In vitro* assembled CRISPR ribonucleoprotein complex was electroporated into *Foxp3*$^{GFP\text{-}}$

^{CNS0fl} zygotes, which were then transplanted into pseudopregnant mice. The resulting mice were screened for CNS1 deletion with PCR, and male founders with deletions similar to the previous described *Foxp3*$^{GFP\text{-}\Delta CNS1}$ (70, 119) mice were bred to *Foxp3*^{GFP} or *Foxp3*$^{GFP\text{-}CNS0fl}$ mice to confirm germline transmission. Two founder lines were initially analyzed and yielded phenotypically similar results. One founder line was then maintained, on which most of the experiments were conducted.

In vitro induction assay

Bone marrow cells were harvested from the femur and tibia of WT, CNS1KO, CNS0KO, and DKO mice and T cells were depleted with Dynabeads FlowComp Mouse Pan T (CD90.2) Kit by recovering the cells not bound to the beads. Bone marrow was transferred into CD45.1 recipients that had been lethally irradiated with 950 rad 24 hrs before. Recipients were rested for 8 weeks and 3 doses of tamoxifen were given via oral gavage every 3 days. One week after the last dose, spleen, peripheral (brachial, axillary, inguinal) and mesenteric lymph nodes were harvested and meshed with the blunt end of a syringe plunger through a 100 μm strainer (Corning, 07-201-432). CD4 T cells were then enriched with the Dynabeads Flowcomp Mouse CD4 Kit (ThermoFisher, 11461D) according to manufacturer's instructions, stained with antibodies, washed extensively, resuspended in isolation buffer (PBS w/ 2% FBS, 10 mM HEPES buffer, 1% L-glutamine, and 2 mM EDTA) containing 0.01% SYTOX Blue dead cell stain (ThermoFisher, S34857) to facilitate dead cell exclusion. Donor-derived naïve

conventional T cells ($CD45.2^{+}CD45.1^{-}TCR\beta^{+}CD4^{+}$Foxp3-$GFP^{-}CD62^{hi}CD44^{lo}$) were sorted on a FACSAria (BD) instrument.

To set up the induction assay, 96-well Flat bottom plates were coated with 200 μL 1 μg/mL α-CD3ε (145-2C11, BioXCell, BE0001-1) and α-CD28 (37.51, BioXCell, BE0015-1) in PBS at 37°C for more than 2 h and then extensively washed. Serial dilutions of TGF-β (ThermoFisher, 240B002), RA (Sigma-Aldrich, R2625), and rhIL-2 (NIH-NCI-FNLCR-BRB, BULK Ro 23-6019) were then set up in the coated plates and 50,000 cells were added to each well to a final volume of 200 μL. When titrating TGF-β, rhIL-2 concentration was kept constant at 50 U/mL. When titrating RA, TGF-β and rhIL-2 concentrations were kept constant at 100 pg/mL and 50 U/mL, respectively. When titrating rhIL-2, TGF-β concentration was kept constant at 1 ng/mL, and 5 μg/mL of each α-mIL-2 antibodies (RRID: AB_1107702, Clone: JES6-1A12, BioXCell BE0043; RRID: AB_1107705, Clone: S4B6-1, BioXCell BE0043-1) were added to neutralize murine IL-2 produced by the cells during the course of the assay. The cells were then cultured 37°C for 24 h and then recorded on an Attune cytometer with a CytKick Max Autosampler (ThermoFisher).

Tamoxifen and 4-hydroxytomaxifen treatment

For tamoxifen administration, 20 mg of tamoxifen (Sigma-Aldrich, T5648) was resuspended in 1 mL corn oil (Sigma-Aldrich, C8267) by rotating and tilting at 37°C until fully dissolved. Each mouse was orally gavaged with 4 mg of tamoxifen per treatment.

4-hydroxytamoxifen (4-OHT, Sigma-Aldrich, H7904) stock solution was made by reconstituting in ethyl alcohol 200 proof (Sigma-Aldrich, E-7023) at a concentration of 20 mg/mL, then diluting 1:1 (v/v) with Cremophor EL (Sigma-Aldrich, 238470). 20 μg/g body weight of 4-OHT diluted in PBS was administered intraperitoneally.

Isolation of cell from lymphoid organs and large intestine lamina propria cells

Cells were retrieved from spleens, peripheral (brachial, axillary and inguinal) lymph nodes, mesenteric lymph nodes, thymuses, and livers by meshing the organs through a 100 μm strainer (Corning, 07-201-432) with a syringe plunger. Cells in the colonic lamina propria were isolated as previously described (119). Briefly, colons were cleaned by flushing the luminal content out with PBS using a syringe, defatted, opened up longitudinally and diced into 1-2 cm pieces. Tissues were then incubated in 25 mL IEL solution [1x PBS w/ 2% FBS (ThermoFisher, 35010CV), 10 mM HEPES buffer (ThermoFisher, MT 25–060-CI), 1% penicillin/streptomycin (ThermoFisher, MT 30–002-CI), 1% L-glutamine (ThermoFisher, MT 25–005-CI), plus 1 mM EDTA (Sigma-Aldrich, E4884) and 1 mM DTT (Sigma-Aldrich, D9779) added immediately before use] for 15 minutes at 37°C with vigorous shaking (250 rpm) to remove the epithelial fraction. Tissues were then retrieved, washed extensively, and digested in 25 mL LPL solution [1x RPMI 1640 w/2% FBS, 10 mM HEPES buffer, 1% penicillin/streptomycin, 1% L-glutamine, 0.2 U/mL collagenase A (Sigma, 11088793001) and 1 U/mL DNase I (Sigma-Aldrich, 10104159001)] for 30 minutes at 37°C with vigorous shaking (250 rpm). ¼inch ceramic beads (MP Biomedicals, 116540034) were added during this

step (3–4 per sample) to facilitate tissue dissociation. The digested samples were passed through a 100 μm strainer, pelleted at 450 g for 5 minutes and washed extensively. Cells from large intestine were centrifugated in 40% PBS-adjusted Percoll (v/v, ThermoFisher, 45–001-747) in PBS to enrich for lymphocytes. Erythrocytes in the spleen were lysed with ACK lysis buffer [150 mM NH_4Cl (Sigma-Aldrich, A9434), 10 mM $KHCO_3$ (Sigma-Aldrich, P7682), 0.1 mM Na_2EDTA, pH 7.4].

Flow cytometric analysis of cytokine production and intracellular antigens

To measure cytokine production after *ex vivo* restimulation, single cell suspensions were incubated at 37°C for 4 hours with 5% CO_2 in 96-well flat-bottom plates in the presence of 50 ng/mL phorbol-12-myristate-13-acetate (PMA, Sigma-Aldrich, P8139) and 500 ng/mL ionomycin (Sigma-Aldrich, I0634) with 1 μg/mL brefeldin A (Sigma-Aldrich, B6542) and 2 μM monensin (Sigma-Aldrich, M5273) to inhibit ER and Golgi transport. Cells were then stained with Zombie NIR Flexible Viability Kit (Biolegend, 423106) in PBS for 10 minutes at 4°C to help identify dead cells and then with purified anti-Mouse CD16/CD32 (2.4G2, Tonbo, 70-0161) in staining buffer [0.5% (w/v) BSA, 2 mM EDTA, 10 mM HEPES, 0.02% NaN_3 (Sigma-Aldrich, S2002) in 1x PBS] for 10 minutes at 4°C to block the Fc receptors. Samples were then incubated with fluorescently conjugated antibodies against cell surface antigens in staining buffer for 25 minutes at 4°C and washed extensively. To access intracellular antigens, cells were fixed and permeabilized with the BD Cytofix/Cytoperm Kit (BDB554714) for measuring cytokine production, or with the ThermoFisher Transcription Factor Fix/Perm Kit (00-5521-00) for staining cytosolic

and nuclear antigens as well as immunoglobulin isotypes, according to manufacturers' instructions. Samples were recorded on an Cytek Aurora cytometer using the SpectroFlo software v2.2.0.3 and analyzed with FlowJo v10.6.1 (BD).

ELISA

ELISA experiments were conducted as previously described(71). Briefly, mouse peripheral blood was collected via cardiac puncture immediately after euthanasia into BD SST microcontainer tubes (02-675-185) and sera were harvested after centrifugation. Flat-bottom 96-well plates were coated with capturing antibodies in 50 μL 0.1 M $NaHCO_3$ solution at pH 9.5 O/N at 4°C. The plates were then emptied, blocked with 200 μL 1% bovine serum albumin (VWR, 97061-422) in PBS, and washed 3 times with PBS containing 0.05% Tween-20 (Sigma-Aldrich, P1379). 50 μL of sera at appropriate dilutions was added and incubated O/N at 4°C. The plate was then incubated in sequential orders with 50 μL of biotinylated detection antibodies for 2-3 hours, 50 μL of avidin-HRP (ThermoFisher, 18-4100-51) for 30 minutes, and 100 μL of TMB solution (ThermoFisher, 00-4201-56) at 25°C , with 3-4 washes with PBS-Tween in between each incubation steps. The colorimetric reaction was stopped with 100 μL of 1M H_3PO_4 (Sigma-Aldrich, P5811) after 5-10 minutes of adding TMB and absorbance at 450 nm was measured with a Synergy HTX plate reader (BioTek). Concentrations of antigens were determined using standard curves constructed with purified recombinant proteins and calculated with Gen5 3.02.2 (BioTek).

Antibodies and reagents

The following antibodies and streptavidin were used in this study for flow cytometry, with clones, venders, catalog numbers, and dilutions indicated in the parentheses: anti-Siglec-F (E50-2440, BD, 562681, 1:400), anti-I-A/I-E (M5/114.15.2, BD, 566086, 1:1200), anti-CD45 (30-F11, BioLegend, 103136, 1:600), anti-CD11b (M1/70, BD, 563553, 1:300), anti-CD3ε (17A2, BioLegend, 100237, 1:400), anti-Ly-6C (HK1.4, BioLegend, 128037, 1:1500), anti-CD90.2 (30-H12, BioLegend, 105331, 1:1500), anti-CD19 (6D5, Biolegend, 115510, 1:600), anti-Gr-1 (RB6-8C5, ThermoFisher, 58-5931-82, 1:1000), anti-TCRβ (H57-597, BD, 748405, 1:300), anti-CD4 (RM4-5, BioLegend, 100553, 1:400), anti-CD8α (53-6.7, BD, 564297, 1:400), anti-CD44 (IM7, BD, 563971, 1:400; ThermoFisher, 48-0441-82, 1:400; BioLegend, 103049, 1:400), anti-CD62L (MEL-14, BioLegend, 104438, 1:1600; BD, 565213, 1:600), anti-Helios (22F6, BioLegend, 137222, 1:400), anti-CD45.1 (A20, BioLegend, 110708, 1:200), anti-CD45.2 (104, ThermoFisher, 17-0454-82, 1:200), anti-IL-2 (JES6-5H4, BioLegend, 503824, 1:500), anti-IL-17A (17B7, ThermoFisher, 48-7177-82, 1:400), anti-IFNγ (XMG1.2, Biolegend, 505836, 1:200), anti-IL-4 (11B11, ThermoFisher, 17-7041-82, 1:400), anti-CD45R/B220 (RA3-6B2, Biolegend, 103261, 1:400), anti-IL-5 (TRFK5, BD, 554395, 1:500), anti-IL-13 (eBio13A, ThermoFisher, 61-7133-82, 1:800), anti-RORgt (Q31-378, BD, 562684, 1:400), anti-CTLA4 (UC10-4B9, Biolegend, 106323, 1:200), anti-CD69 (H1.2F3, ThermoFisher, 15-0691-81, 1:400), anti-Gata-3 (TWAJ, ThermoFisher, 50-9966-42, 1:200), anti-CD64 (X-54-5/7.1, Biolegend, 139314, 1:300), anti-CD95 (Jo2, BD, 557653, 1:300), anti-CD38 (90, ThermoFisher, 46-0381-82, 1:750), anti-IgD (11-26c.2a, BioLegend, 405729,

1:600), anti-IgM (II/41, BD, 743327, 1:200), anti-IgG1 (X56, BD, 742476, 1:200), anti-IgA (mA-6E1, ThermoFisher, 12-4204-82, 1:1000), anti-IgG2b (R12-3, BD Biosciences, 743174, 1:200), anti-Blimp-1 (5E7, BioLegend, 150008, 1:200), anti-CD117 (2B8, BD Biosciences, 553356, 1:200), anti-FcεRIα (2B8, BD, Biosciences, 553356, 1:400).

The following antibodies were used to capture antigens for ELISA in this study: purified anti-mouse IgE (R35-72, BD Pharmingen, 553413), Goat Anti-Mouse IgG1 (RRID: AB_2794408, SouthernBiotech, 1070-01), Goat Anti-Mouse IgG3 (RRID: AB_2794567, SouthernBiotech, 1100-01), Goat Anti-Mouse IgG2a (RRID: AB_2794475, SouthernBiotech, 1080-01), Goat Anti-Mouse IgG2b (RRID: AB_2794517, SouthernBiotech, 1090-01), Goat Anti-Mouse IgG2c (RRID: AB_2794464, SouthernBiotech, 1079-01), Goat Anti-Mouse IgA (RRID: AB_2314669, SouthernBiotech, 1040-01), Goat Anti-Mouse IgM (RRID: AB_2794197, SouthernBiotech, 1020-01).

The following antibodies were used to detect antigens for ELISA in this study: Goat Anti-Mouse Ig-HRP (RRID: AB_2728714, SouthernBiotech, 1010-05), Biotin Rat Anti-Mouse IgE (R35-118, BD Pharmingen, 553419).

The following reagents were used to construct standard curves for ELISA in this study: Purified Mouse IgE, kappa, Isotype Control (C38-2, BD Pharmingen, 557079), Purified Mouse IgA, kappa, Isotype Control (M18-254, BD Pharmingen, 553476), Purified Mouse IgG3, kappa, Isotype Control (A112-3, BD Pharmingen, 553486), Purified Mouse IgG1, kappa, Isotype Control (15H6, SouthernBiotech, 0102-01), Purified Mouse IgG2a, kappa, Isotype Control (UPC-10, Sigma, M5409),

IgM Isotype Control from murine myeloma (MOPC 104E, Sigma, M5909), IgG2b Isotype Control from murine myeloma (MOPC-141, Sigma, M5534), Mouse IgG2c (6.3, RRID: AB_2794064, SouthernBiotech, 0122-01).

CONCLUDING REMARKS

In conclusion, we have presented definitive experimental data demonstrating that Treg cells are fully functional under conditions of established inflammation and are capable of reversing lethal autoimmunity, and that impaired peripheral Treg cell generation in the intestine causes gastrointestinal inflammation and potential food allergy. Taken together, these results not only highlight the importance of Treg cells in the etiology of human autoimmune and inflammatory disorders, but also accentuate the tremendous potential Treg cells harbor as therapeutics. However, heterogeneity within Treg cell populations must be taken into account when developing Treg cell-based therapies, and the distinct Treg cell subsets indicated for each condition must be accurately identified. Such heterogeneity can result from antigenic specificity, tissue adaptation, activation states, effector mechanisms, regenerative potential, migratory properties, and disease-specific remodeling. In addition, novel methods of delivery or *in situ* generation of Treg cells need to be invented for efficient targeting to the diseased tissues. Successful application of Treg cells in the clinic depends on further understanding of and continuous research on Treg cells, and the development of novel molecular, cellular, biophysical, and multi-omic tools to study their biology and disruption thereof in human disorders.

BIBLIOGRAPHY

1. Starr TK, Jameson SC, Hogquist KA. Positive and negative selection of T cells. Annu Rev Immunol. 2003;21:139-76.

2. Lenschow DJ, Walunas TL, Bluestone JA. CD28/B7 system of T cell costimulation. Annu Rev Immunol. 1996;14:233-58.

3. Bonomo A, Kehn PJ, Payer E, Rizzo L, Cheever AW, Shevach EM. Pathogenesis of post-thymectomy autoimmunity. Role of syngeneic MLR-reactive T cells. J Immunol. 1995;154(12):6602-11.

4. Nishizuka Y, Sakakura T. Thymus and reproduction: sex-linked dysgenesia of the gonad after neonatal thymectomy in mice. Science. 1969;166(3906):753-5.

5. Sakaguchi S, Takahashi T, Nishizuka Y. Study on cellular events in postthymectomy autoimmune oophoritis in mice. I. Requirement of Lyt-1 effector cells for oocytes damage after adoptive transfer. J Exp Med. 1982;156(6):1565-76.

6. Asano M, Toda M, Sakaguchi N, Sakaguchi S. Autoimmune disease as a consequence of developmental abnormality of a T cell subpopulation. J Exp Med. 1996;184(2):387-96.

7. Fehervari Z, Sakaguchi S. Development and function of CD25+CD4+ regulatory T cells. Curr Opin Immunol. 2004;16(2):203-8.

8. Shevach EM. Regulatory T cells in autoimmmunity*. Annu Rev Immunol. 2000;18:423-49.

9. Brunkow ME, Jeffery EW, Hjerrild KA, Paeper B, Clark LB, Yasayko SA, et al. Disruption of a new forkhead/winged-helix protein, scurfin, results in the fatal lymphoproliferative disorder of the scurfy mouse. Nat Genet. 2001;27(1):68-73.

10. Bennett CL, Christie J, Ramsdell F, Brunkow ME, Ferguson PJ, Whitesell L, et al. The immune dysregulation, polyendocrinopathy, enteropathy, X-linked syndrome (IPEX) is caused by mutations of FOXP3. Nat Genet. 2001;27(1):20-1.

11. Wildin RS, Ramsdell F, Peake J, Faravelli F, Casanova JL, Buist N, et al. X-linked neonatal diabetes mellitus, enteropathy and endocrinopathy syndrome is the human equivalent of mouse scurfy. Nat Genet. 2001;27(1):18-20.

12. Chatila TA, Blaeser F, Ho N, Lederman HM, Voulgaropoulos C, Helms C, et al. JM2, encoding a fork head-related protein, is mutated in X-linked autoimmunity-allergic disregulation syndrome. J Clin Invest. 2000;106(12):R75-81.

13. Gambineri E, Torgerson TR, Ochs HD. Immune dysregulation, polyendocrinopathy, enteropathy, and X-linked inheritance (IPEX), a syndrome of systemic autoimmunity caused by mutations of FOXP3, a critical regulator of T-cell homeostasis. Curr Opin Rheumatol. 2003;15(4):430-5.

14. Godfrey VL, Rouse BT, Wilkinson JE. Transplantation of T cell-mediated, lymphoreticular disease from the scurfy (sf) mouse. Am J Pathol. 1994;145(2):281-6.

15. Hori S, Nomura T, Sakaguchi S. Control of regulatory T cell development by the transcription factor Foxp3. Science. 2003;299(5609):1057-61.

16. Khattri R, Cox T, Yasayko SA, Ramsdell F. An essential role for Scurfin in CD4+CD25+ T regulatory cells. Nat Immunol. 2003;4(4):337-42.

17. Fontenot JD, Gavin MA, Rudensky AY. Foxp3 programs the development and function of CD4+CD25+ regulatory T cells. Nat Immunol. 2003;4(4):330-6.

18. Liston A, Farr AG, Chen Z, Benoist C, Mathis D, Manley NR, et al. Lack of Foxp3 function and expression in the thymic epithelium. J Exp Med. 2007;204(3):475-80.

19. Fontenot JD, Rasmussen JP, Williams LM, Dooley JL, Farr AG, Rudensky AY. Regulatory T cell lineage specification by the forkhead transcription factor foxp3. Immunity. 2005;22(3):329-41.

20. Wan YY, Flavell RA. Regulatory T-cell functions are subverted and converted owing to attenuated Foxp3 expression. Nature. 2007;445(7129):766-70.

21. Williams LM, Rudensky AY. Maintenance of the Foxp3-dependent developmental program in mature regulatory T cells requires continued expression of Foxp3. Nat Immunol. 2007;8(3):277-84.

22. Kim JM, Rasmussen JP, Rudensky AY. Regulatory T cells prevent catastrophic autoimmunity throughout the lifespan of mice. Nat Immunol. 2007;8(2):191-7.

23. Chinen T, Volchkov PY, Chervonsky AV, Rudensky AY. A critical role for regulatory T cell-mediated control of inflammation in the absence of commensal microbiota. J Exp Med. 2010;207(11):2323-30.

24. Gangaplara A, Martens C, Dahlstrom E, Metidji A, Gokhale AS, Glass DD, et al. Type I interferon signaling attenuates regulatory T cell function in viral infection and in the tumor microenvironment. PLoS Pathog. 2018;14(4):e1006985.

25. Izcue A, Hue S, Buonocore S, Arancibia-Carcamo CV, Ahern PP, Iwakura Y, et al. Interleukin-23 restrains regulatory T cell activity to drive T cell-dependent colitis. Immunity. 2008;28(4):559-70.

26. Nish SA, Schenten D, Wunderlich FT, Pope SD, Gao Y, Hoshi N, et al. T cell-intrinsic role of IL-6 signaling in primary and memory responses. Elife. 2014;3:e01949.

27. Overacre-Delgoffe AE, Chikina M, Dadey RE, Yano H, Brunazzi EA, Shayan G, et al. Interferon-gamma Drives Treg Fragility to Promote Anti-tumor Immunity. Cell. 2017;169(6):1130-41 e11.

28. Pasare C, Medzhitov R. Toll pathway-dependent blockade of CD4+CD25+ T cell-mediated suppression by dendritic cells. Science. 2003;299(5609):1033-6.

29. Pelly VS, Coomes SM, Kannan Y, Gialitakis M, Entwistle LJ, Perez-Lloret J, et al. Interleukin 4 promotes the development of ex-Foxp3 Th2 cells during immunity to intestinal helminths. J Exp Med. 2017;214(6):1809-26.

30. Srivastava S, Koch MA, Pepper M, Campbell DJ. Type I interferons directly inhibit regulatory T cells to allow optimal antiviral T cell responses during acute LCMV infection. J Exp Med. 2014;211(5):961-74.

31. Oldenhove G, Bouladoux N, Wohlfert EA, Hall JA, Chou D, Dos Santos L, et al. Decrease of Foxp3+ Treg cell number and acquisition of effector cell phenotype during lethal infection. Immunity. 2009;31(5):772-86.

32. Schenten D, Nish SA, Yu S, Yan X, Lee HK, Brodsky I, et al. Signaling through the adaptor molecule MyD88 in CD4+ T cells is required to overcome suppression by regulatory T cells. Immunity. 2014;40(1):78-90.

33. Korn T, Reddy J, Gao W, Bettelli E, Awasthi A, Petersen TR, et al. Myelin-specific regulatory T cells accumulate in the CNS but fail to control autoimmune inflammation. Nat Med. 2007;13(4):423-31.

34. Clough LE, Wang CJ, Schmidt EM, Booth G, Hou TZ, Ryan GA, et al. Release from regulatory T cell-mediated suppression during the onset of tissue-specific autoimmunity is associated with elevated IL-21. J Immunol. 2008;180(8):5393-401.

35. Gao Y, Tang J, Chen W, Li Q, Nie J, Lin F, et al. Inflammation negatively regulates FOXP3 and regulatory T-cell function via DBC1. Proc Natl Acad Sci U S A. 2015;112(25):E3246-54.

36. Komatsu N, Okamoto K, Sawa S, Nakashima T, Oh-hora M, Kodama T, et al. Pathogenic conversion of Foxp3+ T cells into TH17 cells in autoimmune arthritis. Nat Med. 2014;20(1):62-8.

37. Bailey-Bucktrout SL, Martinez-Llordella M, Zhou X, Anthony B, Rosenthal W, Luche H, et al. Self-antigen-driven activation induces instability of regulatory T cells during an inflammatory autoimmune response. Immunity. 2013;39(5):949-62.

38. Mottet C, Uhlig HH, Powrie F. Cutting edge: cure of colitis by CD4+CD25+ regulatory T cells. J Immunol. 2003;170(8):3939-43.

39. Uhlig HH, Coombes J, Mottet C, Izcue A, Thompson C, Fanger A, et al. Characterization of Foxp3+CD4+CD25+ and IL-10-secreting CD4+CD25+ T cells during cure of colitis. J Immunol. 2006;177(9):5852-60.

40. Lund JM, Hsing L, Pham TT, Rudensky AY. Coordination of early protective immunity to viral infection by regulatory T cells. Science. 2008;320(5880):1220-4.

41. Ruckwardt TJ, Bonaparte KL, Nason MC, Graham BS. Regulatory T cells promote early influx of CD8+ T cells in the lungs of respiratory syncytial virus-infected mice and diminish immunodominance disparities. J Virol. 2009;83(7):3019-28.

42. Hall AO, Beiting DP, Tato C, John B, Oldenhove G, Lombana CG, et al. The cytokines interleukin 27 and interferon-gamma promote distinct Treg cell populations required to limit infection-induced pathology. Immunity. 2012;37(3):511-23.

43. Durant LR, Makris S, Voorburg CM, Loebbermann J, Johansson C, Openshaw PJ. Regulatory T cells prevent Th2 immune responses and pulmonary eosinophilia during respiratory syncytial virus infection in mice. J Virol. 2013;87(20):10946-54.

44. Schmitz I, Schneider C, Frohlich A, Frebel H, Christ D, Leonard WJ, et al. IL-21 restricts virus-driven Treg cell expansion in chronic LCMV infection. PLoS Pathog. 2013;9(5):e1003362.

45. Zhao J, Zhao J, Perlman S. Virus-specific regulatory T cells ameliorate encephalitis by repressing effector T cell functions from priming to effector stages. PLoS Pathog. 2014;10(8):e1004279.

46. Hu W, Wang ZM, Feng Y, Schizas M, Hoyos BE, van der Veeken J, et al. Regulatory T cells function in established systemic inflammation and reverse fatal autoimmunity. Nat Immunol. 2021;22(9):1163-74.

47. Josefowicz SZ, Lu LF, Rudensky AY. Regulatory T cells: mechanisms of differentiation and function. Annu Rev Immunol. 2012;30:531-64.

48. Liston A, Nutsch KM, Farr AG, Lund JM, Rasmussen JP, Koni PA, et al. Differentiation of regulatory Foxp3+ T cells in the thymic cortex. Proc Natl Acad Sci U S A. 2008;105(33):11903-8.

49. Burchill MA, Yang J, Vang KB, Moon JJ, Chu HH, Lio CW, et al. Linked T cell receptor and cytokine signaling govern the development of the regulatory T cell repertoire. Immunity. 2008;28(1):112-21.

50. Lio CW, Hsieh CS. A two-step process for thymic regulatory T cell development. Immunity. 2008;28(1):100-11.

51. Lu L, Barbi J, Pan F. The regulation of immune tolerance by FOXP3. Nat Rev Immunol. 2017;17(11):703-17.

52. Singer A, Adoro S, Park JH. Lineage fate and intense debate: myths, models and mechanisms of CD4- versus CD8-lineage choice. Nat Rev Immunol. 2008;8(10):788-801.

53. Germain RN. T-cell development and the CD4-CD8 lineage decision. Nat Rev Immunol. 2002;2(5):309-22.

54. Stromnes IM, Cerretti LM, Liggitt D, Harris RA, Goverman JM. Differential regulation of central nervous system autoimmunity by T(H)1 and T(H)17 cells. Nat Med. 2008;14(3):337-42.

55. Moran AE, Holzapfel KL, Xing Y, Cunningham NR, Maltzman JS, Punt J, et al. T cell receptor signal strength in Treg and iNKT cell development demonstrated by a novel fluorescent reporter mouse. J Exp Med. 2011;208(6):1279-89.

56. Kawahata K, Misaki Y, Yamauchi M, Tsunekawa S, Setoguchi K, Miyazaki J, et al. Generation of CD4(+)CD25(+) regulatory T cells from autoreactive T cells

simultaneously with their negative selection in the thymus and from nonautoreactive T cells by endogenous TCR expression. J Immunol. 2002;168(9):4399-405.

57. Apostolou I, Sarukhan A, Klein L, von Boehmer H. Origin of regulatory T cells with known specificity for antigen. Nat Immunol. 2002;3(8):756-63.

58. Walker LS, Chodos A, Eggena M, Dooms H, Abbas AK. Antigen-dependent proliferation of CD4+ CD25+ regulatory T cells in vivo. J Exp Med. 2003;198(2):249-58.

59. Jordan MS, Boesteanu A, Reed AJ, Petrone AL, Holenbeck AE, Lerman MA, et al. Thymic selection of CD4+CD25+ regulatory T cells induced by an agonist self-peptide. Nat Immunol. 2001;2(4):301-6.

60. van Santen HM, Benoist C, Mathis D. Number of T reg cells that differentiate does not increase upon encounter of agonist ligand on thymic epithelial cells. J Exp Med. 2004;200(10):1221-30.

61. Wong P, Barton GM, Forbush KA, Rudensky AY. Dynamic tuning of T cell reactivity by self-peptide-major histocompatibility complex ligands. J Exp Med. 2001;193(10):1179-87.

62. Azzam HS, DeJarnette JB, Huang K, Emmons R, Park CS, Sommers CL, et al. Fine tuning of TCR signaling by CD5. J Immunol. 2001;166(9):5464-72.

63. Hsieh CS, Zheng Y, Liang Y, Fontenot JD, Rudensky AY. An intersection between the self-reactive regulatory and nonregulatory T cell receptor repertoires. Nat Immunol. 2006;7(4):401-10.

64. Hsieh CS, Liang Y, Tyznik AJ, Self SG, Liggitt D, Rudensky AY. Recognition of the peripheral self by naturally arising CD25+ CD4+ T cell receptors. Immunity. 2004;21(2):267-77.

65. Tai X, Cowan M, Feigenbaum L, Singer A. CD28 costimulation of developing thymocytes induces Foxp3 expression and regulatory T cell differentiation independently of interleukin 2. Nat Immunol. 2005;6(2):152-62.

66. Salomon B, Lenschow DJ, Rhee L, Ashourian N, Singh B, Sharpe A, et al. B7/CD28 costimulation is essential for the homeostasis of the CD4+CD25+ immunoregulatory T cells that control autoimmune diabetes. Immunity. 2000;12(4):431-40.

67. Marie JC, Liggitt D, Rudensky AY. Cellular mechanisms of fatal early-onset autoimmunity in mice with the T cell-specific targeting of transforming growth factor-beta receptor. Immunity. 2006;25(3):441-54.

68. Kim HP, Leonard WJ. CREB/ATF-dependent T cell receptor-induced FoxP3 gene expression: a role for DNA methylation. J Exp Med. 2007;204(7):1543-51.

69. Zheng Y, Josefowicz S, Chaudhry A, Peng XP, Forbush K, Rudensky AY. Role of conserved non-coding DNA elements in the Foxp3 gene in regulatory T-cell fate. Nature. 2010;463(7282):808-12.

70. Josefowicz SZ, Niec RE, Kim HY, Treuting P, Chinen T, Zheng Y, et al. Extrathymically generated regulatory T cells control mucosal TH2 inflammation. Nature. 2012;482(7385):395-9.

71. Feng Y, Arvey A, Chinen T, van der Veeken J, Gasteiger G, Rudensky AY. Control of the inheritance of regulatory T cell identity by a cis element in the Foxp3 locus. Cell. 2014;158(4):749-63.

72. Feng Y, van der Veeken J, Shugay M, Putintseva EV, Osmanbeyoglu HU, Dikiy S, et al. A mechanism for expansion of regulatory T-cell repertoire and its role in self-tolerance. Nature. 2015;528(7580):132-6.

73. Dikiy S, Li J, Bai L, Jiang M, Janke L, Zong X, et al. A distal Foxp3 enhancer enables interleukin-2 dependent thymic Treg cell lineage commitment for robust immune tolerance. Immunity. 2021;54(5):931-46 e11.

74. Kawakami R, Kitagawa Y, Chen KY, Arai M, Ohara D, Nakamura Y, et al. Distinct Foxp3 enhancer elements coordinate development, maintenance, and function of regulatory T cells. Immunity. 2021;54(5):947-61 e8.

75. Oh H, Grinberg-Bleyer Y, Liao W, Maloney D, Wang P, Wu Z, et al. An NF-kappaB Transcription-Factor-Dependent Lineage-Specific Transcriptional Program Promotes Regulatory T Cell Identity and Function. Immunity. 2017;47(3):450-65 e5.

76. Hemmers S, Schizas M, Azizi E, Dikiy S, Zhong Y, Feng Y, et al. IL-2 production by self-reactive CD4 thymocytes scales regulatory T cell generation in the thymus. J Exp Med. 2019;216(11):2466-78.

77. Bautista JL, Lio CW, Lathrop SK, Forbush K, Liang Y, Luo J, et al. Intraclonal competition limits the fate determination of regulatory T cells in the thymus. Nat Immunol. 2009;10(6):610-7.

78. Fontenot JD, Dooley JL, Farr AG, Rudensky AY. Developmental regulation of Foxp3 expression during ontogeny. J Exp Med. 2005;202(7):901-6.

79. Fontenot JD, Rasmussen JP, Gavin MA, Rudensky AY. A function for interleukin 2 in Foxp3-expressing regulatory T cells. Nat Immunol. 2005;6(11):1142-51.

80. Vang KB, Yang J, Mahmud SA, Burchill MA, Vegoe AL, Farrar MA. IL-2, -7, and -15, but not thymic stromal lymphopoeitin, redundantly govern CD4+Foxp3+ regulatory T cell development. J Immunol. 2008;181(5):3285-90.

81. Burchill MA, Yang J, Vang KB, Farrar MA. Interleukin-2 receptor signaling in regulatory T cell development and homeostasis. Immunol Lett. 2007;114(1):1-8.

82. Burchill MA, Yang J, Vogtenhuber C, Blazar BR, Farrar MA. IL-2 receptor beta-dependent STAT5 activation is required for the development of Foxp3+ regulatory T cells. J Immunol. 2007;178(1):280-90.

83. Thornton AM, Shevach EM. CD4+CD25+ immunoregulatory T cells suppress polyclonal T cell activation in vitro by inhibiting interleukin 2 production. J Exp Med. 1998;188(2):287-96.

84. Pan F, Yu H, Dang EV, Barbi J, Pan X, Grosso JF, et al. Eos mediates Foxp3-dependent gene silencing in CD4+ regulatory T cells. Science. 2009;325(5944):1142-6.

85. Weist BM, Kurd N, Boussier J, Chan SW, Robey EA. Thymic regulatory T cell niche size is dictated by limiting IL-2 from antigen-bearing dendritic cells and feedback competition. Nat Immunol. 2015;16(6):635-41.

86. Owen DL, Mahmud SA, Vang KB, Kelly RM, Blazar BR, Smith KA, et al. Identification of Cellular Sources of IL-2 Needed for Regulatory T Cell Development and Homeostasis. J Immunol. 2018;200(12):3926-33.

87. Chinen T, Kannan AK, Levine AG, Fan X, Klein U, Zheng Y, et al. An essential role for the IL-2 receptor in Treg cell function. Nat Immunol. 2016;17(11):1322-33.

88. Malin S, McManus S, Cobaleda C, Novatchkova M, Delogu A, Bouillet P, et al. Role of STAT5 in controlling cell survival and immunoglobulin gene recombination during pro-B cell development. Nat Immunol. 2010;11(2):171-9.

89. Kitagawa Y, Ohkura N, Kidani Y, Vandenbon A, Hirota K, Kawakami R, et al. Guidance of regulatory T cell development by Satb1-dependent super-enhancer establishment. Nat Immunol. 2017;18(2):173-83.

90. Placek K, Hu G, Cui K, Zhang D, Ding Y, Lee JE, et al. MLL4 prepares the enhancer landscape for Foxp3 induction via chromatin looping. Nat Immunol. 2017;18(9):1035-45.

91. Curotto de Lafaille MA, Kutchukhidze N, Shen S, Ding Y, Yee H, Lafaille JJ. Adaptive Foxp3+ regulatory T cell-dependent and -independent control of allergic inflammation. Immunity. 2008;29(1):114-26.

92. Curotto de Lafaille MA, Lafaille JJ. Natural and adaptive foxp3+ regulatory T cells: more of the same or a division of labor? Immunity. 2009;30(5):626-35.

93. Mucida D, Kutchukhidze N, Erazo A, Russo M, Lafaille JJ, Curotto de Lafaille MA. Oral tolerance in the absence of naturally occurring Tregs. J Clin Invest. 2005;115(7):1923-33.

94. Hsieh CS, Rudensky AY. The role of TCR specificity in naturally arising CD25+ CD4+ regulatory T cell biology. Curr Top Microbiol Immunol. 2005;293:25-42.

95. Lathrop SK, Bloom SM, Rao SM, Nutsch K, Lio CW, Santacruz N, et al. Peripheral education of the immune system by colonic commensal microbiota. Nature. 2011;478(7368):250-4.

96. Lathrop SK, Santacruz NA, Pham D, Luo J, Hsieh CS. Antigen-specific peripheral shaping of the natural regulatory T cell population. J Exp Med. 2008;205(13):3105-17.

97. Kretschmer K, Apostolou I, Hawiger D, Khazaie K, Nussenzweig MC, von Boehmer H. Inducing and expanding regulatory T cell populations by foreign antigen. Nat Immunol. 2005;6(12):1219-27.

98. Xu M, Pokrovskii M, Ding Y, Yi R, Au C, Harrison OJ, et al. c-MAF-dependent regulatory T cells mediate immunological tolerance to a gut pathobiont. Nature. 2018;554(7692):373-7.

99. Chai JN, Peng Y, Rengarajan S, Solomon BD, Ai TL, Shen Z, et al. Helicobacter species are potent drivers of colonic T cell responses in homeostasis and inflammation. Sci Immunol. 2017;2(13).

100. Zegarra-Ruiz DF, Kim DV, Norwood K, Kim M, Wu WH, Saldana-Morales FB, et al. Thymic development of gut-microbiota-specific T cells. Nature. 2021;594(7863):413-7.

101. Thornton AM, Korty PE, Tran DQ, Wohlfert EA, Murray PE, Belkaid Y, et al. Expression of Helios, an Ikaros transcription factor family member, differentiates

thymic-derived from peripherally induced Foxp3+ T regulatory cells. J Immunol. 2010;184(7):3433-41.

102. Weiss JM, Bilate AM, Gobert M, Ding Y, Curotto de Lafaille MA, Parkhurst CN, et al. Neuropilin 1 is expressed on thymus-derived natural regulatory T cells, but not mucosa-generated induced Foxp3+ T reg cells. J Exp Med. 2012;209(10):1723-42, S1.

103. Yadav M, Louvet C, Davini D, Gardner JM, Martinez-Llordella M, Bailey-Bucktrout S, et al. Neuropilin-1 distinguishes natural and inducible regulatory T cells among regulatory T cell subsets in vivo. J Exp Med. 2012;209(10):1713-22, S1-19.

104. Chen W, Jin W, Hardegen N, Lei KJ, Li L, Marinos N, et al. Conversion of peripheral CD4+CD25- naive T cells to CD4+CD25+ regulatory T cells by TGF-beta induction of transcription factor Foxp3. J Exp Med. 2003;198(12):1875-86.

105. Benson MJ, Pino-Lagos K, Rosemblatt M, Noelle RJ. All-trans retinoic acid mediates enhanced T reg cell growth, differentiation, and gut homing in the face of high levels of co-stimulation. J Exp Med. 2007;204(8):1765-74.

106. Coombes JL, Siddiqui KR, Arancibia-Carcamo CV, Hall J, Sun CM, Belkaid Y, et al. A functionally specialized population of mucosal CD103+ DCs induces Foxp3+ regulatory T cells via a TGF-beta and retinoic acid-dependent mechanism. J Exp Med. 2007;204(8):1757-64.

107. Mucida D, Park Y, Kim G, Turovskaya O, Scott I, Kronenberg M, et al. Reciprocal TH17 and regulatory T cell differentiation mediated by retinoic acid. Science. 2007;317(5835):256-60.

108. Schambach F, Schupp M, Lazar MA, Reiner SL. Activation of retinoic acid receptor-alpha favours regulatory T cell induction at the expense of IL-17-secreting T helper cell differentiation. Eur J Immunol. 2007;37(9):2396-9.

109. Sun CM, Hall JA, Blank RB, Bouladoux N, Oukka M, Mora JR, et al. Small intestine lamina propria dendritic cells promote de novo generation of Foxp3 T reg cells via retinoic acid. J Exp Med. 2007;204(8):1775-85.

110. Selvaraj RK, Geiger TL. A kinetic and dynamic analysis of Foxp3 induced in T cells by TGF-beta. J Immunol. 2007;179(2):11 p following 1390.

111. Horwitz DA, Zheng SG, Gray JD, Wang JH, Ohtsuka K, Yamagiwa S. Regulatory T cells generated ex vivo as an approach for the therapy of autoimmune disease. Semin Immunol. 2004;16(2):135-43.

112. Korn T, Bettelli E, Gao W, Awasthi A, Jager A, Strom TB, et al. IL-21 initiates an alternative pathway to induce proinflammatory T(H)17 cells. Nature. 2007;448(7152):484-7.

113. Nurieva R, Yang XO, Martinez G, Zhang Y, Panopoulos AD, Ma L, et al. Essential autocrine regulation by IL-21 in the generation of inflammatory T cells. Nature. 2007;448(7152):480-3.

114. Zhou L, Ivanov, II, Spolski R, Min R, Shenderov K, Egawa T, et al. IL-6 programs T(H)-17 cell differentiation by promoting sequential engagement of the IL-21 and IL-23 pathways. Nat Immunol. 2007;8(9):967-74.

115. Zhou L, Lopes JE, Chong MM, Ivanov, II, Min R, Victora GD, et al. TGF-beta-induced Foxp3 inhibits T(H)17 cell differentiation by antagonizing RORgammat function. Nature. 2008;453(7192):236-40.

116. Xu L, Kitani A, Stuelten C, McGrady G, Fuss I, Strober W. Positive and negative transcriptional regulation of the Foxp3 gene is mediated by access and binding of the Smad3 protein to enhancer I. Immunity. 2010;33(3):313-25.

117. Tone Y, Furuuchi K, Kojima Y, Tykocinski ML, Greene MI, Tone M. Smad3 and NFAT cooperate to induce Foxp3 expression through its enhancer. Nat Immunol. 2008;9(2):194-202.

118. Josefowicz SZ, Wilson CB, Rudensky AY. Cutting edge: TCR stimulation is sufficient for induction of Foxp3 expression in the absence of DNA methyltransferase 1. J Immunol. 2009;182(11):6648-52.

119. Campbell C, Dikiy S, Bhattarai SK, Chinen T, Matheis F, Calafiore M, et al. Extrathymically Generated Regulatory T Cells Establish a Niche for Intestinal Border-Dwelling Bacteria and Affect Physiologic Metabolite Balance. Immunity. 2018;48(6):1245-57 e9.

120. Arpaia N, Rudensky AY. Microbial metabolites control gut inflammatory responses. Proc Natl Acad Sci U S A. 2014;111(6):2058-9.

121. Smith PM, Howitt MR, Panikov N, Michaud M, Gallini CA, Bohlooly YM, et al. The microbial metabolites, short-chain fatty acids, regulate colonic Treg cell homeostasis. Science. 2013;341(6145):569-73.

122. Wahlstrom A, Sayin SI, Marschall HU, Backhed F. Intestinal Crosstalk between Bile Acids and Microbiota and Its Impact on Host Metabolism. Cell Metab. 2016;24(1):41-50.

123. Campbell C, McKenney PT, Konstantinovsky D, Isaeva OI, Schizas M, Verter J, et al. Bacterial metabolism of bile acids promotes generation of peripheral regulatory T cells. Nature. 2020;581(7809):475-9.

124. Song X, Sun X, Oh SF, Wu M, Zhang Y, Zheng W, et al. Microbial bile acid metabolites modulate gut RORgamma(+) regulatory T cell homeostasis. Nature. 2020;577(7790):410-5.

125. Hang S, Paik D, Yao L, Kim E, Trinath J, Lu J, et al. Bile acid metabolites control TH17 and Treg cell differentiation. Nature. 2019;576(7785):143-8.

126. Allenspach E, Torgerson TR. Autoimmunity and Primary Immunodeficiency Disorders. J Clin Immunol. 2016;36 Suppl 1:57-67.

127. Georgiev P, Charbonnier LM, Chatila TA. Regulatory T Cells: the Many Faces of Foxp3. J Clin Immunol. 2019;39(7):623-40.

128. Park JH, Lee KH, Jeon B, Ochs HD, Lee JS, Gee HY, et al. Immune dysregulation, polyendocrinopathy, enteropathy, X-linked (IPEX) syndrome: A systematic review. Autoimmun Rev. 2020;19(6):102526.

129. Samstein RM, Josefowicz SZ, Arvey A, Treuting PM, Rudensky AY. Extrathymic generation of regulatory T cells in placental mammals mitigates maternal-fetal conflict. Cell. 2012;150(1):29-38.

130. Zong X, Hao X, Xu B, Crawford JC, Wright S, Li J, et al. Foxp3 enhancers synergize to maximize regulatory T cell suppressive capacity. J Exp Med. 2021;218(8).

131. Blaschke K, Ebata KT, Karimi MM, Zepeda-Martinez JA, Goyal P, Mahapatra S, et al. Vitamin C induces Tet-dependent DNA demethylation and a blastocyst-like state in ES cells. Nature. 2013;500(7461):222-6.

132. Yin R, Mao SQ, Zhao B, Chong Z, Yang Y, Zhao C, et al. Ascorbic acid enhances Tet-mediated 5-methylcytosine oxidation and promotes DNA demethylation in mammals. J Am Chem Soc. 2013;135(28):10396-403.

133. Kanangat S, Blair P, Reddy R, Daheshia M, Godfrey V, Rouse BT, et al. Disease in the scurfy (sf) mouse is associated with overexpression of cytokine genes. Eur J Immunol. 1996;26(1):161-5.

134. Chatila TA. Role of regulatory T cells in human diseases. J Allergy Clin Immunol. 2005;116(5):949-59; quiz 60.

135. Godfrey VL, Wilkinson JE, Russell LB. X-linked lymphoreticular disease in the scurfy (sf) mutant mouse. Am J Pathol. 1991;138(6):1379-87.

136. Gavin MA, Rasmussen JP, Fontenot JD, Vasta V, Manganiello VC, Beavo JA, et al. Foxp3-dependent programme of regulatory T-cell differentiation. Nature. 2007;445(7129):771-5.

137. Lin W, Haribhai D, Relland LM, Truong N, Carlson MR, Williams CB, et al. Regulatory T cell development in the absence of functional Foxp3. Nat Immunol. 2007;8(4):359-68.

138. Ohkura N, Hamaguchi M, Morikawa H, Sugimura K, Tanaka A, Ito Y, et al. T cell receptor stimulation-induced epigenetic changes and Foxp3 expression are independent and complementary events required for Treg cell development. Immunity. 2012;37(5):785-99.

139. Ramsdell F, Ziegler SF. FOXP3 and scurfy: how it all began. Nat Rev Immunol. 2014;14(5):343-9.

140. Tian L, Altin JA, Makaroff LE, Franckaert D, Cook MC, Goodnow CC, et al. Foxp3(+) regulatory T cells exert asymmetric control over murine helper responses by inducing Th2 cell apoptosis. Blood. 2011;118(7):1845-53.

141. Scherer MT, Ignatowicz L, Winslow GM, Kappler JW, Marrack P. Superantigens: bacterial and viral proteins that manipulate the immune system. Annu Rev Cell Biol. 1993;9:101-28.

142. Pacholczyk R, Kraj P, Ignatowicz L. Peptide specificity of thymic selection of CD4+CD25+ T cells. J Immunol. 2002;168(2):613-20.

143. Romagnoli P, Hudrisier D, van Meerwijk JP. Preferential recognition of self antigens despite normal thymic deletion of CD4(+)CD25(+) regulatory T cells. J Immunol. 2002;168(4):1644-8.

144. Arvey A, van der Veeken J, Samstein RM, Feng Y, Stamatoyannopoulos JA, Rudensky AY. Inflammation-induced repression of chromatin bound by the transcription factor Foxp3 in regulatory T cells. Nat Immunol. 2014;15(6):580-7.

145. Vignali DA, Collison LW, Workman CJ. How regulatory T cells work. Nat Rev Immunol. 2008;8(7):523-32.

146. Shevach EM. Mechanisms of foxp3+ T regulatory cell-mediated suppression. Immunity. 2009;30(5):636-45.

147. Owen DL, Mahmud SA, Sjaastad LE, Williams JB, Spanier JA, Simeonov DR, et al. Thymic regulatory T cells arise via two distinct developmental programs. Nat Immunol. 2019;20(2):195-205.

148. Levine AG, Hemmers S, Baptista AP, Schizas M, Faire MB, Moltedo B, et al. Suppression of lethal autoimmunity by regulatory T cells with a single TCR specificity. J Exp Med. 2017;214(3):609-22.

149. Ye J, Qiu J, Bostick JW, Ueda A, Schjerven H, Li S, et al. The Aryl Hydrocarbon Receptor Preferentially Marks and Promotes Gut Regulatory T Cells. Cell Rep. 2017;21(8):2277-90.

150. Pritykin Y, van der Veeken J, Pine AR, Zhong Y, Sahin M, Mazutis L, et al. A unified atlas of CD8 T cell dysfunctional states in cancer and infection. Mol Cell. 2021;81(11):2477-93 e10.

151. Pierson W, Cauwe B, Policheni A, Schlenner SM, Franckaert D, Berges J, et al. Antiapoptotic Mcl-1 is critical for the survival and niche-filling capacity of Foxp3(+) regulatory T cells. Nat Immunol. 2013;14(9):959-65.

152. Setty M, Kiseliovas V, Levine J, Gayoso A, Mazutis L, Pe'er D. Characterization of cell fate probabilities in single-cell data with Palantir. Nat Biotechnol. 2019;37(4):451-60.

153. Miragaia RJ, Gomes T, Chomka A, Jardine L, Riedel A, Hegazy AN, et al. Single-Cell Transcriptomics of Regulatory T Cells Reveals Trajectories of Tissue Adaptation. Immunity. 2019;50(2):493-504 e7.

154. Xing S, Gai K, Li X, Shao P, Zeng Z, Zhao X, et al. Tcf1 and Lef1 are required for the immunosuppressive function of regulatory T cells. J Exp Med. 2019;216(4):847-66.

155. Yang BH, Wang K, Wan S, Liang Y, Yuan X, Dong Y, et al. TCF1 and LEF1 Control Treg Competitive Survival and Tfr Development to Prevent Autoimmune Diseases. Cell Rep. 2019;27(12):3629-45 e6.

156. Long SA, Buckner JH. CD4+FOXP3+ T regulatory cells in human autoimmunity: more than a numbers game. J Immunol. 2011;187(5):2061-6.

157. Venken K, Hellings N, Broekmans T, Hensen K, Rummens JL, Stinissen P. Natural naive CD4+CD25+CD127low regulatory T cell (Treg) development and function are disturbed in multiple sclerosis patients: recovery of memory Treg homeostasis during disease progression. J Immunol. 2008;180(9):6411-20.

158. Ferraro A, D'Alise AM, Raj T, Asinovski N, Phillips R, Ergun A, et al. Interindividual variation in human T regulatory cells. Proc Natl Acad Sci U S A. 2014;111(12):E1111-20.

159. Arvey A, van der Veeken J, Plitas G, Rich SS, Concannon P, Rudensky AY. Genetic and epigenetic variation in the lineage specification of regulatory T cells. Elife. 2015;4:e07571.

160. Nasrallah R, Imianowski CJ, Bossini-Castillo L, Grant FM, Dogan M, Placek L, et al. A distal enhancer at risk locus 11q13.5 promotes suppression of colitis by Treg cells. Nature. 2020;583(7816):447-52.

161. Sakaguchi S, Mikami N, Wing JB, Tanaka A, Ichiyama K, Ohkura N. Regulatory T Cells and Human Disease. Annu Rev Immunol. 2020;38:541-66.

162. Tahvildari M, Dana R. Low-Dose IL-2 Therapy in Transplantation, Autoimmunity, and Inflammatory Diseases. J Immunol. 2019;203(11):2749-55.

163. Vogtenhuber C, Bucher C, Highfill SL, Koch LK, Goren E, Panoskaltsis-Mortari A, et al. Constitutively active Stat5b in CD4+ T cells inhibits graft-versus-host disease lethality associated with increased regulatory T-cell potency and decreased T effector cell responses. Blood. 2010;116(3):466-74.

164. Rubtsov YP, Niec RE, Josefowicz S, Li L, Darce J, Mathis D, et al. Stability of the regulatory T cell lineage in vivo. Science. 2010;329(5999):1667-71.

165. Sledzinska A, Hemmers S, Mair F, Gorka O, Ruland J, Fairbairn L, et al. TGF-beta signalling is required for CD4(+) T cell homeostasis but dispensable for regulatory T cell function. PLoS Biol. 2013;11(10):e1001674.

166. Mombaerts P, Clarke AR, Rudnicki MA, Iacomini J, Itohara S, Lafaille JJ, et al. Mutations in T-cell antigen receptor genes alpha and beta block thymocyte development at different stages. Nature. 1992;360(6401):225-31.

167. Madisen L, Zwingman TA, Sunkin SM, Oh SW, Zariwala HA, Gu H, et al. A robust and high-throughput Cre reporting and characterization system for the whole mouse brain. Nat Neurosci. 2010;13(1):133-40.

168. Dobin A, Davis CA, Schlesinger F, Drenkow J, Zaleski C, Jha S, et al. STAR: ultrafast universal RNA-seq aligner. Bioinformatics. 2013;29(1):15-21.

169. McKenna A, Hanna M, Banks E, Sivachenko A, Cibulskis K, Kernytsky A, et al. The Genome Analysis Toolkit: a MapReduce framework for analyzing next-generation DNA sequencing data. Genome Res. 2010;20(9):1297-303.

170. Love MI, Huber W, Anders S. Moderated estimation of fold change and dispersion for RNA-seq data with DESeq2. Genome Biol. 2014;15(12):550.

171. van Dijk D, Sharma R, Nainys J, Yim K, Kathail P, Carr AJ, et al. Recovering Gene Interactions from Single-Cell Data Using Data Diffusion. Cell. 2018;174(3):716-29 e27.

172. Levine JH, Simonds EF, Bendall SC, Davis KL, Amir el AD, Tadmor MD, et al. Data-Driven Phenotypic Dissection of AML Reveals Progenitor-like Cells that Correlate with Prognosis. Cell. 2015;162(1):184-97.

173. Wolf FA, Angerer P, Theis FJ. SCANPY: large-scale single-cell gene expression data analysis. Genome Biol. 2018;19(1):15.

174. Stuart T, Butler A, Hoffman P, Hafemeister C, Papalexi E, Mauck WM, 3rd, et al. Comprehensive Integration of Single-Cell Data. Cell. 2019;177(7):1888-902 e21.

175. Bolotin DA, Poslavsky S, Mitrophanov I, Shugay M, Mamedov IZ, Putintseva EV, et al. MiXCR: software for comprehensive adaptive immunity profiling. Nat Methods. 2015;12(5):380-1.

176. Shugay M, Bagaev DV, Turchaninova MA, Bolotin DA, Britanova OV, Putintseva EV, et al. VDJtools: Unifying Post-analysis of T Cell Receptor Repertoires. PLoS Comput Biol. 2015;11(11):e1004503.

177. Martin-Orozco E, Norte-Munoz M, Martinez-Garcia J. Regulatory T Cells in Allergy and Asthma. Front Pediatr. 2017;5:117.

178. Kim KS, Hong SW, Han D, Yi J, Jung J, Yang BG, et al. Dietary antigens limit mucosal immunity by inducing regulatory T cells in the small intestine. Science. 2016;351(6275):858-63.

179. Ohnmacht C, Park JH, Cording S, Wing JB, Atarashi K, Obata Y, et al. MUCOSAL IMMUNOLOGY. The microbiota regulates type 2 immunity through RORgammat(+) T cells. Science. 2015;349(6251):989-93.

180. Sefik E, Geva-Zatorsky N, Oh S, Konnikova L, Zemmour D, McGuire AM, et al. MUCOSAL IMMUNOLOGY. Individual intestinal symbionts induce a distinct population of RORgamma(+) regulatory T cells. Science. 2015;349(6251):993-7.

181. Littman DR, Rudensky AY. Th17 and regulatory T cells in mediating and restraining inflammation. Cell. 2010;140(6):845-58.

182. Chang D, Xing Q, Su Y, Zhao X, Xu W, Wang X, et al. The Conserved Non-coding Sequences CNS6 and CNS9 Control Cytokine-Induced Rorc Transcription during T Helper 17 Cell Differentiation. Immunity. 2020;53(3):614-26 e4.

183. Akimova T, Beier UH, Wang L, Levine MH, Hancock WW. Helios expression is a marker of T cell activation and proliferation. PLoS One. 2011;6(8):e24226.

184. Zabransky DJ, Nirschl CJ, Durham NM, Park BV, Ceccato CM, Bruno TC, et al. Phenotypic and functional properties of Helios+ regulatory T cells. PLoS One. 2012;7(3):e34547.

185. Zheng SG, Wang JH, Stohl W, Kim KS, Gray JD, Horwitz DA. TGF-beta requires CTLA-4 early after T cell activation to induce FoxP3 and generate adaptive CD4+CD25+ regulatory cells. J Immunol. 2006;176(6):3321-9.

186. Nutsch K, Chai JN, Ai TL, Russler-Germain E, Feehley T, Nagler CR, et al. Rapid and Efficient Generation of Regulatory T Cells to Commensal Antigens in the Periphery. Cell Rep. 2016;17(1):206-20.

187. Davidson TS, DiPaolo RJ, Andersson J, Shevach EM. Cutting Edge: IL-2 is essential for TGF-beta-mediated induction of Foxp3+ T regulatory cells. J Immunol. 2007;178(7):4022-6.

188. Horwitz DA, Zheng SG, Wang J, Gray JD. Critical role of IL-2 and TGF-beta in generation, function and stabilization of Foxp3+CD4+ Treg. Eur J Immunol. 2008;38(4):912-5.

189. Ruzankina Y, Pinzon-Guzman C, Asare A, Ong T, Pontano L, Cotsarelis G, et al. Deletion of the developmentally essential gene ATR in adult mice leads to age-related phenotypes and stem cell loss. Cell Stem Cell. 2007;1(1):113-26.

190. Goodwin LO, Splinter E, Davis TL, Urban R, He H, Braun RE, et al. Large-scale discovery of mouse transgenic integration sites reveals frequent structural variation and insertional mutagenesis. Genome Res. 2019;29(3):494-505.

191. Yang S, Fujikado N, Kolodin D, Benoist C, Mathis D. Immune tolerance. Regulatory T cells generated early in life play a distinct role in maintaining self-tolerance. Science. 2015;348(6234):589-94.

192. Finkelman FD, Madden KB, Morris SC, Holmes JM, Boiani N, Katona IM, et al. Anti-cytokine antibodies as carrier proteins. Prolongation of in vivo effects of exogenous cytokines by injection of cytokine-anti-cytokine antibody complexes. J Immunol. 1993;151(3):1235-44.

193. Moon HB, Severinson E, Heusser C, Johansson SG, Moller G, Persson U. Regulation of IgG1 and IgE synthesis by interleukin 4 in mouse B cells. Scand J Immunol. 1989;30(3):355-61.

194. Xiong H, Dolpady J, Wabl M, Curotto de Lafaille MA, Lafaille JJ. Sequential class switching is required for the generation of high affinity IgE antibodies. J Exp Med. 2012;209(2):353-64.

195. Herschlag D, Johnson FB. Synergism in transcriptional activation: a kinetic view. Genes Dev. 1993;7(2):173-9.

196. Bettelli E, Carrier Y, Gao W, Korn T, Strom TB, Oukka M, et al. Reciprocal developmental pathways for the generation of pathogenic effector TH17 and regulatory T cells. Nature. 2006;441(7090):235-8.

197. Veldhoen M, Hocking RJ, Atkins CJ, Locksley RM, Stockinger B. TGFbeta in the context of an inflammatory cytokine milieu supports de novo differentiation of IL-17-producing T cells. Immunity. 2006;24(2):179-89.

198. Schneider C, O'Leary CE, von Moltke J, Liang HE, Ang QY, Turnbaugh PJ, et al. A Metabolite-Triggered Tuft Cell-ILC2 Circuit Drives Small Intestinal Remodeling. Cell. 2018;174(2):271-84 e14.

199. Ford AC, Sperber AD, Corsetti M, Camilleri M. Irritable bowel syndrome. Lancet. 2020;396(10263):1675-88.

200. Guan Q. A Comprehensive Review and Update on the Pathogenesis of Inflammatory Bowel Disease. J Immunol Res. 2019;2019:7247238.